01 Mar 1973

Plastic subassemblage anlysis and tests for rigid high-rise steel frames

J. Hartley Daniels

S. W. Kim

BULLETIN NO. 23, MARCH, 1973—*Lehigh University*—PLASTIC SUBASSEMBLAGE ANALYSIS AND TESTS FOR RIGID HIGH-RISE STEEL FRAMES

STEEL RESEARCH for construction

PLASTIC SUBASSEMBLAGE ANALYSIS AND TESTS FOR RIGID HIGH-RISE STEEL FRAMES

—Lehigh University

Committee of Structural Steel Producers • Committee of Steel Plate Producers

american iron and steel institute

150 East 42nd Street, New York, N.Y. 10017

BULLETIN NO. 23, MARCH, 1973

Plastic Subassemblage Analysis and Tests for Rigid High-Rise Steel Frames

DEPARTMENT OF CIVIL ENGINEERING
FRITZ ENGINEERING LABORATORY
LEHIGH UNIVERSITY
Bethlehem, Pennsylvania

Committee of Steel Plate Producers and Committee of Structural Steel Producers

american iron and steel institute

150 East 42nd Street, New York, N.Y. 10017

(150) PS 158

Printed in U.S.A. 373/3000

Plastic Analysis of One-Story Assemblages

by

J. HARTLEY DANIELS

ACKNOWLEDGMENTS

The work described herein was performed as part of a general investigation into the plastic design of multistory frames at Fritz Engineering Laboratory, Lehigh University, Bethlehem, Pa. The general investigation was sponsored jointly by the Welding Research Council and the Department of the Navy with funds furnished by the American Institute of Steel Construction, American Iron and Steel Institute, Naval Ship Systems Command and Naval Facilities Engineering Command. Technical guidance was provided by the Subcommittee on Welded Continuous Frames and Their Components of the Structural Steel Committee of the Welding Research Council. Dr. T. R. Higgins was Chairman of the Subcommittee.

The Committees of Structural Steel Producers and Steel Plate Producers of American Iron and Steel Institute sponsored the experimental work reported in this Bulletin.

CONTENTS

ABSTRACT

The plastic subassemblage method of analysis was developed to perform the plastic analysis of one-story assemblages. This method provides a key element in the plastic design of unbraced multi-story rigid steel frames. In the method, a one-story assemblage is assumed isolated from a multistory multibay unbraced frame at the level under consideration. The load-drift behavior of the one-story assemblage approximates the load-drift behavior of a story at that level. This report provides the background information for the two reports which follow.

1. Introduction

The plastic subassemblage method of analysis was developed to provide a story-by-story analysis of an unbraced multistory multibay steel frame such as the one shown in Figure 1 (1–3). The frame is subjected to combined gravity loads w and lateral loads H. In the method, a one-story assemblage is assumed isolated from the frame at the level under consideration. The load-drift behavior of the one-story assemblage is then determined and assumed to approximate the load-drift behavior of a story at that level.

The plastic subassemblage method of analysis is based on the subassemblage concept and uses the results of studies on restrained columns permitted to sway (4). The method accounts for $P-\Delta$ moments as well as plastic hinges in the beams and columns and residual stresses in the columns.

The purpose of this report is to familiarize the reader with the plastic subassemblage analysis of one-story assemblages. It also provides the background information for the two reports which follow, "Experiments on Restrained Columns Permitted to Sway" and "Experiments on Unbraced One-Story Assemblages." These two reports present the results of an extensive experimental program which provides experimental verification of the plastic subassemblage method of analysis.

Nomenclature

d = depth of column section
E = modulus of elasticity
f = shape factor
H = applied horizontal load concentrated at floor level
ΣH = total applied horizontal load above a given floor level
h = story height
I = moment of inertia
K = restraint coefficient
k = nondimensional restraint
L = span length of a beam in a one-story assemblage
M = interior moment at the top of a restrained column
M_p = plastic moment capacity of a beam
M_{pc} = reduced plastic moment capacity of a column (modified plastic moment capacity to account for axial forces)
M_r = restraining moment applied by beams to top of a restrained column
M_r' = maximum value of restraining moment corresponding to a mechanism condition or the value of restraining moment at the occurrence of each plastic hinge in the subassemblage
n = level
p = ratio of M_r' to M_{pc}
P = axial force in a restrained column due to applied loads
P_y = yield stress level of axial force in the restrained column
Q = shear resistance of subassemblage (function of Δ/h)
ΣQ = shear resistance of one-story assemblage (function of Δ/h)
r_x = radius of gyration about x axis
S = section modulus
w = distributed gravity load per unit length of beam (working load value)
h/r_x = slenderness ratio about x axis
P/P_y = axial load ratio of a restrained column
α = ratio of stiffness of column to beam at a joint
α' = ratio of stiffness of column to beam at a joint
β = ratio of stiffness of column to beam at a joint
γ = joint rotation at the top of a restrained column relative to the chord
δ = increment
Δ = story drift; also twice the drift of a restrained column
Δ/h = deflection index or nondimensional drift of a story, a one-story assemblage or a subassemblage
η = ratio of stiffness of column to beam at a joint
θ = joint rotation at the top of a restrained column
θ_p = joint rotation corresponding to occurrence of a plastic hinge at the top of a restrained column
λ = distribution factor
σ_y = yield stress

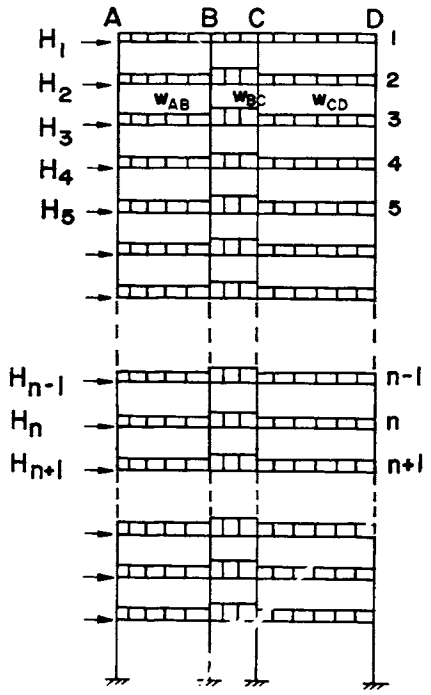

FIGURE 1. Unbraced frame and loading

2. Plastic Subassemblage Analysis Concept

2.1 The One-Story Assemblage

If the frame shown in Figure 1 is a well-proportioned regular rectangular multistory frame with relatively uniform story heights and combined loading along its height, the inflection points in the columns can be expected to occur near mid-height of each story over most of the frame. Assuming that the inflection points in the columns are located at mid-story height a one-story assemblage can be removed at level n of the frame as shown in Figure 2 by passing cuts through the mid-heights of the columns above and below level n. In Figure 2, the story height is h, the applied shear above and below level n is respectively ΣH_{n-1} and ΣH_n. The constants λ define the distribution of the applied shear to the columns. The column axial forces P and the distributed beam loads w are assumed constant and are calculated from the

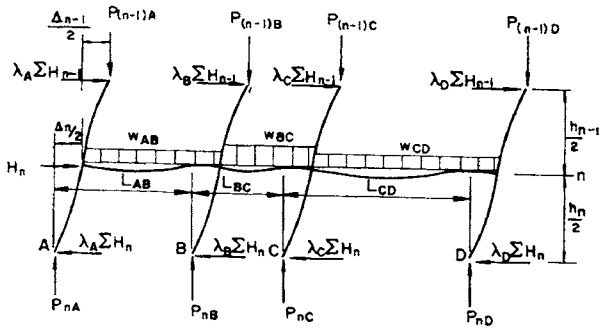

FIGURE 2. One-story assemblage

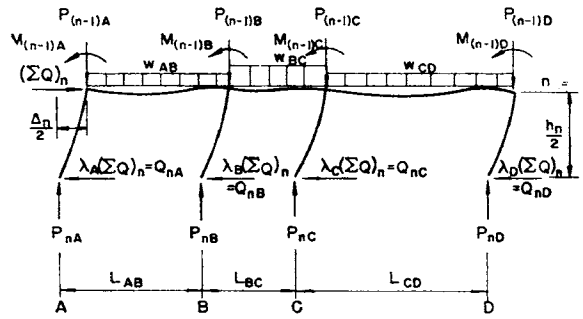

$$M_{(n-1)A} = -(\lambda_A \Sigma Q_{n-1})\frac{h_{n-1}}{2} - P_{(n-1)A}\frac{\Delta_{n-1}}{2}$$

$$M_{(n-1)B} = -(\lambda_B \Sigma Q_{n-1})\frac{h_{n-1}}{2} - P_{(n-1)B}\frac{\Delta_{n-1}}{2}$$

$$M_{(n-1)C} = -(\lambda_C \Sigma Q_{n-1})\frac{h_{n-1}}{2} - P_{(n-1)C}\frac{\Delta_{n-1}}{2}$$

$$M_{(n-1)D} = -(\lambda_D \Sigma Q_{n-1})\frac{h_{n-1}}{2} - P_{(n-1)D}\frac{\Delta_{n-1}}{2}$$

FIGURE 3. Equivalent one-story assemblage

known loads on the frame. The column drift referred to level n is given by $\Delta/2$. The story drift is therefore Δ.

The one-story assemblage can be simplified as shown in Figure 3 by replacing each column above level n with the equivalent joint forces. The columns below level n in Figure 3 are now called restrained columns and the beams provide the restraint for the restrained columns. In the figure the known shear forces ΣH_{n-1} and ΣH_n are also replaced by unknown shear forces ΣQ_{n-1} and ΣQ_n which are functions of Δ. In the analysis the unknown shears ΣQ are to be computed and compared with the applied shears ΣH.

2.2 The Subassemblages

To facilitate the load-drift analysis of the equivalent one-story assemblage, it is assumed to be subdivided into smaller units called subassemblages. Each subassemblage consists of one restrained column plus the adjacent restraining beams at the column top. The three types of subassemblages (windward, interior and exterior) which are possible in any multibay one-story assemblage are shown in Figure 4. Rotational restraints are assumed at the free ends of the beams in each subassemblage to account for the restraining effects of the beams and columns outside the subassemblage. These restraints are shown schematically by springs in Figure 4.

2.3 The Restrained Columns

Figure 5(a) shows a typical restrained column. It is subjected to a constant vertical load, P_n, and to varying lateral force, Q_n, and moment, M_n. The resulting deformed configuration is shown in

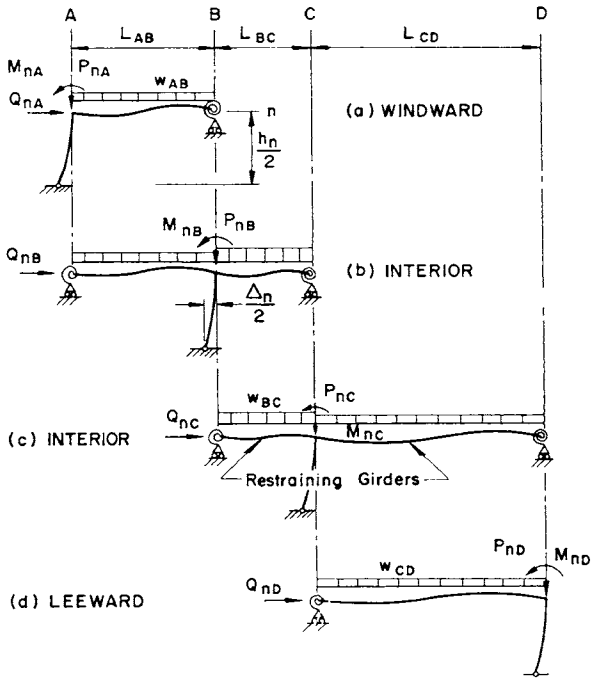

FIGURE 4. The subassemblages

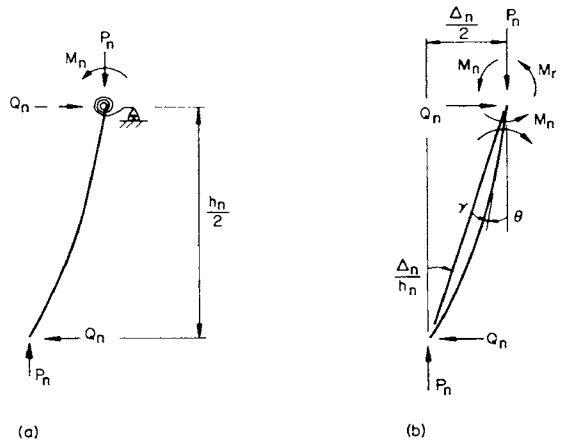

FIGURE 5. The restrained column in a subassemblage

Figure 5(b). A linearly elastic rotational restraint at the column top provides a restraining moment of M_r. The three rotations, Δ_n/h_n, θ and γ are measured from the references lines shown in Figure 5(b) and are positive when clockwise. For any story n, equilibrium requires that

$$M = -\left(Q\frac{h}{2} + P\frac{\Delta}{2}\right) \tag{1}$$

and

$$2M + M_r = 0 \tag{2}$$

For small deformations, the rotations θ, γ and Δ_n/h_n in Figure 5(b) for any story n are related by the compatibility condition:

$$\frac{\Delta}{h} = \theta - \gamma \tag{3}$$

Equation (1) can be nondimensionalized with respect to the reduced plastic moment capacity of the column, M_{pc}, as follows:

$$\frac{Qh}{2M_{pc}} = -\left(\frac{M}{M_{pc}} + \frac{P\Delta}{2M_{pc}}\right) \tag{4}$$

where, for major axis bending of W shapes,

$$M_{pc} = 1.18(1 - P/P_y)M_p;\ P/P_y > 0.15 \tag{5}$$

in which M_p is the full plastic moment and P_y is the axial yield load of the column. Writing

$$M_p = \sigma_y f S = 2P_y f \frac{r_x^2}{d} \tag{6}$$

in which σ_y is the yield stress of the column, f the shape factors, S the section modulus, d the column depth and r_x the radius of gyration about the strong axis, then

$$\frac{Qh}{2M_{pc}} = -\left[\frac{M}{M_{pc}} + \frac{P\,h\,d\,\Delta}{P_y r_x 2 r_x h\ 2.36 f\left(1 - \frac{P}{P_y}\right)}\right] \tag{7}$$

Equation 7 may be simplified by noting that for most wide-flange shapes used for columns f and $d/2r_x$ can be approximated by their respective average values of 1.11 and 1.15. Therefore

$$\frac{Qh}{2M_{pc}} = -\left[\frac{M}{M_{pc}} + \frac{P\,h\,\Delta}{P_y r_x h\ 2.28\left(1 - \frac{P}{P_y}\right)}\right] \tag{8}$$

The load-drift relationship Q vs. $\Delta/2$ for the restrained columns can now be determined by solving Eqs. (2), (3) and (8) together with the moment-rotation relationship, M vs. γ, for the column (5–7).

The nondimensional load-drift relationship, $Qh/2M_{pc}$ vs. Δ/h for a particular restrained column with slenderness ratio, h/r_x, constant axial load ratio, P/P_y, and constant restraint stiffness, k_1, is shown by curve 0–g–b–c–e in Figure 6.

Additional load-drift curves may also be obtained for the column shown in Figure 6. Each curve would correspond to a different value of restraint stiffness, $0 \leq k_1 \leq \infty$. All curves would be similar in shape to 0–g–b–c–e and all would pass through point 0. In addition, all curves would intersect the line d–e, extended, since the maximum restraining moment, M_r' for all curves is independent of the restraint stiffness k_1.

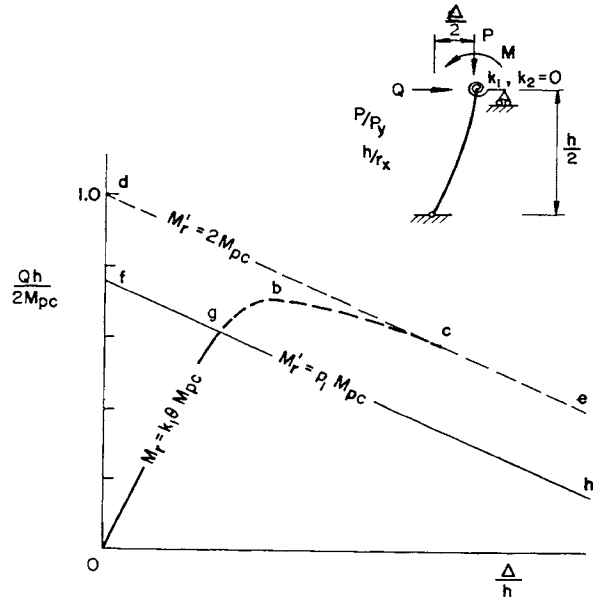

FIGURE 6. Load-deflection curve of a restrained column with constant-zero restraint stiffness

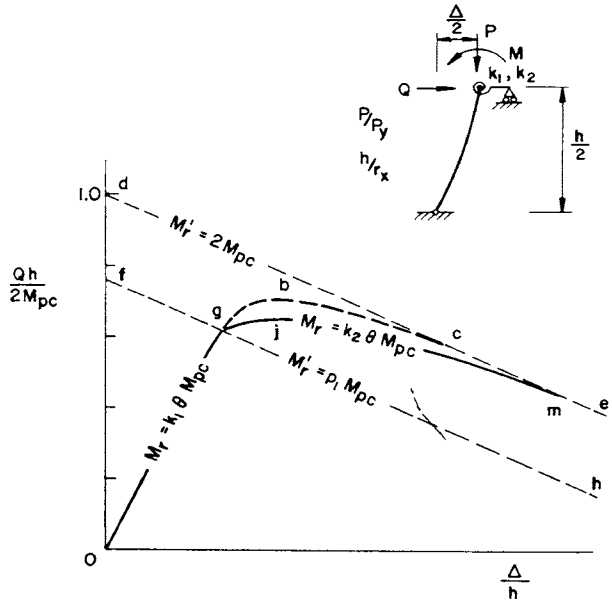

FIGURE 7. Load-deflection curve of a restrained column with constant-constant restraint stiffness

In general, the restraint stiffness, k_1, will not remain constant for all values of joint rotation, θ, but will decrease abruptly at discrete intervals as θ increases due to the successive formation of plastic hinges in the restraining beams. Of the infinite number of k–θ relationships possibly, only two of them are fundamental to subassemblage theory.

1. Constant-Zero Restraint Stiffness—The restraining moment at the column top is defined by the equations

$$M_r = k_1 \theta M_{pc} \qquad (0 \leq \theta \leq \theta_1) \tag{9}$$

$$M_r = M_r' = k_1 \theta_1 M_{pc} = p_1 M_{pc} \qquad (\theta_1 < \theta \leq \infty) \text{ and } (\theta_1 < \theta_p) \tag{10}$$

in which p_1 is a constant and $0 \leq p_1 \leq 2$. The solution of Eq. (8) for the restraining moment defined by Eq. (9) will give the load-deflection curve 0–g in Figure 6. At point g, however, the restraint stiffness becomes zero. Therefore additional restraining moment cannot be generated and a mechanism condition results. The moment at the top of the restrained column will remain constant at $M_r' = p_1 M_{pc}$ and the load-drift curve after the mechanism develops will be curve g–h in Figure 6.

2. Constant-Constant Restraint Stiffness–The restraining moment at the column top will now be defined by the equations

$$M_r = k_1 M_{pc} \qquad (0 \leq \theta \leq \theta_1) \tag{11}$$

$$M_r = k_2 M_{pc} \qquad (\theta_1 \leq \theta \leq \infty) \text{ and } (k_2 < \theta_1) \tag{12}$$

The solution of Eq. (8) for M_r defined by Eq. (11) gives curve segment 0–g in Figures 6 and 7. However, at point g in Figure 7 the restraint stiffness reduces to k_2. Additional restraining moment, M_r, can be developed after point g but at a smaller rate than before. The resulting load-drift curve is shown as curve g–j–m in Figure 7, which intersects the line d–2 at point m with the formation of a plastic hinge in the column top.

2.4 Superposition of Restrained Column Load-Drift Curves

Consider the two restrained column curves shown in Figure 8. Curve 0–a–b–c is for a restrained column whose restraint stiffness decreases from k_1 to k_2 at point a. Curve 0–a'–b'–c', however, is the load-drift curve for the same column but with constant restraint stiffness k_2. Segment 0–a and the complete curve 0–a'–b'–c' may both be obtained by solving Eq. (8) where the restraining moments M_r, are defined by $k_1 \theta M_{pc}$ and

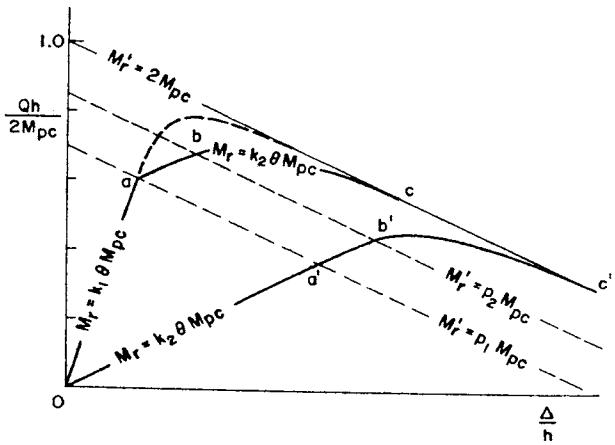

FIGURE 8. Superposition of load-deflection curves

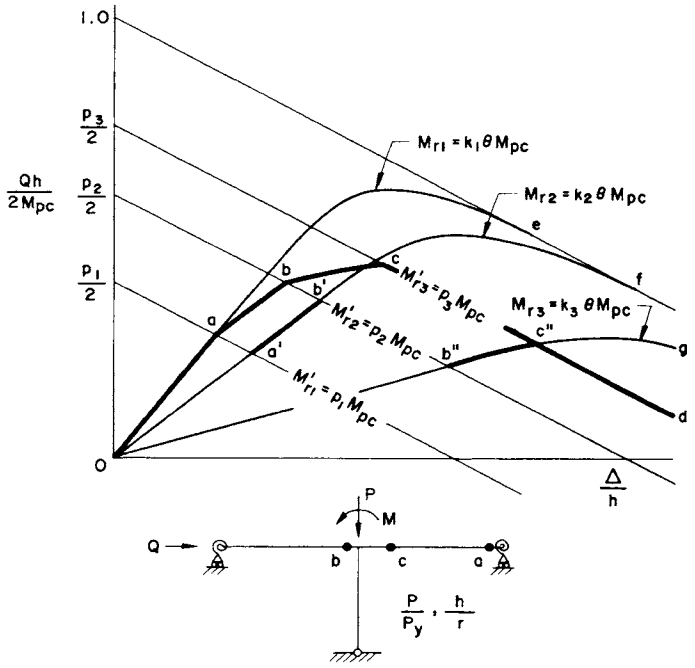

FIGURE 9. Construction of load-deflection curve

$k_2\theta M_{pc}$, respectively. Also segments a–b–c and a'–b'–c' are identical. Therefore it is not necessary to derive the load-drift equation corresponding to each reduced value of restraint stiffness, k. Instead the load-drift curve may be built up from segments of complete load-drift curves which are given by Eq. (8) for the appropriate values of $k(0 \leq k \leq \infty)$.

2.5 Construction of Subassemblage Load-Drift Curve

Figure 9 illustrates the method of constructing a typical load-drift curve for an interior subassemblage. It is assumed that a mechanism occurs with the formation of three plastic hinges in the restraining beams at a, b and c, in that order. An analysis determined that the initial restraint stiffness was k_1 and that the first plastic hinge formed at a joint rotation θ_1 so that $p_1 = k_1\theta_1$. Similarly, prior to the second and third plastic hinges the restraint stiffness was found to be k_2 and k_3, respectively, and it was found that the second and third plastic hinges formed at joint rotations of θ_2 and θ_3. Therefore, $p_2 = k_2\theta_2$ and $p_3 = k_3\theta_3$.

The initial segment of the load-drift curve is 0–a. The second segment is a–b, where point b corresponds to the formation of the second plastic hinge. This segment is obtained by translating segment a'–b' of curve 0–f to points a and b as shown. Similarly, segment b–c is obtained by translating segment b''–c'' of curve 0–g. The final segment c–d of the load-drift curve is the second-order plastic mechanism curve and follows the straight line $M_{r3}' = p_3 M_{pc}$.

Nondimensional restrained column load-drift curves are constructed for each subassemblage in a one-story assemblage. Before combining these curves to obtain the load-drift curve for the one-story assemblage, it is necessary to transform them to Q vs. Δ/h curves by multiplying the ordinates of each curve by the appropriate values of $2M_{pc}/h$.

2.6 Load-Drift Curve of a One-Story Assemblage

The load-drift curve of a one-story assemblage is determined by a superposition of the individual load-drift curves of each subassemblage in the one-story assemblage. The number of subassemblage curves involved will always equal one more than the number of bays comprising the one-story assemblage. Figure 10 illustrates the procedure for the assemblage shown in Figure 3. It requires a summation of the ordinate Q for each subassemblage curve corresponding to arbitrarily chosen values of deflection index Δ/h. Using this procedure the complete ascending and descending portions of the one-story assemblage curve can be determined.

The subassemblage curves for Q_A and Q_C in Figure 10 do not go through the origin. The horizontal axis in these diagrams is shifted to

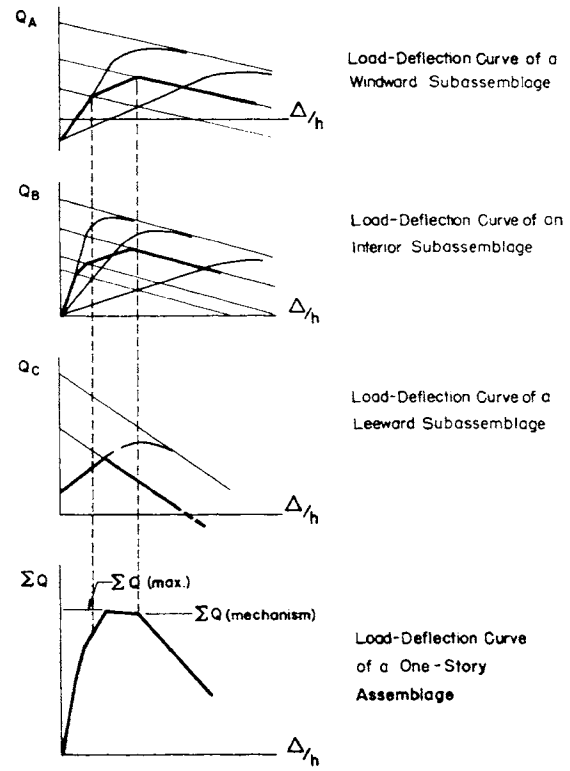

FIGURE 10. Construction of load-deflection curve for a one-story assemblage

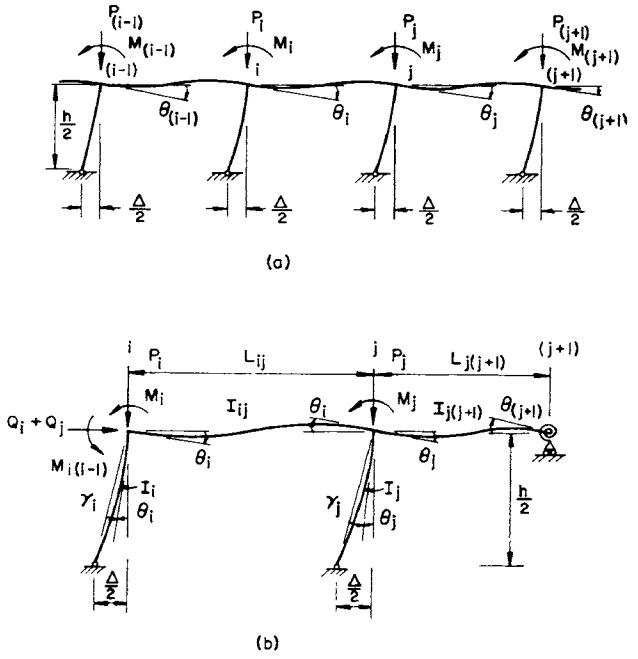

FIGURE 11. Derivation of initial restraint coefficients

account for the column shear caused by gravity loads at zero drift.

2.7 Subassemblage Analysis by Computer

Reference 8 discusses the computer analysis of a one-story assemblage. In effect the computer program solves the approximate equations after each successive increment of drift index Δ/h (arbitrarily small increments) and determines the set of values of M_r and M_r' which will define the load-drift curve of each subassemblage in the one-story assemblage. These curves are then superimposed by the computer to give the load-drift curve of the one-story assemblage. The one-story assemblage curve can also be plotted automatically by including an appropriate subroutine in the program.

3. Restraint Provided by the Beams

3.1 Initial Elastic Restraint

The interior region of a one-story assemblage is shown in Figure 11(a) together with the vertical forces P, and joint moments, M. The beams and columns are initially assumed to be elastic.

Consider the restrained column at joint i. It is desired to calculate the initial elastic value of restraint k_i, which is provided by the beams and columns of the one-story assemblage. The restraining moment, M_r, at joint i will be the sum of the restraining moments on either side of the joint and can be written in nondimensional form as

$$M_r = M_{i(i-1)} + M_{ij} = \left[K_{i(i-1)} \frac{EI_{i(i-1)}}{L_{i(i-1)}M_{pci}} + K_{ij} \frac{EI_{ij}}{L_{ij}M_{pci}}\right] \theta_i M_{pci} \quad (13)$$

in which $M_{i(i-1)}$ and M_{ij} are the moments at i for beams $i(i-1)$ and ij, respectively, and $K_{i(i-1)}$ and K_{ij} are the initial restraint coefficients for the same beams. Also $I_{i(i-1)}$ and I_{ij} are the moments of inertia of beams $i(i-1)$ and ij; θ_i is the rotation of joint i and E is the modulus of elasticity. Also M_{pci} is the reduced plastic moment capacity of the restrained column at joint i corresponding to the axial load ratio P/P_y of column i. Since $M_r = k\theta M_{pc}$, then

$$k_i = K_{i(i-1)} \frac{EI_{i(i-1)}}{L_{i(i-1)}M_{pci}} + K_{ij} \frac{EI_{ij}}{L_{ij}M_{pc}} \quad (14)$$

A good approximation for the initial elastic value of K_{ij} can be obtained by simplifying the one-story assemblage to just those members shown in Figure 11(b):

$$K_{ij} = 6\left[\frac{3 + 0.5\beta + \eta + \frac{\alpha'}{12}K_{i(i-1)}}{3 - 0.5\alpha + \beta + 1.5\eta}\right] \quad (15)$$

where

$$\alpha = \frac{hI_{ij}}{L_{ij}I_i} \qquad \alpha' = \frac{hI_{i(i-1)}}{L_{i(i-1)}I_i}$$

$$\beta = \frac{hI_{ij}}{L_{ij}I_j} \qquad \eta = \frac{hI_{j(j+1)}}{L_{j(j+1)}I_j}$$

The initial elastic restraint to the left of joint j [Fig. 11(a)] K_{ji} is related to K_{ij} as follows:

$$K_{ji} = 4\left[\frac{K_{ij} - 3}{K_{ij} - 4}\right] \quad (16)$$

Similarly

$$K_{i(i-1)} - 4\left[\frac{K_{(i-1)i} - 3}{K_{(i-1)i} - 4}\right] \quad (17)$$

where joint i is an interior joint.

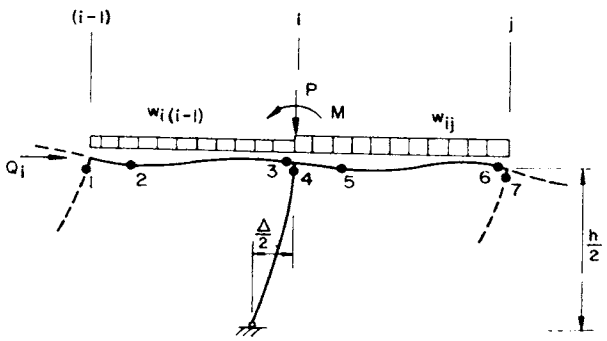

FIGURE 12. Possible plastic hinge locations

3.2 Reduced Restraint

As the lateral shear force, ΣQ on a one-story assemblage increases the successive formation of plastic hinges in the beams and columns will reduce the restraint stiffness at the top of each restrained column. Figure 12 shows the locations of the possible plastic hinges within an interior subassemblage. Referring to the numbered locations of plastic hinges shown in Figure 12, and assuming that hinges 3 and 6 will form before hinges 2 and 5, respectively, the reduced values of restraint, k_i, can be determined from the following:

1. *1 occurs before 3:* Since additional moment cannot be developed at joint $(i-1)$, beam $i(i-1)$ may be considered pinned at $(i-1)$. Thus $K_{i(i-1)}$ reduces to 3.0.
2. *3 occurs after 1:* $K_{i(i-1)}$ reduces from 3.0 to 0.
3. *3 occurs before 1:* $K_{i(i-1)}$ reduces to zero.
4. *6 or 7 occurs:* K_{ij} reduces to 3.0.
5. *5 occurs after 6 or 7:* K_{ij} reduces from 3.0 to 0.
6. *4 occurs:* $K_{i(i-1)}$ and K_{ij} remain unchanged from their values at the time 4 develops.

4. Summary and Conclusions

A second-order elastic-plastic method of analysis has been described in this paper which can be used to perform a plastic analysis of one-story assemblages under combined gravity and lateral loads. If the one-story assemblage is taken from a region of an unbraced multistory frame where the columns can be expected to be in nearly symmetrical double curvature under the combined loads, then the load-drift curve of the story is closely approximated by that of the one-story assemblage. Although beyond the scope of this report, the method can be extended to handle conditions where the column inflection points are shifted from mid-story height.

The method of analysis is based on the concepts of restrained columns and subassemblages and uses directly the results of previous research on restrained columns permitted to sway. The analysis of one-story assemblages can be carried out either manually, with the aid of specially prepared design charts, or by computer.

The plastic subassemblage method provides a key element opening the way to plastic design of unbraced multi-story rigid steel frames (8). A design example is presented in Part 4 of the Bulletin. The analytical and experimental results presented in this Bulletin are recommended for careful study by steel frame designers and specification committees.

5. References

1. Daniels, J. H., and Lu, L. W., "Plastic Subassemblage Analysis for Unbraced Frames," *Journal of the Structural Division*, ASCE, Vol. 98, ST 8, Proc. Paper 9148, August, 1972.
2. Daniels, J. H., "Combined Load Analysis of Unbraced Frames," Ph.D. Dissertation, Lehigh University, 1967, University Microfilm, Inc., Ann Arbor, Mich.
3. Daniels, J. H., and Lu, L. W., "Design Charts for the Sway Subassemblage Method of Designing Unbraced Multi-Story Frames," Report No. 273.54, Fritz Engineering Laboratory, Lehigh University, Dec. 1966.
4. Levi, V., Driscoll, G. C., Jr., and Lu, L. W., "Analysis of Restrained Columns Permitted to Sway," *Journal of the Structural Division, ASCE*, Vol. 13, ST1, Proc. Paper 5092, Feb. 1967.
5. Driscoll, G. C. Jr., et al., "Plastic Design of Multistory Frames Lecture Notes," Report No. 273.20, Fritz Engineering Laboratory, Lehigh University, Sept. 1965.
6. Parikh, B. P., Daniels, J. H., and Lu, L. W., "Plastic Design of Multistory Frames- Design Aids," Report No. 273.24, Fritz Engineering Laboratory, Lehigh University, Sept. 1965.
7. *Plastic Design in Steel (A Guide and Commentary)*, American Society of Civil Engineers Manual of Engineering Practice, No. 41, 2nd Edition, 1970.
8. Driscoll, G. C., Jr., Armacost, J. O., III, and Hansell, W. C., "Plastic Design of Multistory Frames by Computer," *Journal of the Structural Division, ASCE*, Vol. 96, ST1, Jan. 1970.

Experiments on Restrained Columns Permitted to Sway

by

S. W. KIM and J. HARTLEY DANIELS

ACKNOWLEDGMENTS

The work reported herein was performed at the Fritz Engineering Laboratory, Department of Civil Engineering, Lehigh University. Dr. David A. VanHorn is the Chairman of the Civil Engineering Department and Dr. Lynn S. Beedle is Director of the Fritz Engineering Laboratory. The results presented form part of a general investigation in "Strength of Beam-and-Column Subassemblages in Unbraced Multistory Frames." Sponsorship of the program was provided by the Committees of Structural Steel Producers and Steel Plate Producers, American Iron and Steel Institute. Technical guidance was provided by the Task Force on AISI Project 150, consisting of W. C. Hansell (Chairman), R. G. Dean, I. M. Hooper, F. R. Khan, E. O. Pfrang and I. M. Viest (Project Supervisor). The authors are grateful for the guidance and assistance of the Task Force.

The authors gratefully acknowledge the assistance of Dr. L. W. Lu, Director of the Plastic Analysis Division and Messrs. H. Yoshida and L. D. Carpenter, who gave unvaluable suggestions in planning the tests and their help during testing. The work of Kenneth R. Harpel and the technicians in setting up the tests is gratefully appreciated. Thanks are due also to Miss Karen Philbin who typed the report and Mr. John Gera who prepared the drawings.

CONTENTS

ABSTRACT

Experiments were conducted on full-scale restrained columns permitted to sway in order to study their lateral-load vs. drift behavior with a variable rotational restraint stiffness. These tests also provided experimental verification of some aspects of the sway subassemblage method of analysis. Three restrained columns were tested, simulating the restrained columns in a windward, an interior and a leeward sway subassemblage. The column axial load ratio for all the restrained columns was maintained constant at 0.7. Each test specimen consisted of one column and one or two restraining beams welded to the column. The rotational restraint stiffness of restrained column varied during the test due to the formation of a plastic hinge. The test results show good agreement with the predictions from restrained column theory.

1. Introduction

In the sway subassemblage method of analysis a one-story assemblage [Fig. 1(a)] at level n is subdivided into sway subassemblages as shown in Figure 1(b). Each sway subassemblage consists of a restrained column, which is permitted to sway, together with the adjacent restraining beams. A spring at each end of the restraining beams represents the rotational restraint offered by the members outside a sway subassemblage. The columns above level n are replaced by the equivalent joint forces where, conservatively it is assumed that $\Sigma H_{n-1} = \Sigma H_n$ [Fig. 1(a)]. The behavior of a sway subassemblage is then described by the behavior of a restrained column at level n, which is subjected to the forces shown in Figure 2. The behavior of a one-story assemblage is determined by suitably combining the individual behavior of the sway subassemblages, each one containing a restrained column (1–3). The behavior of a restrained column can be determined either manually with the aid of prepared charts, or by computer (1, 4–6).

A numerical method of analysis for restrained columns having any type of rotational and lateral restraints and subjected to any combination of external moments and forces was first presented by Levi (7). The restrained column shown in Figure 2 is a special case of the general restrained column problem. This column, of height $h/2$, is pinned at the lower end, and subjected at the upper end to constant axial load P_n, variable lateral load Q_n, variable joint moment M_n and a restraining moment which is a function of a variable rotational restraint stiffness k. The variation of the rotational restraint stiffness results from the formation of plastic hinges in the restraining beams.

This report presents the results of an experimental investigation of three restrained columns permitted to sway. This is the first phase of a two-phase experimental program to investigate the behavior of restrained columns and one-story assemblages. Each restrained column consisted

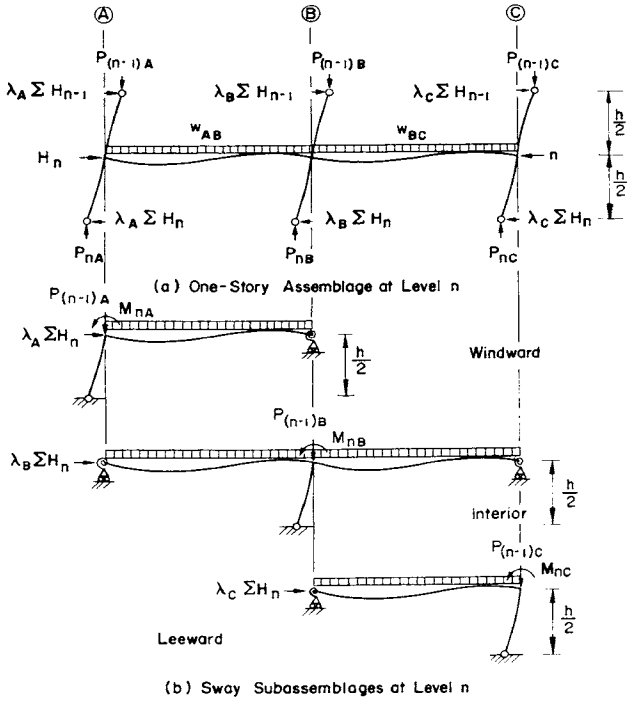

FIGURE 1. One-story assemblage and sway subassemblages at level n

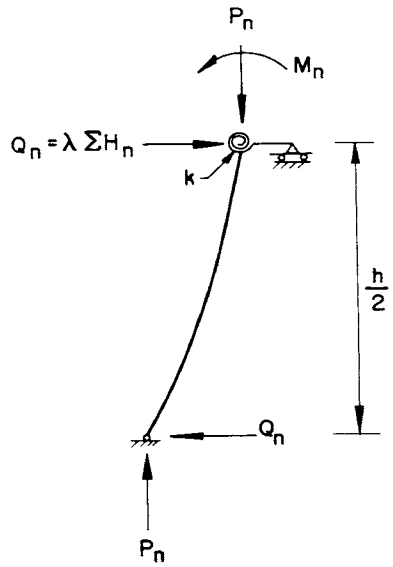

FIGURE 2. Restrained column permitted to sway

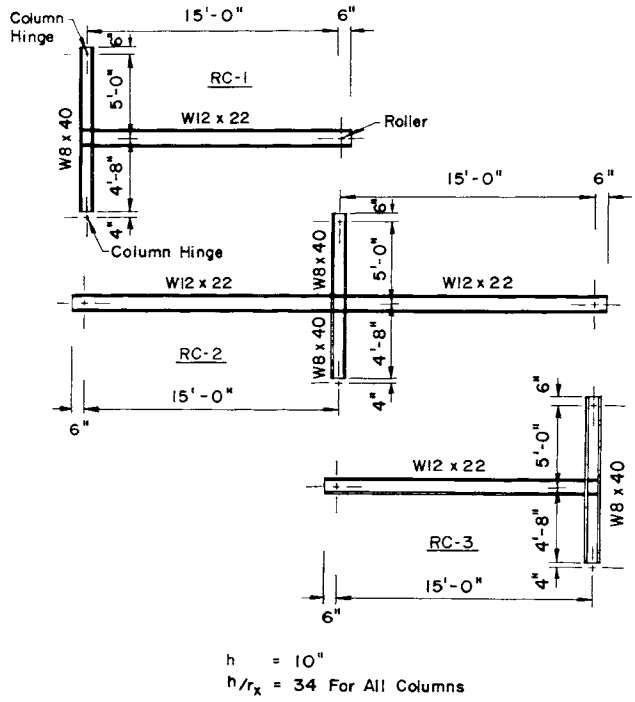

FIGURE 3. Test specimen details

of a column 10 ft long with either one or two restraining beams 15 ft long welded to column flanges at midheight of the column. The three restrained columns therefore simulated restrained columns in windward, interior or leeward sway subassemblages as shown in Figures 1 and 3. The restrained columns were tested under nonproportional loading. The total gravity loads applied to the beams and columns were maintained constant. The lateral load was applied to the top of the column using a horizontal screw jack. The data obtained from the tests was reduced to determine all stress resultants and deformations. The load-drift behavior was compared to predictions from restrained column theory.

In two of the tests, a variable restraint stiffness was obtained by ensuring that a plastic hinge developed in the restraining beam before the attainment of the stability limit load. The column axial load ratio for all the restrained columns was maintained constant at 0.7. This value was chosen to maximize the $P\Delta$ effects and to include the effects of residual stresses in the columns at every stage of loading. The assumption implied in using such a high axial load is that if reasonably good correlation with restrained column theory is obtained with such loads, excellent agreement should be obtained at much smaller loads.

Each restrained column was subjected to approximately two cycles of reversed loading to fairly large values of drift following the initial tests discussed above. These results are not presented in this report.

Nomenclature

A = area of cross section
b = flange width
d = depth
H = horizontal wind load
h = story height
I_x = moment of inertia about major axis
k = restraint stiffness
M = bending moment
M_B = bending moment at joint computed from measured beam strains
M_C = bending moment on beam at column face
M_D = bending moment on beam at a depth of beam away from column face
M_f = bending moment on beam under load point
M_L = bending moment at joint computed from measured strain of upper column
M_p = plastic moment capacity of cross section
M_{pc} = reduced plastic moment capacity considering axial load
M_u = bending moment at joint computed from measured strains of restrained column
n = level
P = axial force in column
P_y = axial yield load of cross section
Q = horizontal force
r_x = radius of gyration about major axis
t = flange thickness
w = web thickness
Z_x = plastic section modulus about major axis
Δ = relative lateral deflection of two consecutive stories
$\Delta/2$ = joint deflection
δ = axial deformation
ϵ_y = yield strain
λ = distribution factor of shear
σ_y = static yield stress level

2. Experiment Design

Each test specimen consisted of one or two restraining beams welded to a column as shown in Figure 3. The restrained column (lower half of each column in Fig. 3) in each test specimen was designed to represent a restrained column in either a windward, an interior, or a leeward sway subassemblage [see Fig. 1(b)]. In order to provide more or less realistic geometry, rotational restraint stiffness and column slenderness ratios, the test specimens were designed to represent part of a one-story assemblage with two 15-ft bays and a 10-ft story height. A column slenderness ratio of approximately 40 for all three speci-

mens was chosen to represent the maximum slenderness ratio found in the middle and lower stories of an unbraced frame. A W8×40 section was selected for all columns and a W12×22 section for all beams. The ratio of strong axis moments of inertia for the sections is also typical of that found in the middle and lower stories of an unbraced frame. The dimensions of the three specimens, RC-1, RC-2 and RC-3, are shown in Figure 3.

It is very difficult experimentally to provide a rotational restraint at the free end of a restraining beam, as required by sway subassemblage theory. Therefore, it was decided to test restrained columns with pin ended restraining beams (8). In effect, these restrained column tests thus represent the tests of sway subassemblages after a plastic hinge has formed at the far end of a restraining beam. The results of the restrained column tests can be used to predict the experimental behavior of sway subassemblages with realistic boundary conditions imposed.

In order to obtain considerable plastification of the columns and to explore the effect of column residual stresses on the experimental results, it was decided to use a high value of the column axial load ratio P/P_y, where P is the applied column load and P_y the yield load. The axial load ratio for each restrained column was arbitrarily chosen as 0.7. No attempt was made to relate the experiment design to a set of probable working loads, load factors and bent spacings for a frame containing the assumed one-story assemblage mentioned before. An analysis of the restrained columns indicated that the variation in the axial load ratio for each restrained column during testing would be insignificant. It was therefore decided that the vertical column load which was computed to give an axial load ratio of 0.7 at the start of each test would be maintained constant throughout the test.

The vertical beam loads were applied approximately at the quarter points in order to accommodate the available gravity load simulators (9). These loads were to be maintained constant and at magnitudes that would ensure the formation of plastic hinges at the desired locations as follows: For specimen RC-1, a plastic hinge was expected to occur in the restraining beam under the load point nearest the column, shown in Figure 4. For RC-2, the first plastic hinge was expected to occur in the restraining beam at the column face with the second plastic hinge at the top of the restrained column. The plastic hinge in RC-3 was expected to form at the top of the restrained column. The constant values of vertical column and beam loads are shown in Figure 4. These values were determined on the basis of the measured yield stress level of the materials.

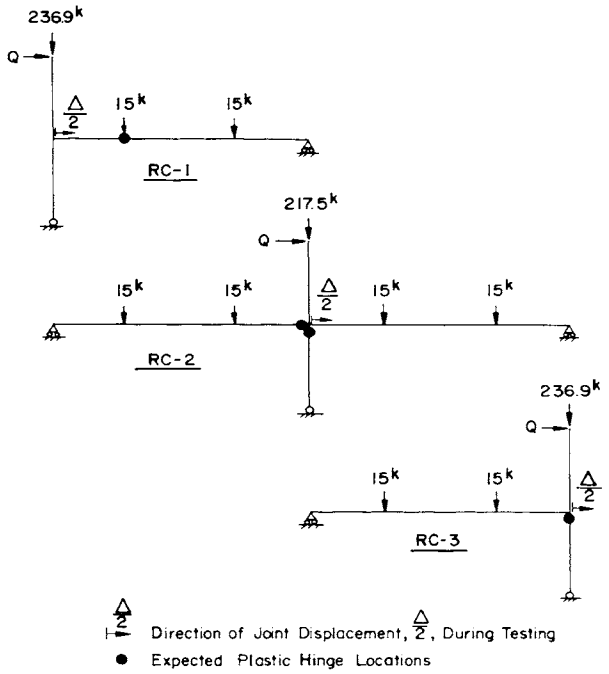

FIGURE 4. Loading and expected plastic hinge locations for each test specimen

Each restrained column was designed to be displaced horizontally during testing in the direction shown in Figure 4. The primary behavior to be determined from each test was the relationship between the resulting lateral force Q at the top of the upper column and the drift $\Delta/2$ at the top of the restrained column (joint). In the zero-sway position an initial value of horizontal load Q was required to maintain equilibrium of the test specimen. For specimen RC-1, Q was initially −5.68 kips. For specimen RC-3, Q was initially +5.68 kips. Due to symmetry of geometry and loading, no initial horizontal load was required for RC-2.

3. Mechanical and Cross-Section Properties

A number of control tests were performed on the materials used for the test specimens. The purpose of these control tests was to determine the material properties and geometry of the sections used.

3.1 Tensile Coupon Tests

ASTM A36 rolled steel was used for all test specimens. The chemical composition and mill test results, as furnished by the manufacturer,

TABLE I. Chemical Composition and Mill Tests Results

Section	Chemical Composition (%)				Mechanical Property		
	C	Mn	P	S	Yield Point (ksi)	Tensile Strength (ksi)	Elongation (8 in.) (%)
W12×22	0.18	0.63	0.010	0.036	47.3	67.5	29.5
W8×40	0.20	0.56	0.014	0.034	51.0	68.4	22.9

are given in Table I. Nine tensile coupons, five from the flanges and four from the web, were tested from the W12×22 beam section. For the W8×40 column section, eight tension tests, (five from flanges and three from web) were performed. The average of the flange and web static yield stress levels for each section are given in Table II, along with the ultimate stress attained and the percent elongations.

TABLE II. Summary of Tension Tests

		Static Yield Stress (ksi)	Ultimate Stress (ksi)	Elongation (8 in.) (%)
W12×22	Web	38.5	62.7	29.0
	Flange	33.6	59.5	30.3
W8×40	Web	33.3	61.0	30.2
	Flange	32.2	60.7	31.0

3.2 Residual Stress Measurement

One residual strain measurement was performed on the W8×40 section used for the columns of the test specimens. The residual stresses were determined by the method of sectioning. The calculated residual stresses are shown in Figure 5.

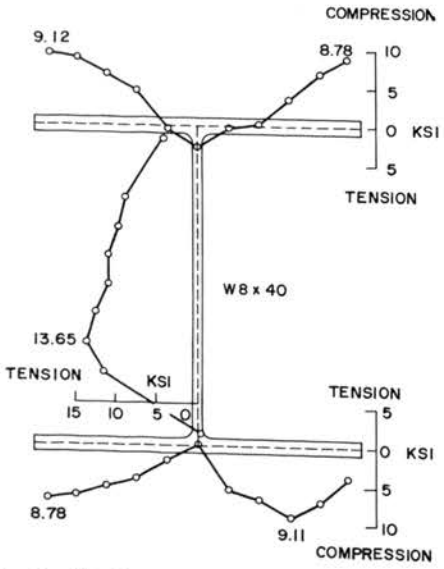

FIGURE 5. Residual stress distribution

The average residual stress at the flange tips was 7.5 ksi or $0.23\sigma_y$. The residual stress distribution obtained was typical for a cross-section which is cold-straightened by gagging.

3.3 Stub Column Test

One stub column test was performed on the W8×40 section to determine the axial yield load, P_y. The load-deformation relationship obtained in the test is given in Figure 6. The value of P_y obtained from the stub column test was about 370 kips, which resulted in an average static yield stress of 32.1 ksi. The value of P_y calculated from the measured cross-sectional area of the section (Article 3.4) and the yield stress levels of the flanges and web as shown in Table II was 367 kips. The two values of P_y are in very good agreement. For all the theoretical computations, the calculated value of P_y (367 kips) was used.

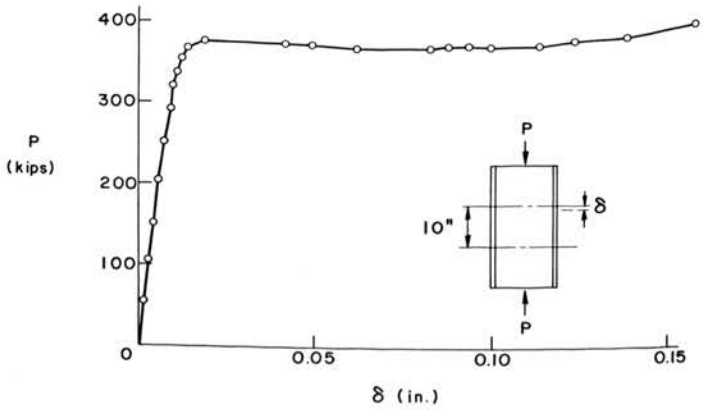

FIGURE 6. Load deformation curve from stub column test

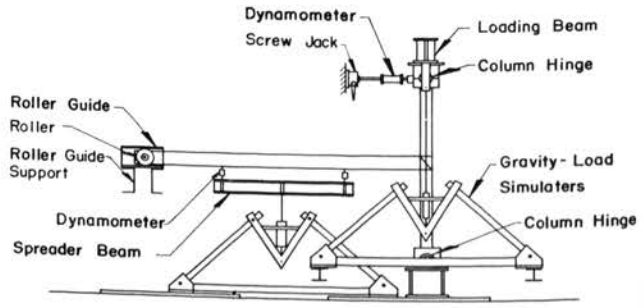

FIGURE 7. Schematic sketch of test setup for test specimens RC-1 and RC-3

TABLE III. Average Section Properties

Section		d (in.)	b (in.)	t (in.)	w (in.)	A (in.^{2})	I_x (in.^{4})	Z_x (in.^{3})	M_p (kip-in.)	P_y (kips)
W12×22	Handbook	12.31	4.03	0.424	0.260	6.47	156	29.3	1060*	—
	Measured	12.35	4.04	0.412	0.266	6.41	153.1	28.8	1020	—
W8×40	Handbook	8.25	8.08	0.558	0.365	11.8	146	39.8	1435*	423*
	Measured	8.28	8.09	0.536	0.366	11.32	141.8	38.4	1240	367

* Yield stress taken as 36 ksi.

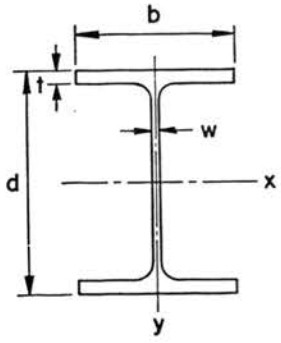

3.4 Cross-Section Measurement

The cross-section dimensions of each shape were measured at various locations along the length of each beam and column using micrometers and calipers. Measurements of web thickness were taken only at the cut ends of each length. The average measured sectional properties are given in Table III, and compared with the corresponding handbook values. There were no large differences between the measured and handbook properties. The measured values were used to determine the area, A, the moment inertia, I_x, and the plastic section modulus, Z_x, for each shape. The calculated plastic moment capacities of the W12×22 and W8×40 sections were 1020 and 1240 k-in., respectively. This compares with the nominal values of 1060 and 1435 k-in., based on handbook properties.

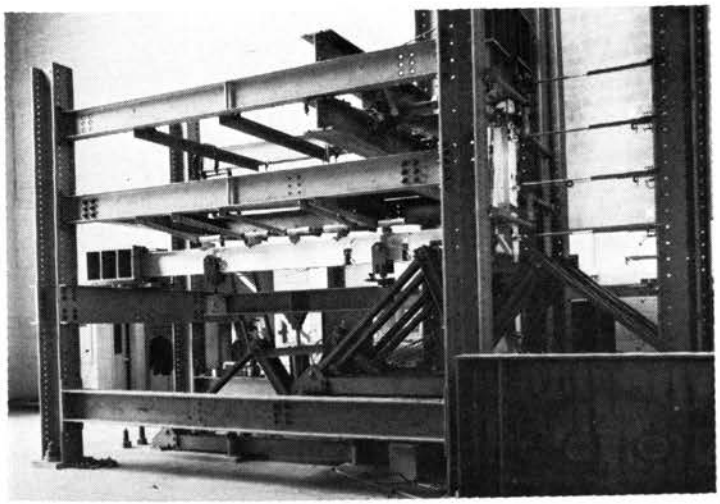

FIGURE 8. Overall view of test setup for test specimens RC-1 and RC-3

4. Test Setup and Procedure

4.1 General

Two different types of test setups were used, one for tests RC-1 and RC-3, and the other for test RC-2. Overall views of the test setups for RC-1 and RC-3 are shown in Figures 7 and 8. Similarly, Figures 9 and 10 show the test set-up for test RC-2.

In the tests, the top and the bottom ends of the columns were hinged. Figure 11 shows a typical view of the column hinge and hinge support detail used in the tests. A large roller bearing was used to ensure that there would be no bending moments at the ends of the columns.

The restraining beams were fully welded to the column flanges at one end using standard welding procedures. The other end of each beam was supported by rollers positioned on either side of the beam. The rollers were free to rotate on large

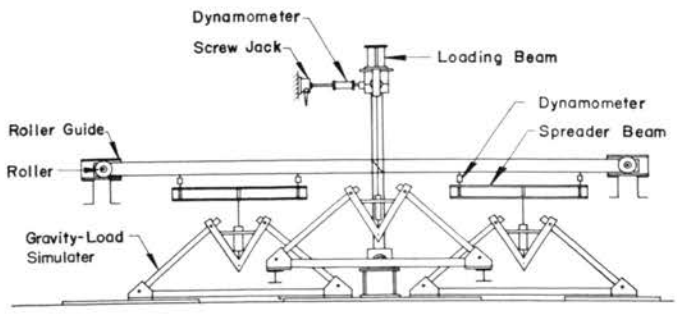

FIGURE 9. Schematic sketch of test setup for test specimen RC-2

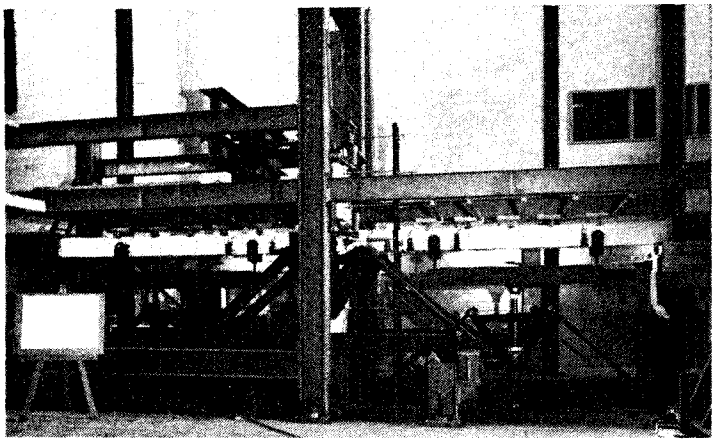

FIGURE 10. Overall view of test setup for test specimen RC-2

roller bearings mounted on a shaft welded perpendicular to the web of the beam. Each roller was free to move horizontally in a roller guide which provided vertical support and alignment of the end of the beam. Schematic views of the rollers and roller guides are shown in Figures 7 and 9. Figure 12 shows a typical end view of a beam together with the rollers and the roller guides. By using this beam support system, the end of a restraining beam could be moved horizontally without restraint, while maintaining the same span length, regardless of the horizontal deflection of the column.

Planar motion of each test specimen under load was ensured by means of lateral bracing perpendicular to the plane of the test specimen as shown in Figure 13 (9). The bracing system used prevented lateral and torsional movement of the beam but did not offer restraint to inplane deformation. The braces were placed at the locations recommended for use in plastic design (10).

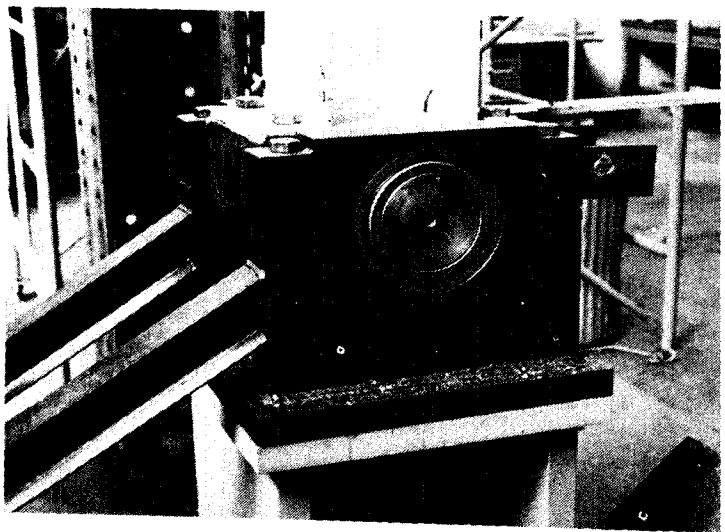

FIGURE 11. Column hinge and hinge support detail

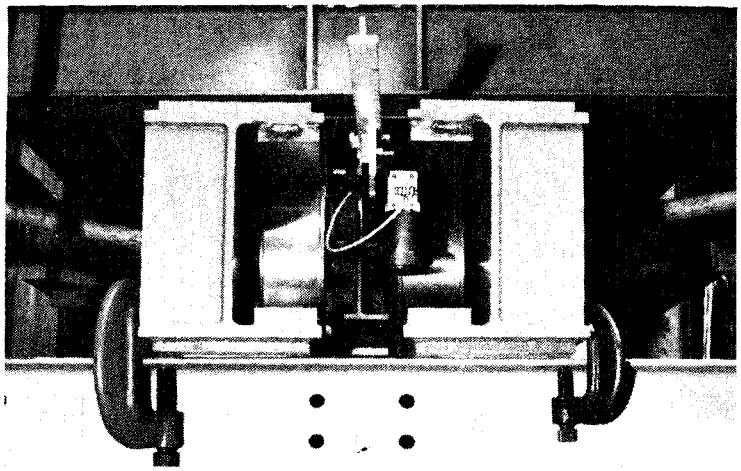

FIGURE 12. Rollers and roller guides at exterior end of beam

Five braces were used for each beam as shown in the figure. The columns were braced using the same type of bracing members. They were located at the level of the restraining beam and at each column top. All braces were in turn attached to an independent supporting frame.

4.2 Load Application

The column axial loads were applied to the tops of the columns through a beam which was connected to the tension jacks of four gravity load simulators (9). The gravity load simulators were symmetrically placed in pairs on either side of a column as shown in Figure 14. Thus the applied column loads remained vertical throughout each test. In order to transmit the large loads from the tension jacks to the column top, a substantial loading beam was fabricated. The loading beam was mounted on the column hinge and hinge support assemblage at the top of a column. Weak axis bending was eliminated by aligning the loading beam to ensure axial distribution of the load.

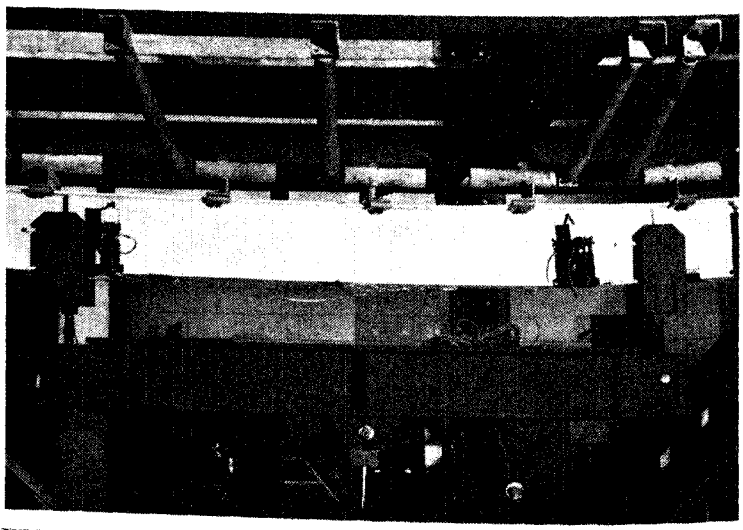

FIGURE 13. Lateral bracing system for the restraining beams

Four tension rods were used to connect the tension jacks of the simulators to the loading beam and were calibrated to determine the load from each jack. The four calibrated rods are also shown in Figure 14. A common hydraulic line was connected to each of the four tension jacks to maintain as nearly as possible the same load on each jack.

Vertical loads were applied approximately at the quarter points of each restraining beam through a spreader beam which was attached at its midpoint to the tension jack of a gravity load simulator as shown in Figure 13. Dynamometers were used to connect the spreader beam to the test specimen and also to measure the applied loads. In test RC-2, the tension jacks of two simulators which were used to apply the vertical beam loads were connected to a common hydraulic line.

The horizontal displacement of the column top was controlled by a screw jack mounted horizontally as shown in Figure 15. The jack was pin connected to the column top through a dynamometer to measure the horizontal load applied by the jack. The jack was also pin connected to an independent supporting frame.

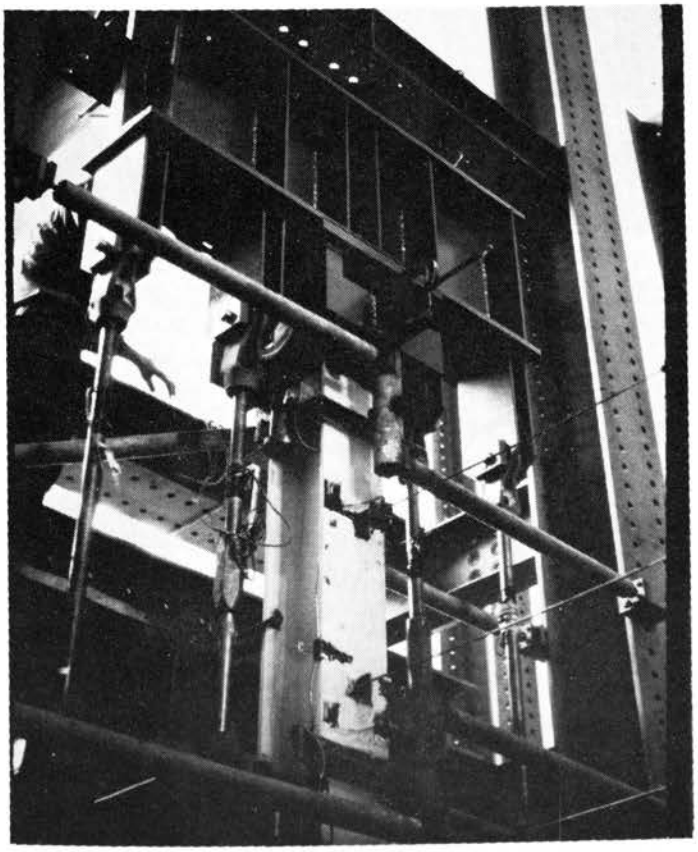

FIGURE 14. Loading beam used to apply vertical load to column top

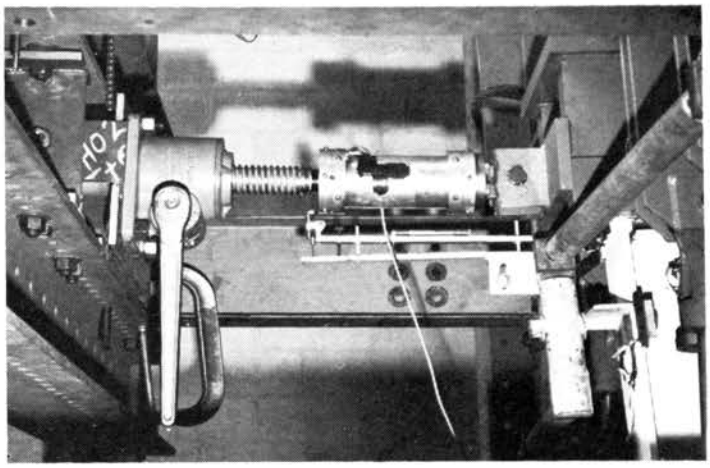

FIGURE 15. Horizontal screw jack used to displace column tops

4.3 Instrumentation

The instrumentation used for each test setup was designed to obtain strain data which could be used to monitor the applied loads, to determine overall deformations and to calculate the internal stress resultants in each test specimen. Strains in the beams and columns were measured using SR-4 electrical resistance strain gages. Four strain gages were used at each instrumented cross-section so that the axial face and bending moment at the cross-section could be calculated. Four cross-sections were gaged on each column and six cross-sections were gaged on each beam as shown in Figure 16.

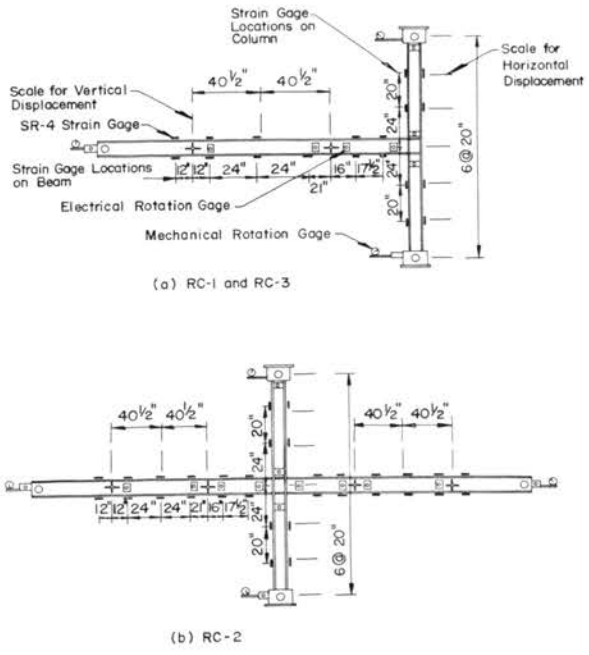

FIGURE 16. Location of electrical strain gages for each test specimen

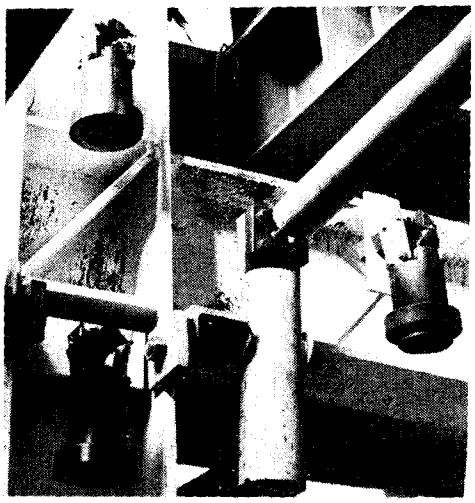

(a) Electrical Rotation Gage

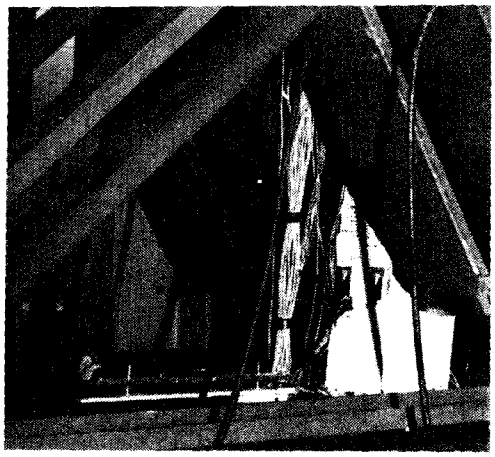

(b) Mechanical Rotation Gage

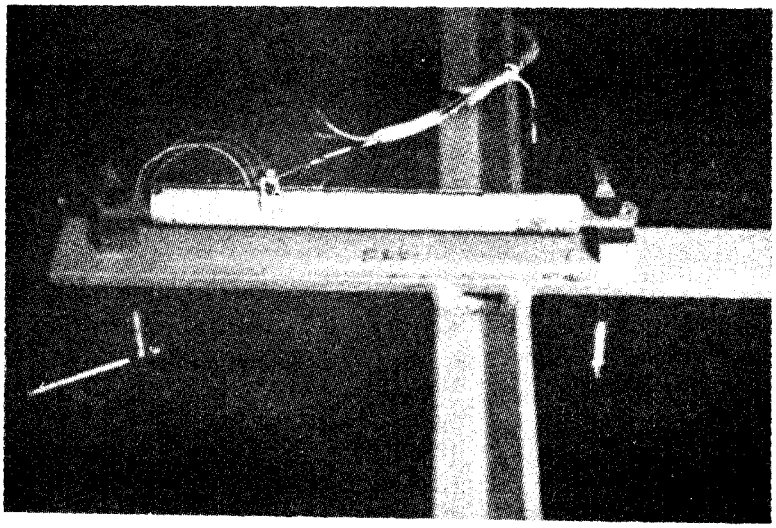

(c) Electrical Displacement Gage

FIGURE 17. Rotation and deflection measuring devices

A transit was used to measure the horizontal movements of the columns by reading scales attached to an outside face of each column at the locations shown in Figure 16. The vertical movements of the beams were also measured by taking level readings on scales positioned as shown in Figure 16. In addition to the direct readings from scales, electrical displacement gages were also used to measure the vertical and horizontal displacements of the beams and columns. A typical electrical displacement gage used in the tests is shown in Figure 17(c).

Rotations were measured using both electrical and mechanical rotation gages as shown in Figures 17(a) and (b). Electrical rotation gages were placed at the top and bottom of each column, at the beam-to-column connections, at locations of potential plastic hinges and at the exterior end of each beam. Mechanical rotation gages were placed at the top and bottom of each column and at the exterior end of each beam to check the readings from the electrical rotation gages at those locations. The locations of rotational gages are also shown in Figure 16.

Each test specimen was whitewashed prior to testing in order to observe the progression of yielding. All readings from SR-4 strain gages, electrical rotation gages and electrical displacement gages were read by a multichannel strain gage recording system and punched automatically onto computer cards. This procedure allows a systematic data reduction to be performed later using a computer program.

4.4 Alignment Procedure

Each column was first placed on its pin-base support (Fig. 11) and aligned with a transit to

ensure that it was plumb. Each restraining beam was also aligned with a plumb line and a carpenter's level to ensure that it was in the correction position. The roller guides at the exterior end of each beam were also aligned so that they were parallel to the beam and horizontal. After all alignment was complete each beam was welded to the column. Then all lateral braces were attached.

After setting up each test specimen, it was necessary to adjust the loading beam at the column top to eliminate the eccentricity of the axial load. Using standard stub-column test procedures strain readings were taken at several load levels. Based on the strain readings which were obtained, the position of the loading beam was adjusted to reduce the eccentricity of load. The tests did not proceed until the column load was applied with negligible eccentricity.

4.5 Test Procedure

At the start of each test, one half of the design column load and the design beam loads were simultaneously applied. The column load was then gradually increased to its full load while the beam loads were held constant. The resulting column and beam loads were maintained constant throughout each test. Before beginning each test, but after all vertical loads had been applied, the restrained column was plumbed by making a small in-plane displacement of the column top in order to reduce the deflection $\Delta/2$ at the center of the joint to zero. The lateral load at the column top required to maintain the test frame in this position was then recorded. This lateral load in addition to the vertical column and beam loads previously applied were as the initial test loads corresponding to zero drift of the restrained column. From this initial point the drift $\Delta/2$ of the joint was incremented using the horizontal jack at the column top. In test RC-1, the drift of the joint was incremented in approximately 0.1-in. intervals. Approximately 0.05-in. increments were used for RC-2 and RC-3. Readings of all the strain gages, dynamometers and rotation and deflection gages were recorded after each increment of displacement. When inelastic action was evident in the test specimen, all readings were taken after approximately a 10- to 15-min waiting period in order to allow the yielding process to stop and the specimen to come to static equilibrium.

Using the screw jack at the top of the column monotonically increasing drift $\Delta/2$, was applied to each restrained column until the joint displacement exceeded that corresponding to the stability limit load. This meant that for RC-1, the initial lateral load at the column top decreased at first with increasing lateral drift and then increased after the stability limit load was reached. For RC-2 and RC-3, the initial lateral load increased at first and then decreased following the stability limit load.

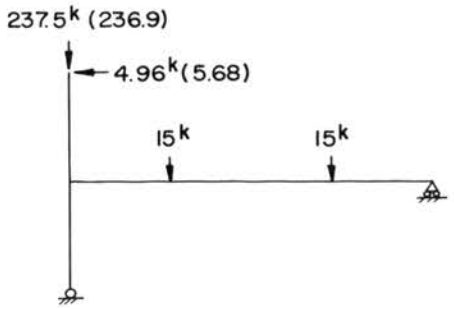

FIGURE 18. Loads on test specimen RC-1 at zero-swayed position

5. Test Results

5.1 Initial Moments

The theoretically calculated loads which were to be applied to each specimen at the start of each test are shown in Figure 4. However, the loads actually applied corresponding to zero-sway position were slightly different from the theoretical ones in tests RC-1 and RC-3. The loads applied to RC-1 and RC-3 are shown in Figures 18 and 19, respectively. The numbers in parentheses correspond to the theoretical values. The differences in the horizontal loads resulted from initial imperfection of the columns and the small misalignments during the test setups. In the presence of high axial loads in these tests, a slight imperfection or misalignment of a column results in a considerable change in the horizontal load. The differences in column axial loads were due to the small variation in oil pressure of the hydraulic jacks of gravity load simulators during the tests.

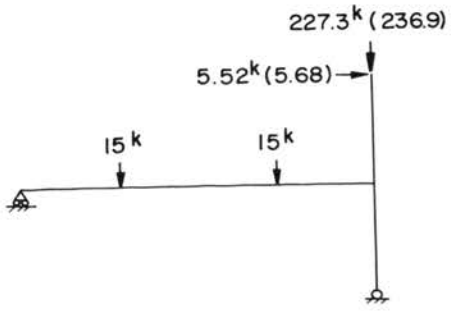

FIGURE 19. Loads on test specimen RC-3 at zero-swayed position

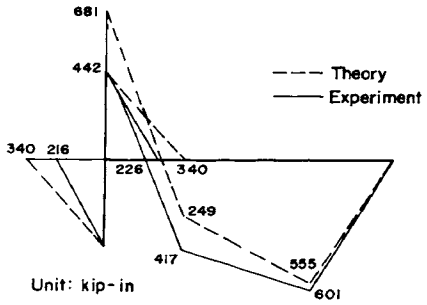

FIGURE 20. Moment diagram for test specimen RC-1 at zero-swayed position

The bending moment diagrams (plotted on tension sides of members) for three test specimens in the zero sway position are shown in Figures 20, 21 and 22. In the figures the dotted lines indicate the theoretical moment diagrams determined from the loads actually applied. The solid lines indicate the moment diagrams computed from measured strains. The differences between the theoretical and computed moment diagrams are fairly significant for specimens RC-1 and RC-2. The rather large difference between moment diagrams can arise from: (1) loads acting through initial imperfections in a specimen, (2) welding residual moments, (3) elastic shortening of the restrained column under axial loads, and (4) moments due to eccentricities of the column axial load with respect to the column centerline.

The analysis of the experimental data from test RC-1 indicated that there was a restraint coming from the roller guides at the exterior end of the beam. About 30% of the horizontal load in the zero-swayed position was being resisted in the roller guides. Therefore an important source for the large discrepancy between the moment diagrams for specimen RC-1 was the effect of the restraint in the roller guides. The restraint resulted from a small misalignment of the roller guides. In tests RC-2 and RC-3, this restraint was reduced considerably by aligning the roller guides much more carefully.

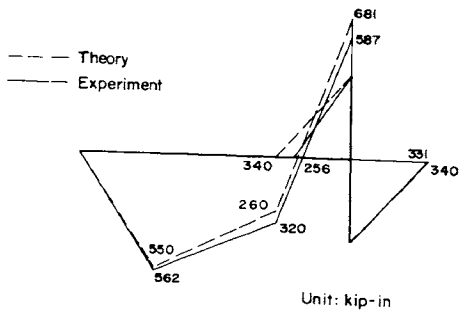

FIGURE 21. Moment diagram for test specimen RC-3 at zero-swayed position

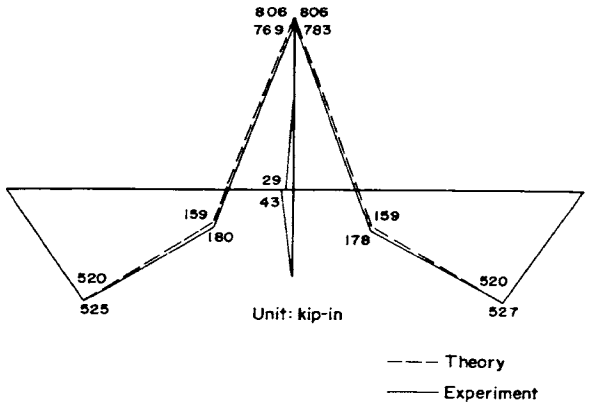

FIGURE 22. Moment diagram for test specimen RC-2 at zero-swayed postion

5.2 Experimental Behavior

The experimental behavior of the three test specimen will now be presented and discussed with reference to Figures 23–36. Theoretical comparisons and detailed analysis of test results is discussed in Chapter 6.

In each figure the load points corresponding to applying the initial increments of column axial load P and beam loads are not shown. The indentifying load numbers for each increment of the horizontal joint deflection $\Delta/2$ are shown on each experimental curve as the solid line in the figures. The theoretical predictions are shown by the dashed curves.

All the plotted points on the curves represent static equilibrium positions of the specimen. After passing the elastic range, the redistribution of strains in the regions loaded above the yield point was relatively slow. This redistribution of strains resulted in increases in horizontal joint deflections and a decrease in the horizontal jack load from the condition immediately after incrementing the joint deflection. The stabilization of the horizontal load monitored from the load cell at the top of the column was used to indicate when the redistribution of strains had essentially halted and static equilibrium had been attained.

5.2.1 Restrained Column The experimental horizontal-load vs. drift curve for test specimen RC-1 is shown in Figure 23. In the figure, the nondimensionalized horizontal load, $Qh/2M_{pc}$ and drift Δ/h are used, where M_{pc} is the reduced column plastic moment in the presence of axial load and h and Δ are shown in the figure.

In the zero-drift position, a few yield lines were present in both flanges of the column and distributed throughout the length. This was due to high axial load ratio used ($P/P_y = 0.7$) and the magnitude of residual stresses in the flanges (Fig.

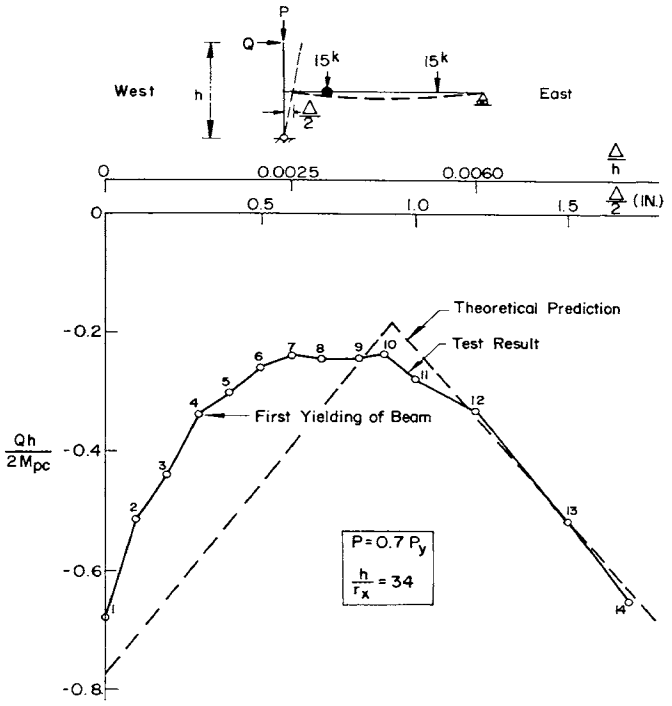

FIGURE 23. Load deflection curve for test specimen RC-1

5). However, there was no yielding observed in the beam. As previously shown in Figure 18, the initial value of Q was -4.96 kips. As the column top deflection was incremented in the direction of Q as shown in Figure 23, the absolute value of Q initially decreased.

At Load No. 4 in Figure 23, the top flange of the beam at the two load points started to yield. As the sway deflection increased, yielding was observed in both flanges. At Load No. 6, the web started to yield under the east load point where a plastic hinge was expected to form. At Load No. 8, the web yielding at the east load point had propagated to the center and the web at the west load point started to yield.

At Load No. 11 there were indications of lateral buckling of the beam, and at Load No. 12 definite lateral buckling was observed of the compression flange midway between the west load point and the center of the beam. Following Load No. 12 the horizontal load increased rapidly (in the direction opposite to the joint deflection) as the lateral buckling progressed. The observed lateral buckling was attributed to the movement of a brace near the buckled region, which might have been the result of slippage of the brace. At Load No. 14, the test was concluded and the specimen was then subjected to cyclic loading.

Figure 24 shows the deflected shape of test specimen RC-1 at a number of drift increments (the numbers on the shapes correspond to the load

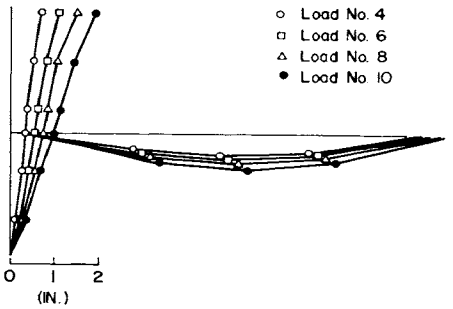

FIGURE 24. Deflections of test specimen RC-1

numbers in Fig. 23). Due to the effects of the extensive yielding of the beam in the region between two load points, a relatively large deflection of the beam was observed. The horizontal deflection of the column top was about twice that of the joint at each stage, as expected.

Figure 25 shows the variation in the axial load ratio of test specimen RC-1. There were no significant changes from the theoretically assumed value of $P/P_y = 0.7$.

The deformed specimen after the completion of cyclic testing is shown in Figure 26. The severe deformation and yielding on the beam and the column shown in the figure can be partially attributed to the cyclic test. However, similar deformation appeared but to a lesser extent during the test reported herein.

5.2.2 Restrained Column The nondimensionalized horizontal-load vs. drift curve obtained from the test is given in Figure 27. Because of the symmetry of the specimen and its vertical loads, there was no initial horizontal force in the zero sway position ($Q = 0$, $\Delta/h = 0$).

As in test RC-1, compression yield lines were observed on the flange tips of the column and were scattered throughout the length in the zero-drift position. At Load No. 4 severe yielding was observed in the flanges of the west beam adjacent to the column, where the first plastic hinge was expected to form. At Load No. 5 the yielding had progressed to the inside face of flanges but there was no apparent yielding on the web. From Load No. 6 the yielding of the west beam near the

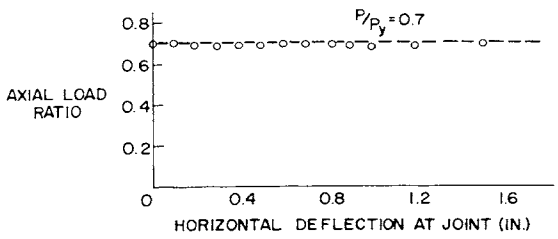

FIGURE 25. Variation in axial load ratio in test specimen RC-1

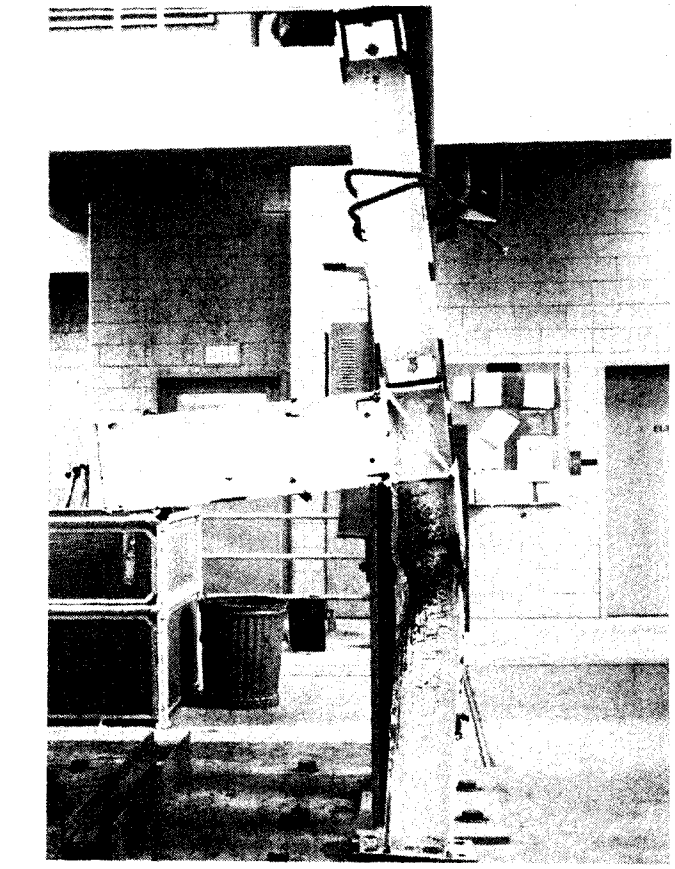

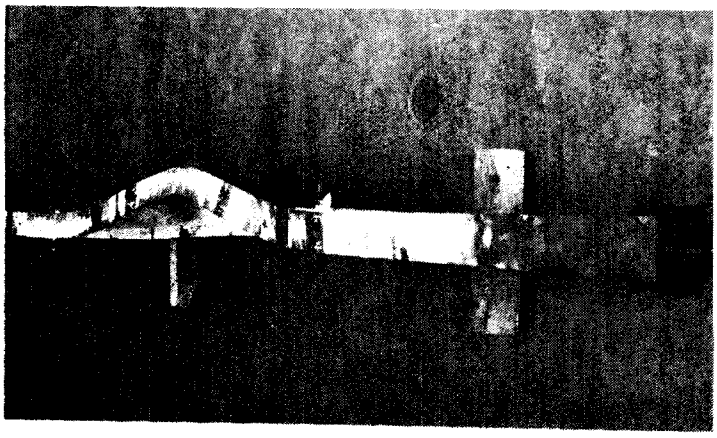

FIGURE 26. Deformed specimen after cyclic testing RC-1

joint progressed rather slowly as the drift increased. Up to Load No. 10, there was no pronounced indication of the formation of a plastic hinge in the west beam. At Load No. 11, the yielding had penetrated into the web of the beam. A significant amount of yielding was also observed in the west flange of the column just below the joint. At Load No. 13 the maximum horizontal load of 4.45 kips was attained. On further incrementing the deflection, the horizontal load started to drop rather slowly. At Load No. 16 the test was terminated.

The deflected shape of the beams and columns is plotted in Figure 28. The increase in column

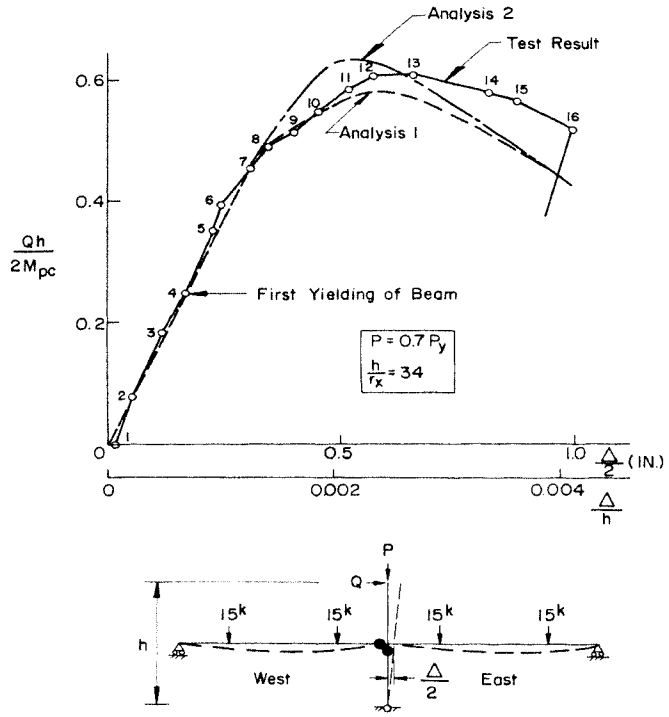

FIGURE 27. Load deflection curve for test specimen RC-2

deflection was almost linear in the elastic range However, as the moment at the top of the re strained column approached its reduced plasti moment value and considerable plastification o the column occurred in that region, a slight "kink' developed in the yielded zone and nonlinear de flections were then obtained. The column de flection below the joint was then observed to in crease with the increasing rate while the rate o deflection of the column above the joint reduced This behavior is to be expected and is a conse quence of the column hinge action.

Figure 29 shows the variation in axial load rati in the restrained column during the test. Th applied axial load ratios were slightly on the higl side.

The measured rotations near the joint wer plotted for each load number in Figure 30. Th locations of the rotation gages are as shown i Figure 30. The numbers on the plots correspon to the load numbers in Figure 27. Except fo the irregular rotation measured at Location 4

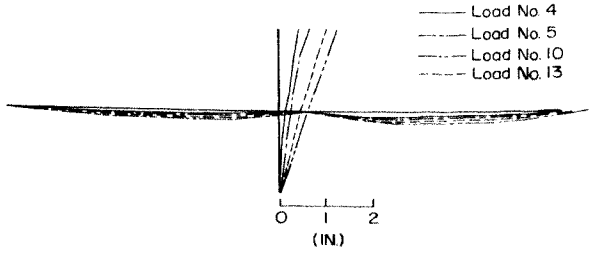

FIGURE 28. Deflections of test specimen RC-2

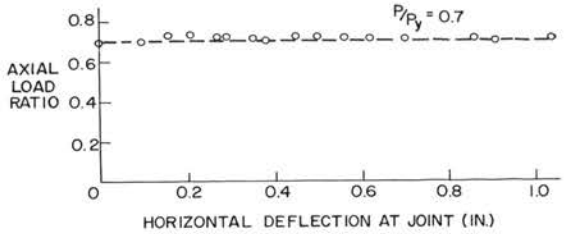

FIGURE 29. Variation in axial load ratio in test specimen RC-2

the curves confirm the previously described behavior of the specimen near the joint. Comparing the rotations at Locations 1 and 2, the difference in magnitudes becomes significant as the drift increases, due to the effects of the gradual plastification of the restrained column and the subsequent plastic hinge formation. Similar behavior is also observed in the rotations at Locations 3 and 4.

The specimen after cyclic testing is shown in Figure 31. The yielding of the restrained column has been amplified by the cyclic tests. It can be seen that there was little yielding of the beams.

5.2.3 Restrained Column RC-3 The nondimensionalized horizontal-load vs. drift curve for test specimen RC-3 is shown in Figure 32. The initial horizontal load at the zero-drift position was 5.52 kips and in the same direction as the imposed sway deflection. As in the previous tests, at zero drift compression yield lines developed in the flange tips of the column. At Load No. 2, the severe yielding progressed in the west flanges of the restrained column and throughout the length. At Load No. 3, the yielding penetrated into the web of the column, resulting in an extensive yielding of the west half of the restrained column near the connection.

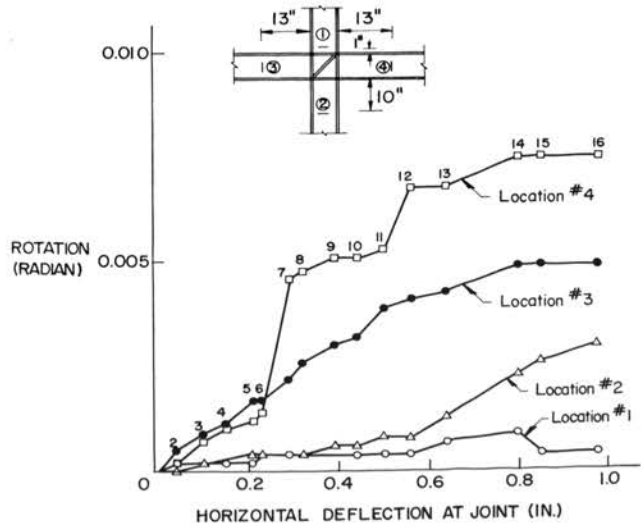

FIGURE 30. Rotations near joint in test specimen RC-2

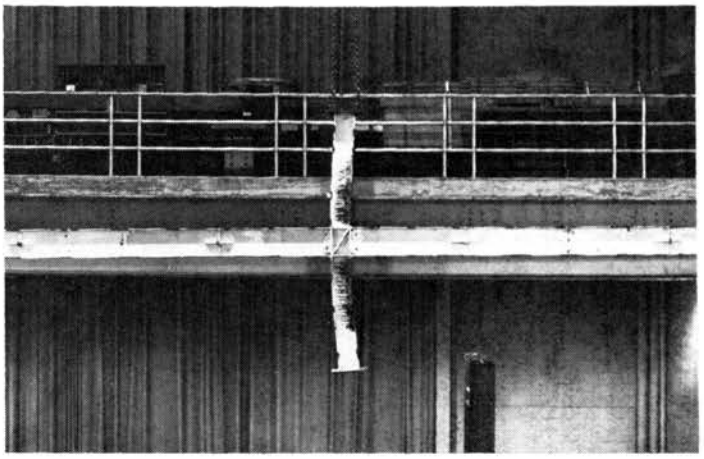

FIGURE 31. Deformed specimen after cyclic testing RC-2

On further loading the frame continued to deflect under the almost constant horizontal load. From Load No. 6 the horizontal load dropped slowly. At Load No. 8, the test was terminated.

The deflected shape of specimen RC-3 is shown in Figure 33. The nature of the column deformation was similar to that of RC-2. The kink near the top of the restraining column was even more distinct in this case. As the drift was increased after the formation of the column plastic hinge, the hinge action was so marked that there was almost no relative increase in deflection between the joint and the top of the column. Nearly all the deformations resulted

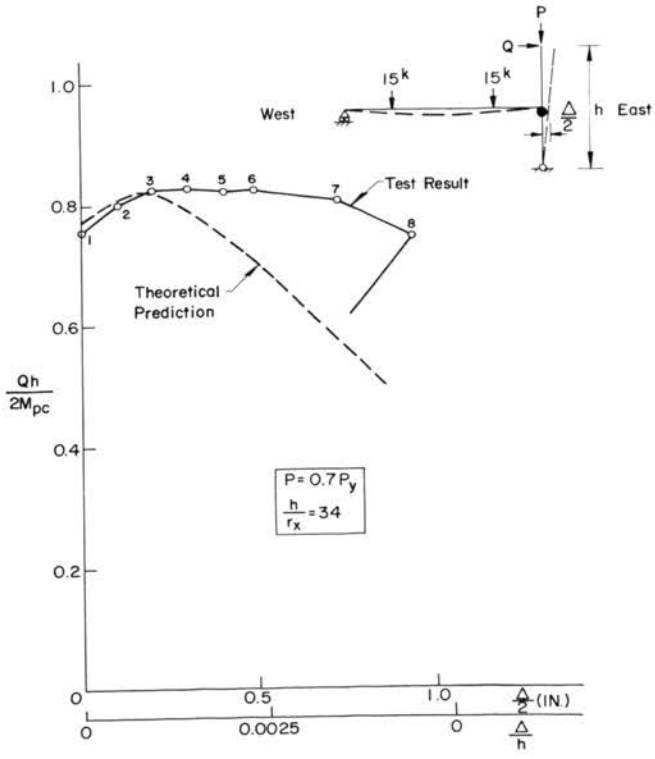

FIGURE 32. Load deflection curve for test specimen RC-3

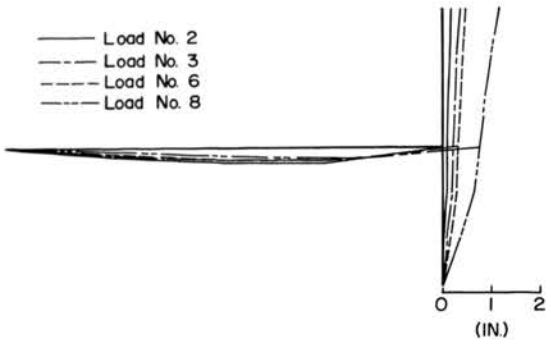

FIGURE 33. Deflections of test specimen RC-3

from the drift increment were concentrated in the plastic hinge region.

The variation in axial load during the test is plotted in Figure 34. The variation was rather scattered, compared with RC-1 and RC-2. However, the magnitude was not appreciably different from the theoretically assumed value of 0.7.

Figure 35 shows the measured rotations near the connection. The locations of the measuring gages are given in the figure.

The deformed specimen after cyclic testing is shown in Figure 36. The lateral buckling of the beam shown in the figure occurred during the cyclic loading. There was no indication of the lateral buckling during the test reported herein.

6. Theoretical Analysis and Discussion

6.1 Theoretical Prediction

The theoretical horizontal-load vs. drift curves for each of the restrained columns can be generated from restrained column theory (7) and sway subassemblage theory (1). The theoretical prediction curves for the three restrained columns are shown as the dashed lines in Figures 23, 27 and 32.

In the theoretical calculations, the column height was taken as the total distance between the pinned ends, which resulted in a strong axis slenderness ratio h/r_x of 34. The clear span of each beam (column face to roller support) was used in all calculations except when calculating the initial (zero-sway) bending moments in the test specimens. In this case, the distance between the

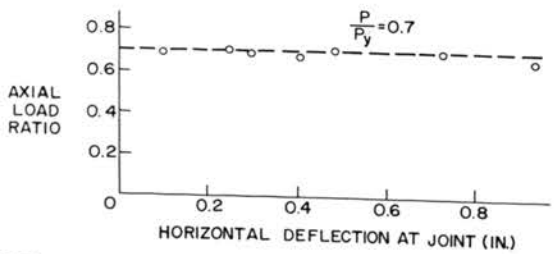

FIGURE 34. Variation in axial load ratio in test specimen RC-3

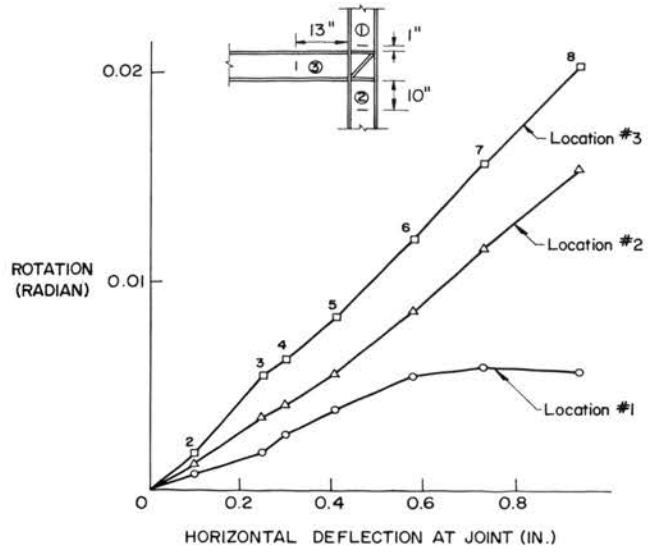

FIGURE 35. Rotations near joint in test specimen RC-3

column centerline and the roller support was used. Since a beam is able to form a plastic hinge adjacent to the face of a column, the effective length of the beam is assumed to be the clear span length. In calculating the theoretical prediction curves, an axial load ratio of $P/P_y = 0.70$ was used. In addition the measured yield stress levels of the steel were used. For residual stress distribution, the standard residual stress pattern was used (10).

6.2 Comparative Behavior

6.2.1 Restrained Column RC-1 The difference between the theoretical and experimental values of $Qh/2M_{pc}$ in Figure 23 in the zero-drift position can likely be attributed to the misalignment of the rollers as discussed in Chapter 5, as well as the initial out of straightness of the column. The horizontal force exerted by the rollers was observed to be present up to about Load No. 2 which could account for the marked difference in slope between the theoretical and experimental curves in that region. Beyond Load No. 2 it was apparent that the rollers had aligned themselves so that little or no horizontal force was being taken by the rollers. Consequently the slopes of the theoretical and predicted curves in Figure 23 between Load Nos. 2 and 4 (first yielding) are more nearly the same.

Therefore, the apparent increased stiffness of test specimen RC-1 as shown in Figure 23 can be attributed mainly to the small friction developed in the roller supports due to the observed initial misalignment. It can be appreciated from observing the small values of horizontal load Q required to cause drift that very little friction was required to substantially alter the experimental

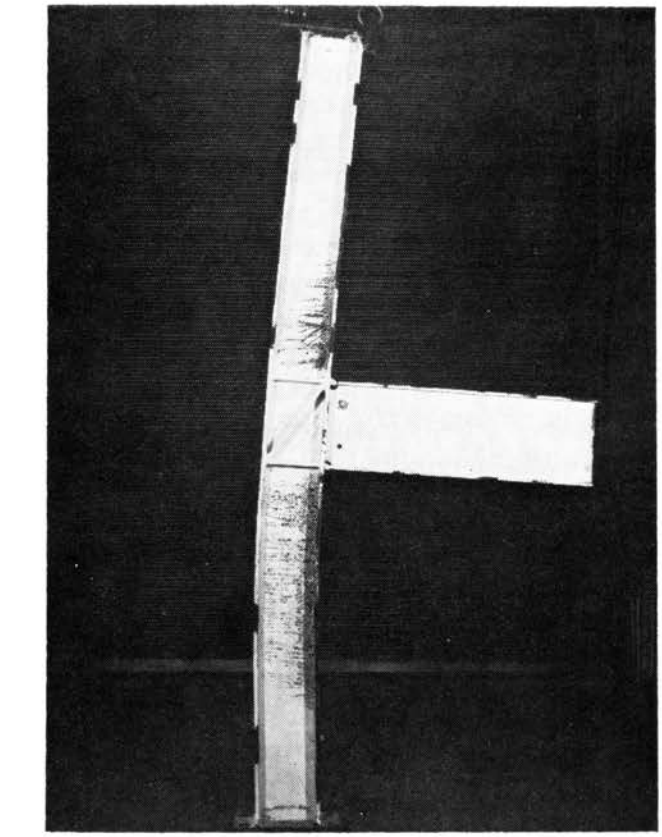

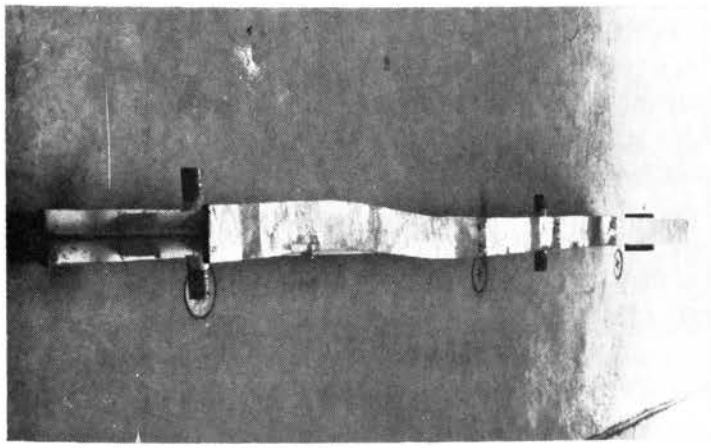

FIGURE 36. Deformed specimen after cyclic testing RC-3

behavior. The small lateral force requirements, of course, are a result of the very high level of axial column load.

Theoretically the lateral load Q for test specimen RC-1 is expected to decrease almost linearly until a plastic hinge forms under the load point nearest the column which results in the failure mechanism for the specimen. As shown in Figure 23, the lateral load was nearly constant between Load Nos. 6 and 10. The difference between the experimental and theoretical results can be explained by considering the gradual yielding process in the vicinity of the plastic hinge location. Figure 37 shows the experimental variation in the bending moments in test specimen RC-1 at the center of the joint and under the load point closest to the column. In the figure, M_u and M_L are the bending moments at the joint as calculated from the measured strains in the columns above and below the joint, respectively. M_f is the bending moment under the load point as calculated from the measured beam strains. M_B is the bending moment at the joint computed from the measured beam strains. M_B is to be compared with the curve showing $-(M_u + M_L)$.

Although first yielding of the beam was calculated to occur at Load No. 7 (Fig. 37), it occurred as early as Load No. 4 (Fig. 23). This was probably due to welding residual stresses at the load point. It can be observed from Figure 37 that the gradual plastification of the beam under the load point after first yielding would have the effect of decreasing the lateral stiffness of the test specimen, thus increasing lateral deflection and $P\Delta$ effects. As a result, for test specimen RC-1 the applied lateral load for a particular value of lateral deflection would be expected to be greater than predictions based on elastic-plastic beam behavior. Although Figure 37 indicates that M_p of the beam was not quite reached, some experimental error should be expected as indicated by the difference in calculated joint moments [M_B vs. $-(M_u + M_L)$]. It was observed during the test that a

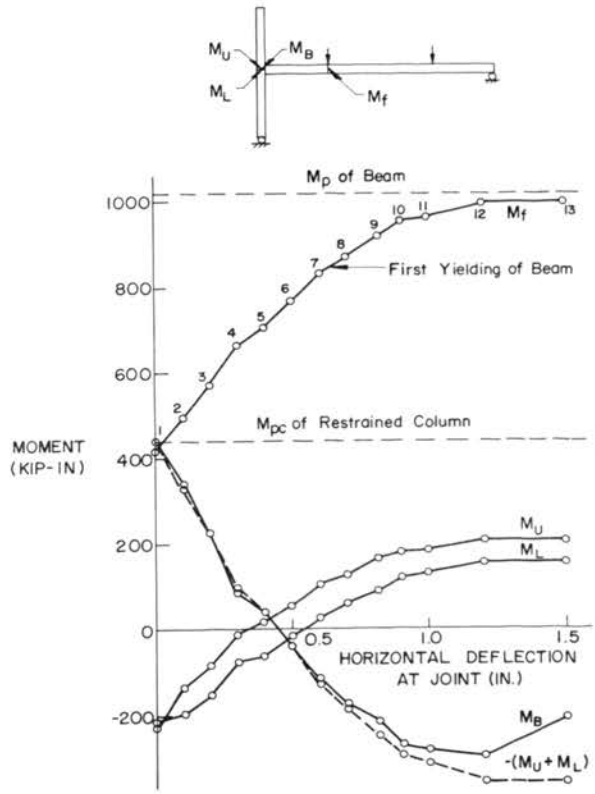

FIGURE 37. Variation in moment in test specimen RC-1

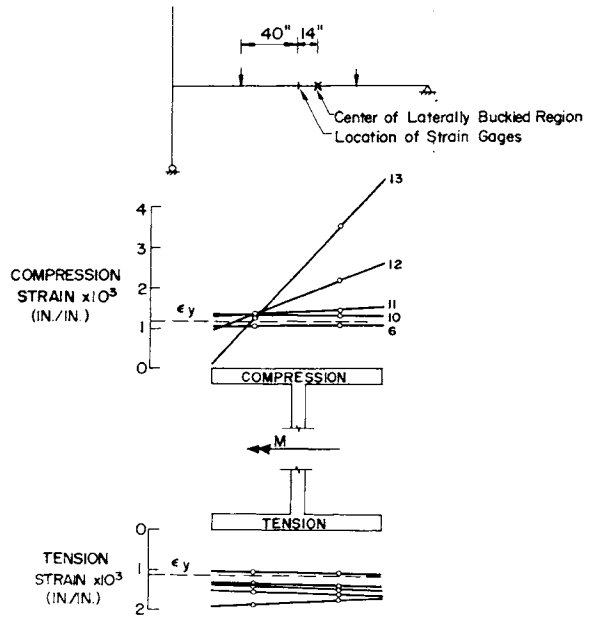

FIGURE 38. Strain distribution in beam flanges near the center of the laterally buckled region RC-1

plastic hinge had developed in the beam under the load point at Load No. 10. As previously discussed in Chapter 5, the beam began to exhibit lateral buckling of the compression flange between the two load points. This was observed to begin after Load No. 10, with definite lateral buckling at Load Nos. 11 and 12.

Figure 38 shows the strain distribution in the beam flanges at the strain gage location nearest the center of the laterally buckled region. The numbers in the figure correspond to the load numbers in Figure 23. It can be seen that the first indication of lateral buckling was at Load No. 11 and there was a definite lateral buckling at Load No. 12. Since the strain gage location was about 14 in. away from the center of the laterally buckled region, the strains shown in Figure 38 will be somewhat smaller than the maximum strains in the beam due to lateral buckling. From Figures 37 and 38 it is evident that in the vicinity of Load Nos. 10 and 11 a plastic hinge had almost developed in the beam under the load point nearest the column, which is in fairly good agreement with observed behavior. In addition lateral buckling of the beam was well developed, at least after Load No. 11. As a result, additional beam restraint was no longer available to the restrained column following Load Nos. 10 and 11. The subsequent unloading of the restrained column could therefore be expected and is confirmed by Figure 23. Since no strain-hardening occurred in the beam following unloading (except that associated with lateral buckling), the unloading slope of the restrained column curve could be expected to agree closely with theoretical predictions as shown in Figure 23.

In conclusion, considering the difficulties with the initial alignment of the rollers and the initial lateral friction force which was developed at the start of the test of specimen RC-1, the experimental and theoretical behaviors of this restrained column are in fairly good agreement.

6.2.2 Restrained Column RC-2 Figure 27 shows the experimental load-drift curve and the theoretically predicted curves for test specimen RC-2. In the theoretical calculations, two different analyses were made. In analysis 1, the beam plastic hinge is assumed to form at the face of the column. In analysis 2, the beam plastic hinge is assumed to form away from the column face, at a distance equal to the beam depth (11, 12).

The prediction based on analysis 1 indicated that the first plastic hinge forms in the beam (Fig. 4). The second plastic hinge occurs at the top of the restrained column following an instability failure of the restrained column at a lateral load of 4.25 kips ($Qh/2M_{pc} = 0.58$). The theoretical prediction based on analysis 2 indicates that the first and only plastic hinge occurs at the top of the restrained column at a maximum lateral load of 4.60 kips ($Qh/2M_{pc} = 0.63$).

As shown in Figure 27, the initial behavior of test specimen RC-2 was almost linear and followed very closely the predicted curves. Theoretically, the load-deflection curve should start at the origin ($Qh/2M_{pc} = 0$, $\Delta/h = 0$). However, there was a small initial deflection with zero lateral load at the start of the test. This can be attributed to the errors occurred during alignment.

As previously stated, according to analysis 1, the first plastic hinge should form in the beam at the column face with a horizontal joint deflection of about 0.33 in. In the test, at Load No. 8 where nearly the same deflection was attained, the moment in the beam at the column face was considerably below the plastic moment. This moment is plotted in Figure 39 as M_c. In Figure 39, moments M_c, M_D and M_L were calculated from measured strains in the beam and the column as described before. At Load No. 11 the moment M_c exceeded the theoretical plastic moment capacity which was in good agreement with visual observation, since it was observed that yielding had penetrated the web of the beam near the column face. After reaching the theoretical plastic moment, the moment at the column face was continued to in-

crease, but at a smaller rate. This increase can be attributed to the effects of the constraint from the connection and the strain-hardening at the yielded region. It is apparent from Figure 39 that a plastic hinge at the top of the restrained column was obtained at Load No. 14. This was also observed during the test. This resulted in the attainment of the collapse mechanism assumed in analysis 1. The experimental behavior as shown in Figure 27 is in fairly good agreement with the predicted results based on analysis 1.

Theoretically, the horizontal deflection of the column is assumed to increase linearly along the column length. In the test, this behavior was observed in the elastic range. However, as yielding of the restrained column progressed and localized curvature change of the yielded zone occurred, the increase in column deflection became nonlinear and a kink developed in the yielded region just below the joint. The kink became more distinctive with the formation of the column plastic hinge. As a result, the relative change in deflection along the upper column was considerably smaller than that of the restrained column. The $P\Delta$ moment coming from the upper column became less than the theoretically assumed value. This difference in $P\Delta$ moment could be a source of the discrepancy between the predicted and the experimental curves near the instability limit load and in the subsequent unloading curves, where the experimental curve remain higher than the predicted curve as shown in Figure 27.

During the unloading part of the test, the specimen exhibited somewhat greater stiffness than predicted. This could be attributed to the following sources: (1) the effect of joint stiffness, (2) the effect of strain-hardening, and (3) the smaller $P\Delta$ moment coming from the upper column than that theoretically assumed. The influence of these effects which result in conservative behavior can be observed from the following analysis of the test data, where an attempt was made to eliminate strain-hardening from the test results. For Load Nos. 14, 15 and 16, the lateral loads Q corresponding to the measured column moments above M_{pc} were computed and subtracted from the experimentally obtained values of Q. The results are shown in Figure 40 by the solid circles. The modified test curve is compared with two theoretical curves based on analysis 1, using two different column slenderness ratios; one with the distance between pinned ends as the column length and the other with the distance between pinned ends less

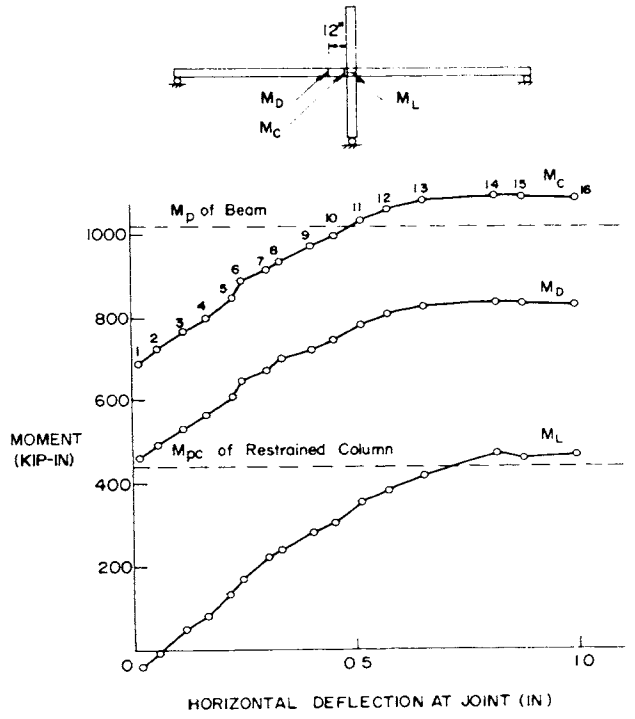

FIGURE 39. Variation in moment in test specimen RC-2

the length of the connection. The experimental results closely agree with analysis 1, assuming that the total column length is the distance between pinned ends. A similar result was found by C. K. Yu and reported in Ref. 13.

6.2.3 Restrained Column RC-3 Figure 32 shows the experimental load-deflection curve and the theoretically predicted curves for test specimen RC-3. The small difference between the theoretical and experimental values of Qh $2M_{pc}$ in the zero-swayed position can be attributed to a small misalignment during the test setup and out

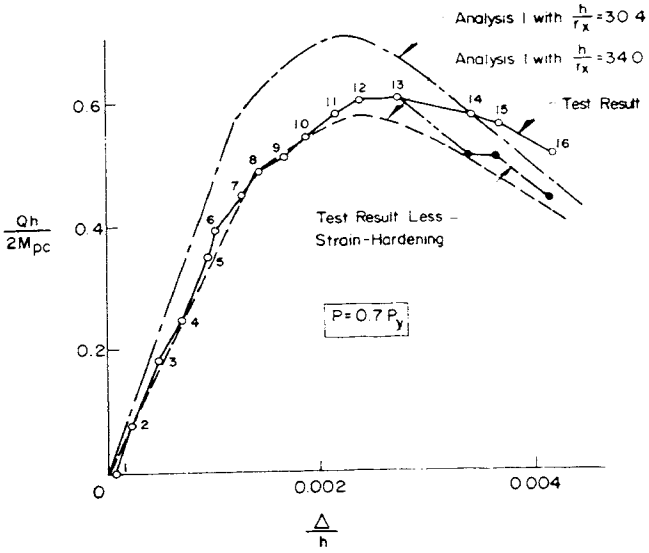

FIGURE 40. Comparison study of test data for test specimen RC-2

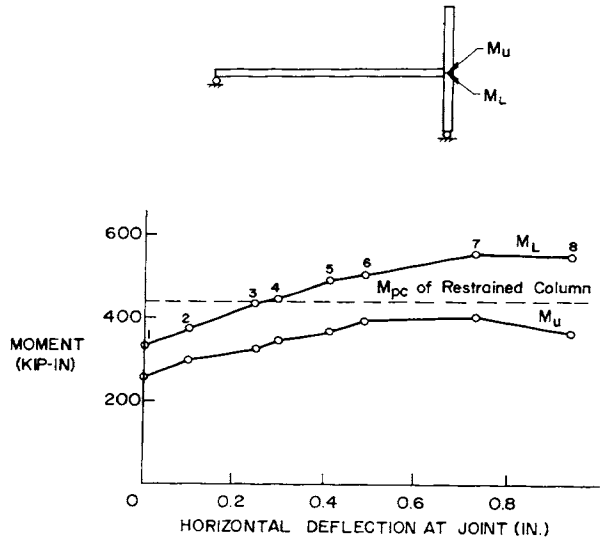

FIGURE 41. Variation in moment in test specimen RC-3

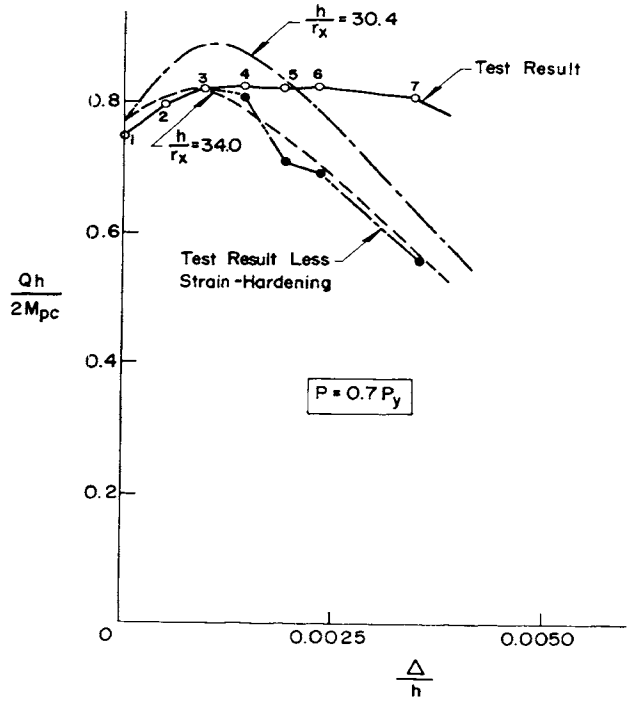

FIGURE 42. Comparison study of test data for test specimen RC-3

of straightness of the members. At zero-sway the theoretical lateral load at the column top is 5.68 kips ($Qh/2M_{pc} = 0.78$) while the load applied in the test was 5.52 kips ($Qh/2M_{pc} = 0.75$) as shown in Figure 19.

In the theoretical analysis, the first plastic hinge occurs at the top of the restrained column, which results in the failure of the specimen. In the test, M_{pc} was reached at the top of the restrained column between Load Nos. 3 and 4 as shown in Figure 41, where the experimental variation of joint moments in the test specimen is plotted. However, the moment at the joint continued to increase up to Load No. 7 while an almost constant value of horizontal load was maintained as the sway deflection increased (Fig. 32). As discussed in Section 6.2, this behavior probably resulted from the effects of the joint stiffness, strain-hardening and the smaller $P\Delta$ moment contributed by the upper column due to the hinge action.

In test specimen RC-3, the hinge action on the horizontal deflection of the column was more distinctive than in test specimen RC-2. The deflection at the column top was much smaller than predicted after the reduced plastic moment in the restrained column was reached. This was an important factor contributing to the significant increased stiffness of the specimen beyond the theoretical mechanism.

In order to evaluate the effects of strain-hardening, the same analysis as in the test specimen RC-2 was performed on the experimental results. Figure 42 shows the modified experimental results as the solid circles where strain-hardening has been eliminated from the test results. The modified test curve is in very good agreement with the theoretical unloading curve. In the figure, the experimental curve is also compared with the theoretical curve determined with the column slenderness of $h/r_x = 30.4$. As in the test specimen RC-2, the experimental result closely agree with the theoretical curve with the total column length between pinned ends ($h/r_x = 34.0$) (13).

Although there is a small difference between the theoretical and experimental curves at the start of the test, two curves are in fairly good agreement during the initial loading part of the load-deflection curve. The maximum horizontal load attained during the test was 6.06 kips ($Qh/2M_{pc} = 0.83$) which gives a good agreement with the predicted value of 6.00 kips ($Qh/2M_{pc} = 0.82$). Since the conservative effects, such as joint stiffness, strain-hardening and reduced $P\Delta$ effect, are not considered in the theoretical prediction, there was a considerable discrepancy between the experimental and predicted unloading curves. However, the test of specimen RC-3 was in good agreement with prediction based on restrained column and sway subassemblage theory.

7. Summary and Conclusions

Tests were conducted on three restrained columns permitted to sway. Each test specimen represented a restrained column in either a windward, an interior, or a leeward sway subassemblage. The main purpose of the tests was to study

the load-drift behavior of such restrained columns and to compare the experimental results with the predictions from restrained column and sway subassemblage theory. The most important observations are summarized below:

1. The behavior and the strength of all test specimens were in fairly good agreement with the theoretical predictions. The order and location of plastic hinge formation were the same as predicted.

2. As yielding of restrained column progressed, a kink developed in the yielded region and the $P\Delta$ moment contributed by the upper column at the joint became considerably less than the theoretically assumed value.

3. The beam moment at the column face exceeded the full plastic moment capacity of the section, M_p, in a test. However, the experimental result closely agree with the prediction assuming that the beam plastic hinge forms at the face of the column.

4. Due to the effects of the joint stiffness and strain-hardening, the moment at the top of a restrained column exceeded its reduced plastic moment capacity, M_{pc}, when a column plastic hinge was expected to form. Consequently, the specimens were stiffer than the prediction in the unloading part of the tests. The behavior modified by eliminating the effects of strain-hardening from the experimental results is in very good agreement with the theoretical behavior.

5. Although there is an effect of joint stiffness, the experimental results closely agree with predictions, assuming that the total column length is the distance between pinned ends.

The following conclusions are based on the test results of this investigation:

1. The behavior and the strength of restrained columns permitted to sway with a constant or a variable rotational stiffness can be closely predicted by restrained column and sway subassemblage theory.

2. In the theoretical calculations, the total height of a column and the clear span of a beam should be used, except when calculating the initial (zero-sway) bending moment. In this case, the center-to-center span of a beam should be used.

References

1. Daniels, J. H., and Lu, L. W., "Sway Subassemblage Analysis for Unbraced Frames," ASCE Meeting Preprint 717, Oct. 1968.
2. Daniels, J. H., "A Plastic Method for Unbraced Frame Design," *AISC Engineering Journal*, Vol. 3, No. 4, Oct. 1966).
3. Daniels, J. H., "Combined Load Analysis of Unbraced Frames," Ph.D. Dissertation, Fritz Engineering Laboratory Report No. 338.2, Lehigh University, July 1967.
4. Daniels, J. H., and Lu, L. W., "Design Charts for the Subassemblage Method of Designing Unbraced Multistory Frames," Fritz Engineering Report No. 273.54, Lehigh University, Nov. 1966.
5. Armacost, J. O., III, and Driscoll, G. C., Jr., "The Computer Analysis of Unbraced Multistory Frames," Fritz Engineering Laboratory Report No. 345.5, Lehigh University, May 1968.
6. Driscoll, G. C., Jr., Armacost, J. O., III, and Hansell, W. C., "Plastic Design of Multistory Frames by Computer," *Proc. ASCE*, Vol. 96, No. ST1, Jan. 1970.
7. Levi, V., Driscoll, G. C., Jr., and Lu, L. W., "Analysis of Restrained Columns Permitted to Sway," *Proc. ASCE*, Vol. 93, No. ST1, Feb. 1967.
8. Kim, S. W., Daniels, J. H., and Lu, L. W., "Technical Proposal No. 1 – Restrained Column Tests," Fritz Engineering Laboratory Report No. 346.1, Lehigh University, Sept. 1967.
9. Yarimci, E., Yura, J. A., and Lu, L. W., "Techniques for Testing Structures Permitted to Sway," Fritz Engineering Laboratory Report No. 273.40, Lehigh University, May 1966.
10. Driscoll, G. C., Jr., et al., "Plastic Design of Multistory Frames – Lecture Notes," Fritz Engineering Laboratory Report No. 273.20, Lehigh University, Sept. 1965.
11. Lay, M. G., and Galambos, T. V., "Tests on Beam-and-Column Subassemblages," Fritz Engineering Laboratory Report No. 278.10, Lehigh University, June 1964.
12. Yarimci, E., "Incremental Inelastic Analysis of Frames Structures and Some Experimental Verifications," Ph.D. Dissertation, Lehigh University, May 1966.
13. Yu, C. K., "Inelastic Columns with Residual Stresses," Ph.D. Dissertation, Lehigh University, April 1968.

Experiments on Unbraced One-Story Assemblages

by

S. W. KIM and J. HARTLEY DANIELS

ACKNOWLEDGMENTS

The work reported herein was performed at Fritz Engineering Laboratory, Department of Civil Engineering, Lehigh University. Dr. David A. VanHorn is the Chairman of the Civil Engineering Department and Dr. Lynn S. Beedle is Director of Fritz Engineering Laboratory. The results presented form part of a general investigation in "Strength of Beam-and-Column Subassemblages in Unbraced Multistory Frames." Sponsorship of the program was provided by the Committees of Structural Steel Producers and Steel Plate Producers, American Iron and Steel Institute. Technical guidance was provided by the Task Force on AISI Project 150, consisting of W. C. Hansell (Chairman), R. G. Dean, I. M. Hooper, F. R. Khan, E. O. Pfrang and I. M. Viest (Project Supervisor). The authors are grateful for the guidance and assistance of the Task Force.

The authors acknowledge the assistance of Dr. L. W. Lu, Director of the Building Systems Division. The work of Kenneth R. Harpel and his technicians in setting up the tests is appreciated. Thanks are due also to Miss Karen Philbin who typed the report and Mr. John Gera who prepared the drawings.

CONTENTS

ABSTRACT

Tests were conducted on two full-sized one-story two-bay assemblages. One test assemblage was designed to simulate a story near the top of an unbraced multistory frame. The other assemblage was designed to simulate a story near the bottom of a frame. In each test the total gravity loads applied to the beams and columns was maintained constant as drift increments were given to the assemblage. However, the distribution of gravity loads to the columns was varied linearly with the applied drift. This loading condition thus represented a realistic combined loading condition for an unbraced frame in a high-rise building. The lateral-load vs. drift behavior of the assemblage was compared with predicted load-drift behavior computed from sway subassemblage theory. The predicted behavior of the assemblages was in very close agreement with the experimental behavior.

1. Introduction

The sway subassemblage method of analysis was developed to determine the approximate second-order elastic-plastic behavior of individual stories of an unbraced multistory frame (1–5). In the method, a story, called a one-story assemblage is isolated from the frame. Using sway subassemblage theory, the complete lateral-load vs. drift curve for the one-story assemblage is then determined for either proportional or nonproportional loads up to or beyond the stability limit load. The load-drift relationship for the one-story assemblage is obtained by superimposing the load-drift relationships for each sway subassemblage in the one-story assemblage. A sway subassemblage consists of a restrained column plus one or two restraining beams.

A two-phase experimental program was undertaken at Lehigh University to provide an experimental evaluation of restrained column theory and sway subassemblage theory (6, 7). In Phase I, three restrained columns were tested and the results reported (8). The tests showed that good correlation with predicted behavior was obtained. These studies therefore provided an important first step in the experimental verification of sway subassemblage theory. Phase II of the program is an experimental investigation of two one-story assemblages and a comparison of the test results with predictions obtained from a sway subassemblage analysis.

The column axial loads in an unbraced frame subjected to combined loads, whether proportional or nonproportional, vary with increasing lateral load and drift. The variation for a particular story column is the summation of the variations in each column directly above the column considered. In the sway subassemblage method of analysis the actual variation in axial loads cannot be exactly accounted for. Therefore some assumptions are required regarding the magnitude and distribution of the total gravity loads to the columns within the one-story assemblage.

In an analysis considering nonproportional loads, where the gravity loads are held constant, it is assumed that the column axial loads in the one-story assemblage are constant. The sum of the column axial loads by statics is equal to the total of all the gravity loads above the one-story assemblage. The distribution of the total gravity loads to each column of the one-story assemblage is taken as that obtained from a moment-balancing solution for the frame corresponding to the frame mechanism condition (3, 9). An analysis considering proportional loads would also eventually arrive at the same column loads but would arrive there after several proportional increments of loading starting with zero gravity and lateral loads.

Analytical studies indicated that within the range of expected axial load ratios in a frame the behavior of a one-story assemblage is insensitive to the distribution of the axial loads to the columns. In fact these studies indicate that one-story assemblage behavior is unaffected by the distribution of the total gravity loads to the columns providing that no plastic hinges form in the columns.

The reasoning for this is as follows: First, an examination of the equilibrium equations for a one-story assemblage show that overall equilibrium is dependent only upon the magnitude of the total gravity loads and not on their distribution (4). Second, the primary effect of the axial load for any particular column is to establish the magnitude of the reduced plastic moment capacity M_{pc} for that column. Thus in the absence of plastic hinges in the columns a variation of the total gravity loads to the columns will not change the one-story assemblage response.

Two tests of one-story assemblages were conducted in Phase II. Each assemblage consisted of three columns and two beams forming two equal bays of 15 ft and a story height of 10 ft. The assemblages were tested under nonproportional loading, which is considered to be the more realistic case for practical frames. The total gravity load

applied to the columns was maintained constant, as were the gravity loads applied to the beams. The lateral load was applied to the top the interior column using a horizontal screw jack. The data obtained from the tests was reduced to determine all stress resultants and deformations. The load-drift behavior was compared to predictions from sway subassemblage theory.

The results of the Phase II studies are reported herein. Experimental evaluation of sway subassemblage theory, as applied to the two one-story assemblages is reported, and includes an evaluation of the effect of variations of the total gravity loads to the columns.

Each assemblage was subjected to approximately two cycles of reversed loading to fairly large values of drift following the initial tests discussed above. These results are not presented in this report.

Nomenclature

A = area of cross section
b = flange width
d = depth
H = horizontal wind load
I_x = moment of inertia about major axis
M = bending moment
M_p = plastic moment capacity of cross section
M_{pc} = reduced moment capacity considering axial load
P = axial force in column
P_y = axial yield load of cross section
Q = horizontal force
t = flange thickness
w = web thickness
Z = plastic section modulus about major axis
$\Delta/2$ = joint deflection

2. Experiment Design

Since only two assemblages were to be tested a decision was made that one should be designed to simulate the expected behavior of a story close to the top of an unbraced frame, in the vicinity of the stability limit load. The other would simulate the expected behavior of a story near the bottom of the frame. Such simulations can be achieved by selecting beam and column sizes and loading such that near the stability limit load, the plastic hinge locations in the test assemblage are similar to the expected locations in the corresponding stories of the frame. At the same time, in order to facilitate some comparison with the results of the Phase I studies it is desirable to maintain the same story and bay dimensions and member sizes as closely as possible (8).

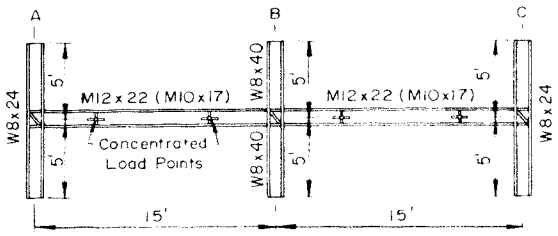

Note: Members for SA-2 shown in parentheses where different from SA-1.
Shapes correspond to those listed in AISC Manual of Steel Construction - 6th Edition

FIGURE 1. One-story assemblages SA-1 and SA-2

The dimensions and member sizes selected for the two test assemblages reported herein are shown in Figure 1. Assemblage SA-1 is designed to simulate the behavior of a story near the top of a frame, while SA-2 is designed to simulate the behavior of a story near the bottom of a frame. ASTM A36 steel is used throughout. All sections are oriented for strong axis bending. The ratios of strong axis moments of inertia are typical of those found in the upper and lower stories of unbraced frames.

Figure 2 shows the beam and column loads selected for each test assemblage and the expected plastic hinge locations. For assemblage SA-1, plastic hinges are expected to occur in the windward beam and at the tops of the interior and leeward columns. This is a typical plastic hinge pattern for a story close to the top of an unbraced frame. The plastic hinges in assemblage SA-2 are expected to occur only in the beams which is

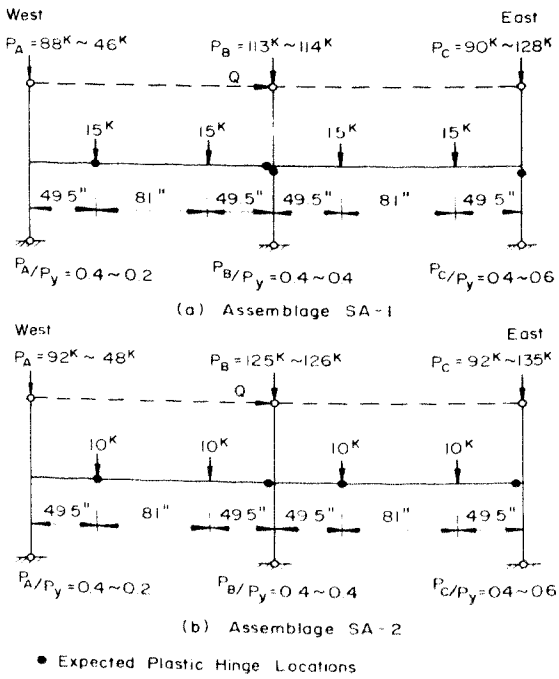

FIGURE 2. Design loads and expected plastic hinge locations

typical for a story located near the bottom of a frame.

The concentrated beam loads shown in Figure 2 are maintained constant and simulate the effect of a constant uniformly distributed gravity floor loading. The column axial loads are varied according to a preselected program to simulate constant gravity loading above the assemblage but the distribution to the columns is varied as would be expected to occur during application of the lateral loads. This is discussed further in Chapter 4. Since assemblage SA-2 is designed to achieve a mechanism with plastic hinges occurring only in the beams the effect of varying the column loads is expected to be detected only from the SA-1 test results.

The ranges of variation of the columns axial load ratios, P/P_y, shown in Figure 2, are chosen to represent as closely as possible a practical range, as well as to be within the capabilities of the available laboratory testing equipment. The column loads shown in the figure are computed using measured mechanical and cross section properties. Referring again to Figure 2, each assemblage is designed to be subjected to increments of drift applied to the tops of the interior columns in a west-to-east direction. The relationship between the resulting lateral force Q (shown positive to the right) at the column top and the drift $\Delta/2$ measured at the center of the interior joint is used to describe the behavior of an assemblage. The column tops are connected by a pinned strut (shown dashed in the figure) designed to maintain a nearly constant distance between the column tops.

In the design calculations, plastic hinges at the ends of the beams are assumed to form at the column faces. Plastic hinges in the columns are assumed to occur at the centers of the joints.

3. Mechanical and Cross-Section Properties

3.1 Tensile Coupon Tests

A total of 32 tension tests were performed to determine the mechanical properties of the ASTM A36 steel used. The static yield stress level, ultimate stress and percent elongation were determined from eight tension coupons cut from each section, four from the flanges and four from the web. A summary of the data obtained from the tension tests is given in Table I. A numerical average for each of the three properties was determined for the webs and flanges separately for each section. Based upon these average values, the plastic moment capacity M_p and the axial yield load P_y of each section were calculated.

TABLE I. Summary of Tension Tests

Section		*Static Yield Stress (ksi)*	*Ultimate Stress (ksi)*	*Elongation (8 in.) (%)*
M10×17	Web	41.6	64.5	26.2
	Flange	36.5	63.0	31.0
M12×22	Web	38.5	62.7	29.0
	Flange	33.6	59.5	30.3
W8×24	Web	33.6	61.4	30.1
	Flange	33.3	60.6	28.6
W8×40	Web	33.3	61.0	30.2
	Flange	32.2	60.7	31.0

3.2 Cross-Section Properties

The cross-section dimensions of each shape were determined at various locations along the length of each beam and column using micrometers and calipers. Measurements of web thickness were taken only at the cut ends of each length. The average cross-section properties of each shape are given in Table II and compared with the corresponding handbook values. There were no significant differences between the measured and handbook properties. The measured values were used to determine the area A, the moment of inertia I_x, and the plastic section modulus Z for each section. The value of the calculated plastic moment capacities M_p and axial yield loads P_y are also shown in Table II.

4. Test Setup and Procedure

4.1 General

The overall view of the test setup used for the two assemblage tests is shown in Figure 3. Figure 3 actually shows assemblage SA-1 after two cycles of reversed loading and shows the frame

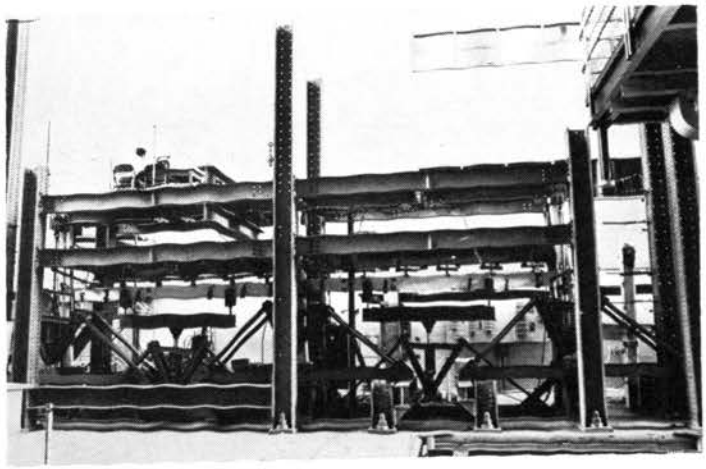

FIGURE 3. Overall view of test setup

TABLE II. Average Cross-Section Properties

Section		d (in.)	b (in.)	t (in.)	w (in.)	A (in.^{2})	I_x (in.^{4})	Z (in.^{3})	M_p (kip-in.)	P_y (kips)
M10×17	Handbook	10.12	4.01	0.329	0.240	4.98	8.18	18.6	670*	—
	Measured	10.12	3.97	0.326	0.233	4.81	79.6	18.0	688	—
M12×22	Handbook	12.31	4.03	0.424	0.260	6.47	155.7	29.4	1060*	—
	Measured	12.35	4.04	0.412	0.266	6.41	153.1	28.8	1020	—
W8×24	Handbook	7.93	6.50	0.398	0.245	7.06	82.5	23.3	831*	254*
	Measured	7.96	6.54	0.402	0.276	7.23	86.13	23.4	780	241
W8×40	Handbook	8.25	8.08	0.558	0.365	11.76	146.3	39.9	1435*	423*
	Measured	8.28	8.09	0.536	0.366	11.32	141.8	38.4	1240	367

* Yield stress taken as 36 ksi.

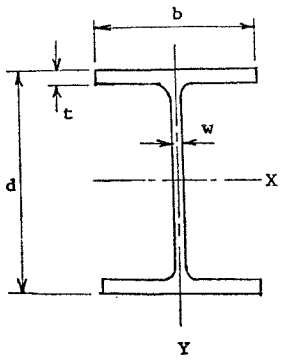

displaced in a westerly direction. In the tests reported herein drift was applied in an easterly direction. A more detailed view of the west bay of SA-1 during testing is shown in Figure 4. The test assemblage is shown in white. The darker members are all part of the testing equipment. A gravity load simulator applying loads to the columns can be seen at the left and right edges of Figure 4.

Figure 5 shows the pinned connections that were used at the ends of the column and the strut joining the column tops. The strut consisted of two channels spaced about 12 in. apart. Large roller bearings were used to ensure that there would be no bending moments at the ends of the columns. A more detailed view of the strut between an interior and an exterior column is shown in Figure 6. At the middle of each strut (near the top of Fig. 6) four small steel rods were inserted and provided with strain gages so that the lateral force in the strut could be calculated during testing. A close-up view of these rods is shown in Figure 7.

Planar motion of each test assemblage was ensured by means of specially designed lateral bracing perpendicular to the place of the test specimen

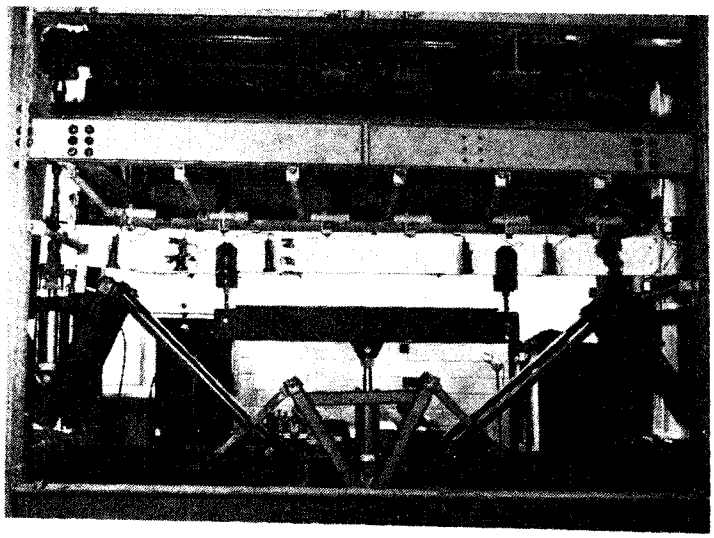

FIGURE 4. View of the west bay of SA-1 during test

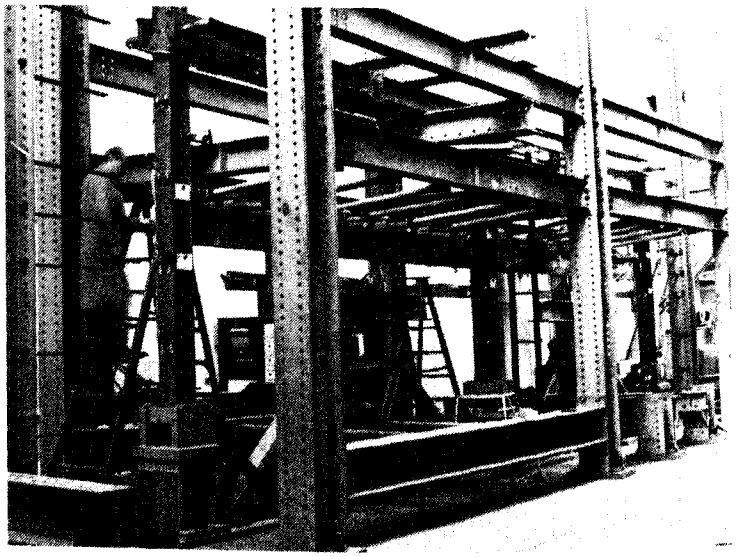

FIGURE 5. View showing pinned connections at the ends of the columns and the strut joining the column tops

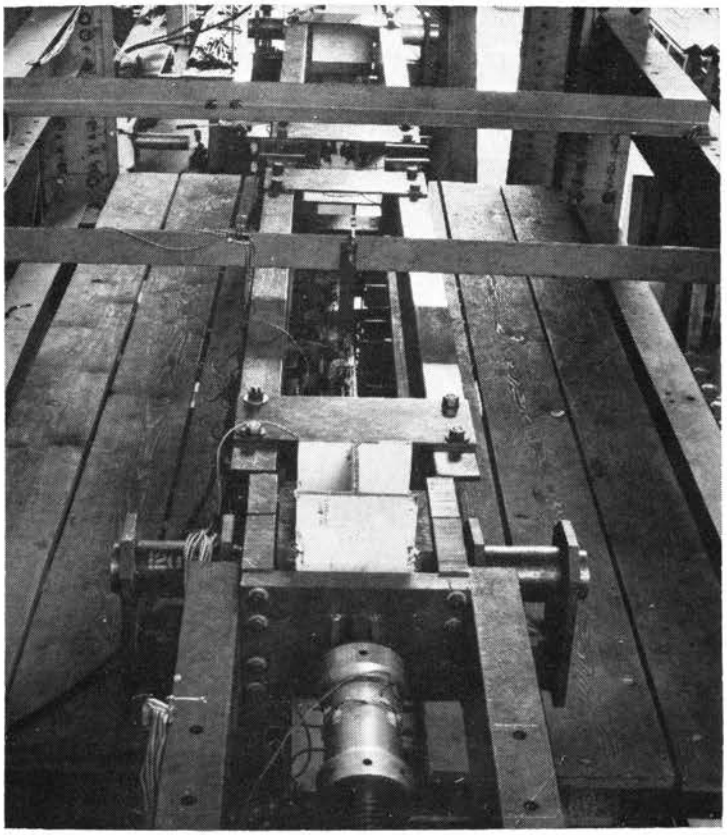

FIGURE 6. Detailed view of strut between columns tops—an interior column is in the foreground

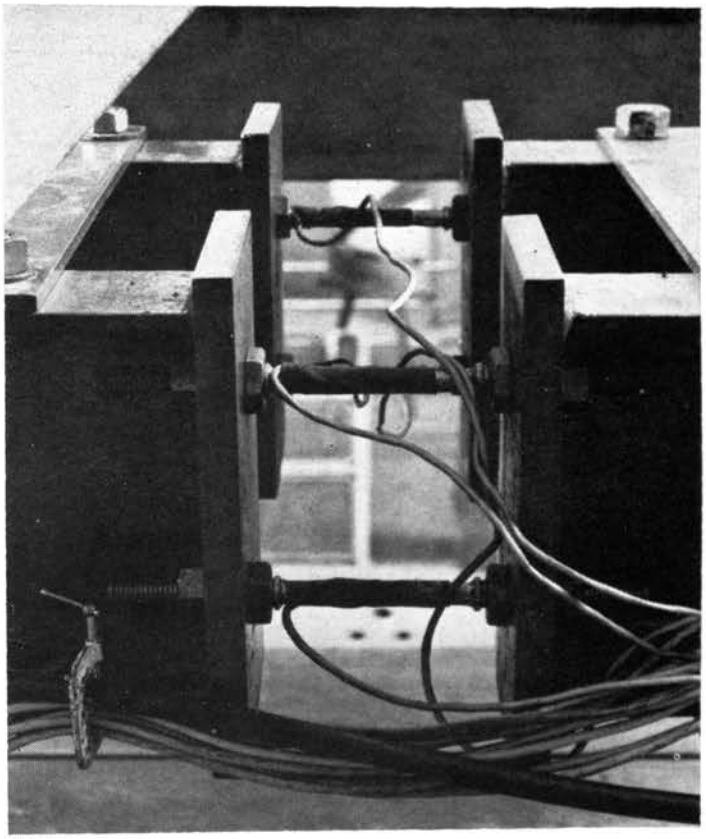

FIGURE 7. Dynamometers used to determine the force in a strut

as can be seen in Figures 4 and 5. The bracing prevented lateral and torsional movement of the beams but did not offer restraint to in-plane deformation (10). The braces for the beams were placed at the locations recommended for use in plastic design (11). The beams were also braced in accordance with the requirements for reverse cyclic loading, the results of which are not reported herein. Six braces were used for each beam. The columns were braced using the same type of bracing members. Each column was braced at the level of the beams as shown in Figure 4. All braces were in turn attached to an independent supporting frame.

4.2 Load Application

Vertical beam loads were applied approximately at the quarter points of each beam through a spreader beam which was attached at its midpoint to the tension jack of a gravity load simulator as shown in Figures 3 and 4 (10). Tension dynamometers were used to connect the spreader beam to the test specimen and also to measure the applied loads. The tension jacks of the two simulators were connected to a common hydraulic line to ensure that the same loads would be applied in both spans. Once the beam loads were applied, they were maintained constant for the duration of the test.

Each column load was applied to the top of the column by means of tension rods connected to two gravity load simulators placed on either side of each column, as shown in Figure 8. The tension rods were provided with strain gages and calibrated so that the load applied by each simulator jack could be calculated. A common hydraulic line was connected to each pair of simulator jaks at each column. The column loads could therefore be controlled by adjusting the hydraulic pressure in each pair of jacks and checked by taking readings on the tension rods.

The column loads were varied as discussed in Chapter 2 to maintain the desired axial load ratio P/P_y in each column at every stage of the test. In order to accomplish this a loading program was determined for each column for each test assemblage. Figure 9 shows the column loading program used for the two subassemblages. For SA-1, the calculated drift corresponding to the theoretical mechanism condition was divided into ten drift increments. The load was adjusted at the end of each drift increment in order to maintain the desired axial load ratios in the columns. The open circles in Figure 9(a) show the desired values

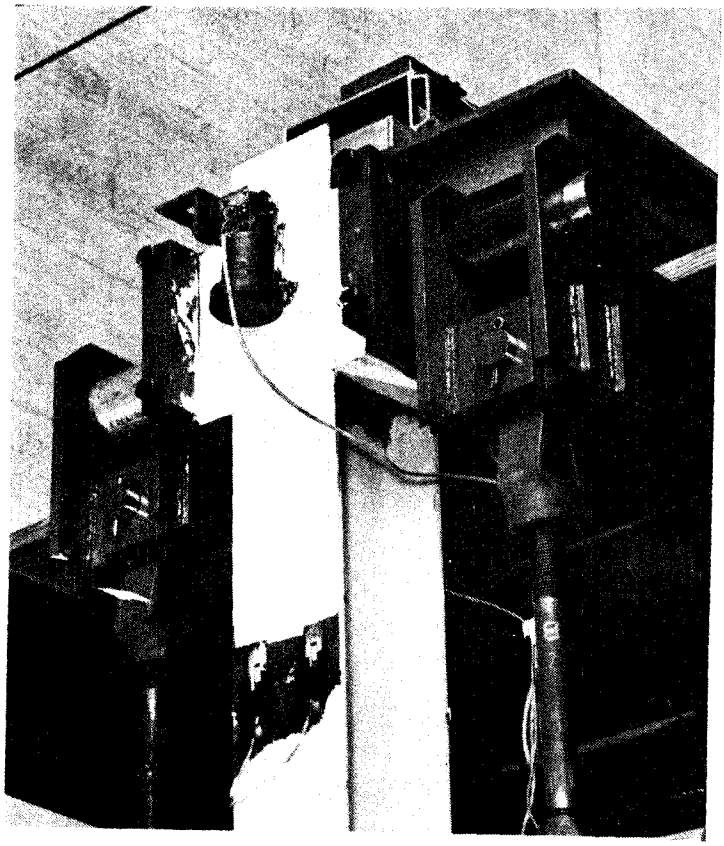

FIGURE 8. Tension rods used to apply column loads

of P/P_y for each column for each drift increment. The column load used during each drift increment was the average of the desired axial load ratios at the beginning and the end of each increment. All strain and deflection readings were taken at the midpoint of a drift increment.

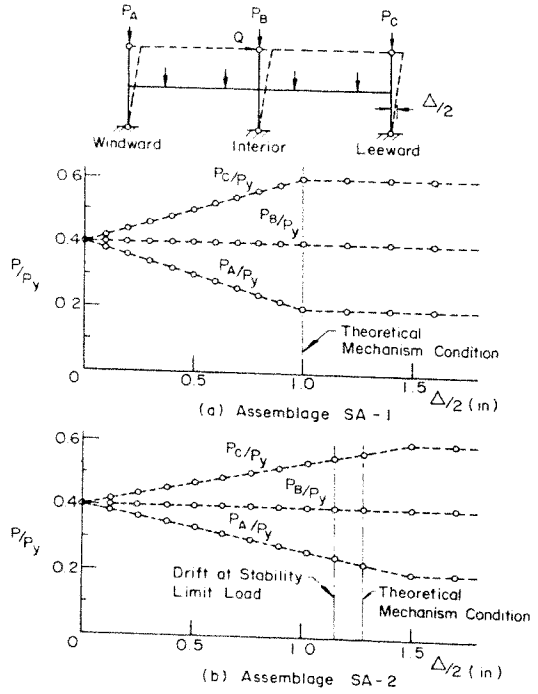

FIGURE 9. Column loading programs

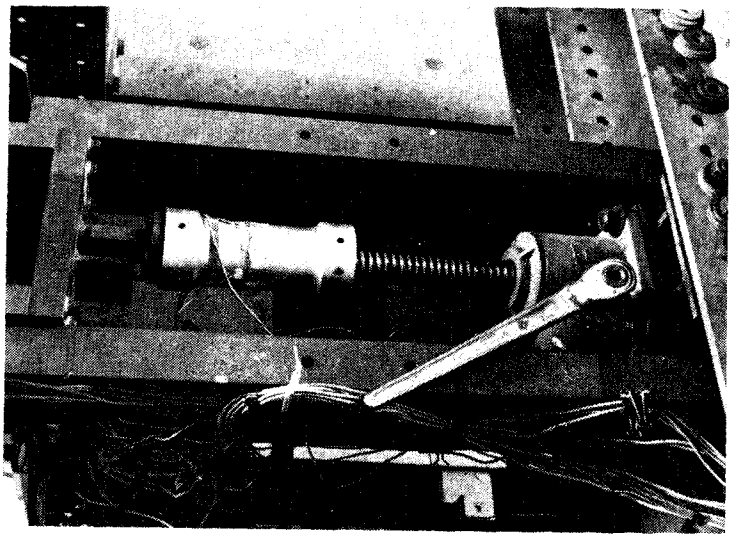

FIGURE 10. Horizontal screw jack used to apply drift increments to the assemblages

The column loading program for assemblage SA-2 is shown in Figure 9(b). For this test the column loads were varied up to and somewhat beyond the mechanism condition. This was to account for the effect of strain hardening which can occur in the beams in the lower stories of a frame after the stability limit load is reached.

The drift increments at the top of the interior columns were applied by a mechanical screw jack mounted horizontally at the top of the interior column as shown in Figures 6 and 10. The jack was pin connected to the column top through a dynamometer used to measure the lateral load applied by the jack. The jack was also pin connected to the independent supporting frame.

4.3 Instrumentation

The instrumentation used in the tests was designed to obtain strain data which could be used to (1) calculate the applied loads, (2) determine deformations and (3) calculate the internal stress resultants in the assemblages. Calibrated dynamometers were used to measure all applied loads.

Strains in the beams and columns were obtained from SR-4 electrical resistance strain gages. Four

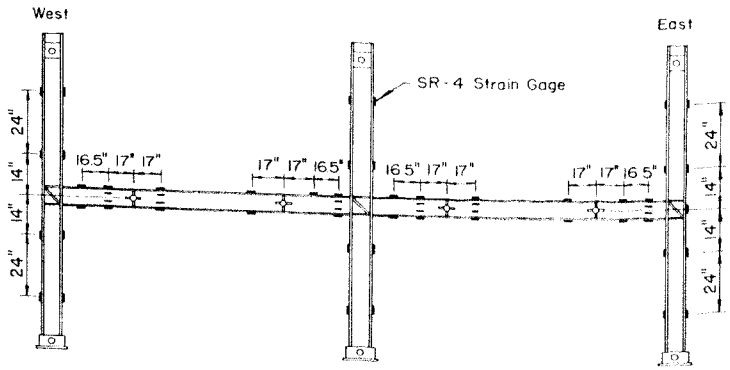

FIGURE 11. Location of electrical resistance strain gages

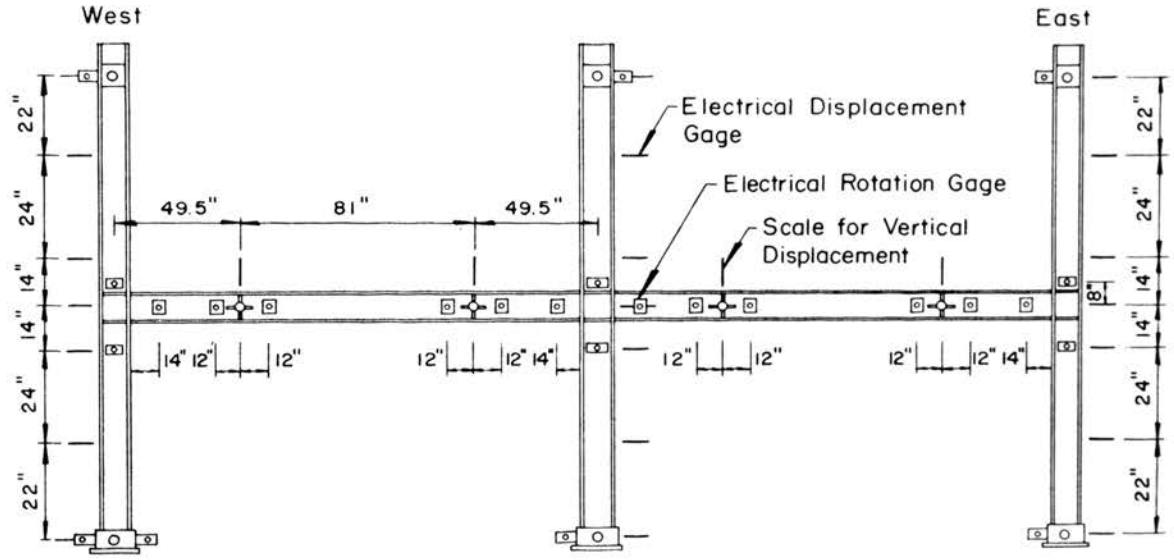

FIGURE 12. Location of displacement and rotation gage

strain gages were used at each instrumented cross-section so that the axial force and bending moment at the cross-section could be calculated. Four cross-sections were gaged on each column and six were gaged on each beam as shown in Figure 11. In addition, another four gages were mounted on the beam webs at six instrumented cross-sections of each assemblage. These cross-sections were chosen near the locations of potential plastic hinges so that some strain measurements would be available after the occurrence of yielding in the flanges at those cross sections.

Electrical displacement gages were used to measure drift and vertical beam deflections at the locations indicated in Figure 12. A transit was also used to measure drift at the level of the beams by reading a scale attached to the face of each column.

Rotations were measured using electrical rotation gages (10). These gages were placed at the top and bottom of each column, at the joints and at either side of the concentrated beam loads as shown in Figure 12.

Each test assemblage was whitewashed prior to testing in order to observe the progression of yielding. All electrical SR-4 strain gages, electrical displacement and rotation gages and dynamometers were read by a multichannel strain gage recording system and punched automatically onto computer cards. This procedure enabled a systematic data reduction to be performed using a computer program.

4.4 Alignment Procedure

During erection of an assemblage the three columns were first placed on their pin-base supports, lightly attached to the surrounding framework at the beam level and aligned with transits to ensure that each beam was horizontal, in the correct position and in the plane of the assemblage. After all alignment was complete and all instrumentation in place, the initial set of strain and deflection readings was taken. Then the beams were welded to the columns. After the welding was completed, the lateral bracing in place and the temporary attachments removed a second set of readings was taken to isolate the effect of welding. At this point the horizontal struts between the column tops were loosely fitted so that no stresses would be developed in the columns above the beam level.

After erecting and aligning each assemblage, it was necessary to adjust the positions of the load hangers on either side of the columns (Fig. 8) to eliminate any eccentricity of the applied column load. Strain readings were taken at several small column load levels. Based on the strains obtained, the positions of the load hangers were adjusted to reduce the eccentricity of column load. The adjustment was continued for each column until all column loads were applied with negligible eccentricities. At this point the horizontal struts were fitted snugly between the column tops by adjusting the rods at the center of each strut.

4.5 Test Procedure

At the start of each test and with the assemblage in a zero drift position, one-half of the initial column loads (Figs. 2 and 9) and the full beam loads were gradually applied simultaneously. The column loads were then gradually increased to their full values while the beam loads were held constant. After all the vertical loads had been

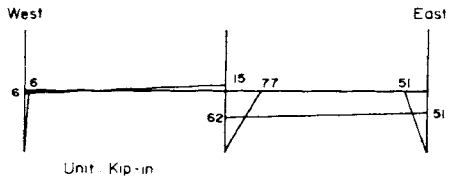

(a) ASSEMBLAGE SA-1

(Bending Moments Plotted on Tension Side)

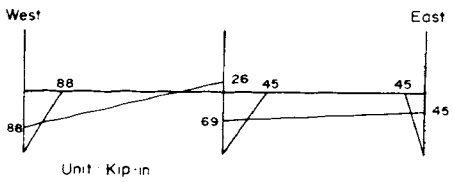

(b) ASSEMBLAGE SA-2

FIGURE 13. Welding residual moments

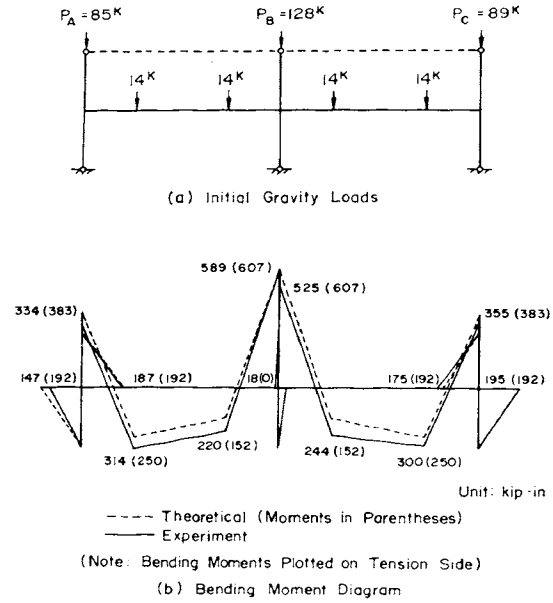

(a) Initial Gravity Loads

(b) Bending Moment Diagram

FIGURE 14. SA-1: Load and moment conditions at zero drift

applied all strain and deflection readings were again recorded to isolate the effect of the initial gravity loads.

From this initial stage the drift of the interior column was incremented following the predetermined program using the horizontal screw jack at the interior column top. A particular drift increment was applied in two steps. First, one-half of the drift increment was applied with the column loads maintained equal to the average value desired for that interval. Then, all strain and deflection readings were taken. After taking all readings, the second half of the required drift increment was applied. At the end of the increment, the column loads were adjusted to the average value required for the next increment in the load program. These procedures were repeated until the total drift exceeded the drift corresponding to the stability limit load for the assemblage.

When inelastic action was evident in an assemblage, all readings were taken after approximately a 10–30-min waiting period in order to allow the yielding process to stop and the assemblage to come to static equilibrium.

5. Test Results

5.1 Welding Residual Moments

Since the fabricated assemblages are statically indeterminate the welding operation can introduce residual stresses into the beams and columns. The calculated moments resulting from the welding are shown plotted in Figure 13 on the tension side of each member. No particular welding order was maintained. The moments shown in the figure apply only to the test assemblages and could be entirely different in a one-story portion of an actual frame.

A certain amount of error is evident since the residual moments shown in the figure should theoretically be in self equilibrium. This error can be attributed mainly to (1) experimental accuracy; strains were recorded to an accuracy of about ± 5 micro-in., and (2) probable restraints provided by the attachments used to align the members prior to welding.

Even though the absolute error indicated in Figure 13 is fairly large the relative error is probably small. For instance, the largest residual moment at a potential plastic hinge location in a beam is about $0.09M_p$, and for a column, about $0.12M_{pc}$. The probable error in the residual moments is likely to be somewhat smaller than this. Therefore the measured residual moments are considered to be sufficiently accurate to include in Chapter 6 where a detailed analysis of the test results is made.

5.2 Initial Gravity Load Moments

The constant gravity loads which were actually applied to the two test assemblages are shown in Figures 14 and 15. These loads are to be compared with the design loads which are shown in Figure 2. During each test the constant gravity loads were maintained using calibrated pressure gages which determined the oil pressure delivered to the several hydraulic jacks. The differences between the design and actual loads arise mainly from the accuracy with which the pressure gages

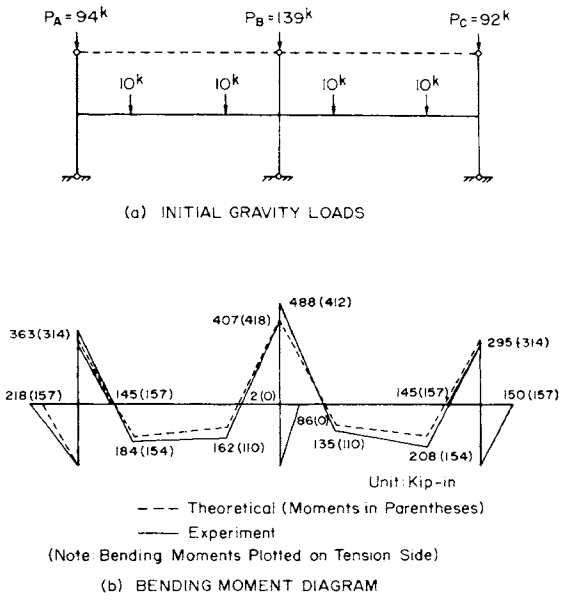

FIGURE 15. SA-2: Load and moment conditions at zero drift

could be read. The actual gravity load carried by an assemblage was calculated after the test using data recorded from the calibrated tension dynamometers previously discussed in Chapter 4. The average applied gravity load during a test is shown in Figures 14 and 15.

The bending moments for each test assemblage corresponding to the initial constant gravity loads are also shown in Figures 14 and 15. The theoretical bending moments which are shown in parentheses and the theoretical moment diagrams which are shown dotted were obtained from an analysis of each assemblage using the loads shown in the figures. The solid lines represent the bending moments computed from the strains measured on the beams and columns. Fairly good correlation was obtained between the theoretical and experimental values except mainly in the interior region of the beams. However, some differences can be expected to occur since the theoretically computed moments do not take into account deformations of the members (column shortening, initial crookedness of the columns, etc.), slight eccentricities of load or slight variations in cross-section dimensions. The experimentally obtained moments are used in Chapter 6 where a detailed analysis of the test results is made.

5.3 Experimental Behavior

The experimental behavior of the two test assemblages will be discussed with reference to Figures 16 to 22 inclusive. Comparison with theoretical predictions and a detailed analysis of the test results will be presented in Chapter 6.

The experimental load-drift behavior of each assemblage is shown by the solid lines in Figures 16 and 19. The numbered circles on these curves correspond to the numbered drift increments (DI) shown on Figures 18 and 21, respectively. Two theoretical load-drift curves for each assemblage, as determined by two sway subassemblage analyses are shown by the dashed curves in Figures 16 and 19. These analyses were performed prior to testing and were used during testing to gage the progress of the tests. These two curves differ only in the assumed location of beam plastic hinges adjacent to the columns. Further discussion of these analyses is deferred to Chapter 6.

5.3.1 Assemblage SA-1 The experimental load-drift behavior of assemblage SA-1 is shown in Figure 16. The onset of yielding was first observed in the flanges of the windward (west) beam adjacent to the windward face of the interior column at drift increment number 3 (DI3). At DI4 yielding was also observed in the flanges at the top of the leeward (east) restrained column; (i.e., below the joint). At DI5 a considerable amount of yielding was observed in the flanges and webs at both of these locations.

Yielding of the flanges at the top of the interior restrained column was first observed at DI10, followed by initial yielding of the flanges of the windward beam under the windward loading point at DI11. At this point the maximum applied lateral load Q of 25.75 kips was reached. Between DI11 and DI13 the lateral load decreased slightly.

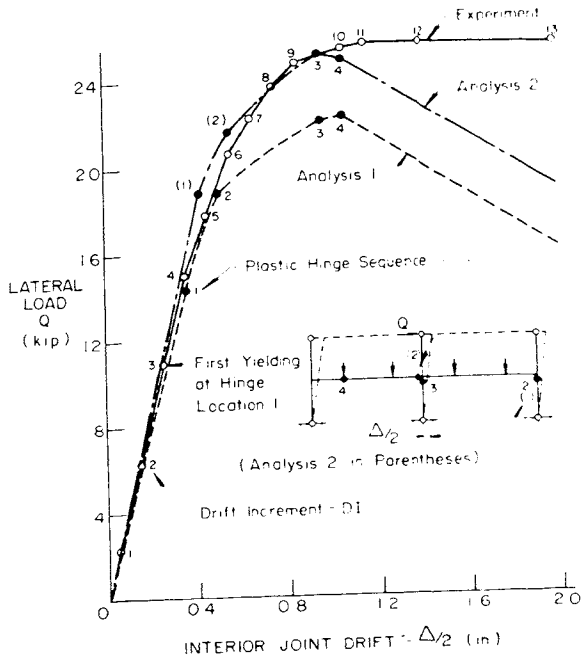

FIGURE 16. SA-1: Lateral load vs. drift behavior

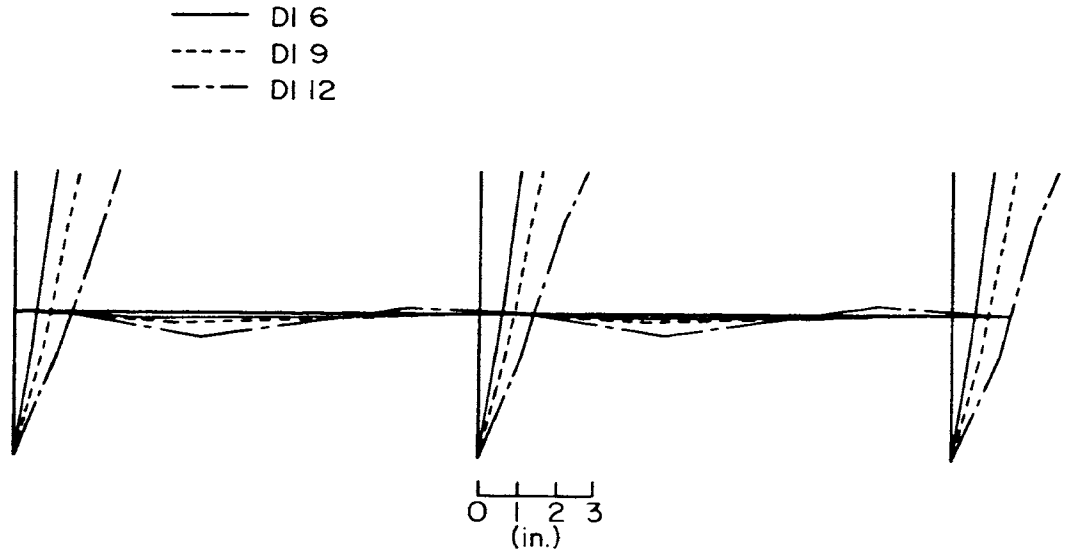

FIGURE 17. SA-1: Experimental drift and beam deflections

The test was terminated at DI13. No lateral-torsional or local buckling was observed prior to DI13. Four plastic hinges were observed to form in the sequence predicted by Analysis 1 and in the same locations (Fig. 16). Yielding was also observed in the beam between the windward column and hinge location 4.

The deflections of the assemblage at three stages of the test are shown in Figure 17. Even though the figure shows the measured deflection points connected by straight line segments, the angle changes at the locations of the plastic hinges are quite noticeable. This is particularly evident at the locations of the first three plastic hinges.

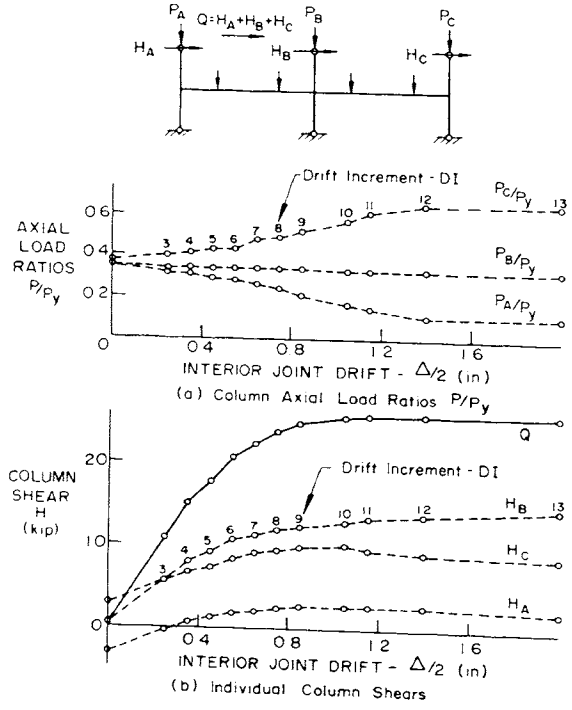

FIGURE 18. SA-1: Experimental column loads and shears

The experimental variations in the axial load ratios P/P_y for each of the three columns of assemblage SA-1 are shown in Figure 18(a). These ratios were computed using the applied loads P determined from the calibrated tension dynamometers connected to the gravity load simulators and the calculated values of P_y shown in Table II. The applied loads were also checked with the axial loads indicated by the column strain gages.

Figure 18(b) shows the experimental variation in shear at the top of each column of assemblage SA-1. These values were computed using the calibrated dynamometers in the horizontal struts between the column tops and checked with the shears indicated by the column strain gages. The shear H_A taken by the windward column reversed direction as expected. In addition the shears taken by the windward and leeward columns reached their maximum values and began to reduce prior to the drift increment corresponding to the maximum load carrying capacity of the assemblage. The total applied lateral load Q is the sum of the individual column shears, $H_A + H_B + H_C$.

5.3.2 Assemblage SA-2 The experimental load-drift behavior of assemblage SA-2 is shown in Figure 19. The onset of yielding was first observed at DI3 in the flanges of both beams adjacent to the windward faces of the interior and leeward columns. At DI5 yielding was also observed in the flanges of the beams at the windward loading points of both beams.

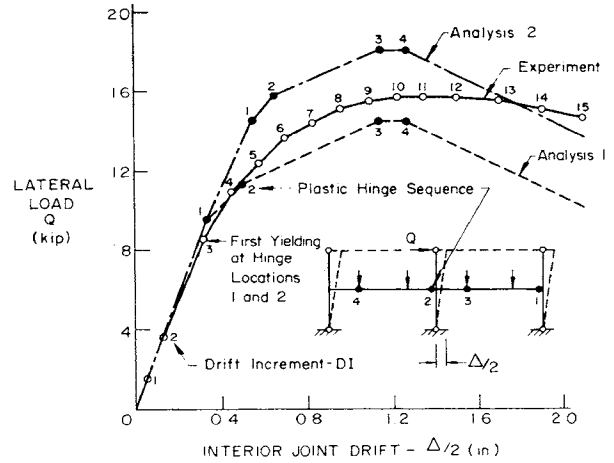

FIGURE 19. SA-2: Lateral load vs. drift behavior

Yielding of the flanges and webs of the beams at all four locations steadily progressed from DI5 until DI12 when the maximum load carrying capacity of 15.69 kips was reached. At this point a few yield lines were also visible in the leeward flanges at the tops of all three restrained columns. Between DI12 and DI15 the applied lateral load gradually reduced. The test was terminated at DI15. No lateral-torsional local buckling was observed prior to DI15. Four plastic hinges were observed to occur in the sequence predicted by Analyses 1 and 2 and in the same locations (Fig. 19). Yielding was also observed in the beams between the windward and interior columns and hinge locations 3 and 4.

The deflections of the assemblage at three stages of the test are shown in Figure 20. The columns remained essentially straight while the angle changes in the beams at the locations of plastic hinges are particularly noticeable.

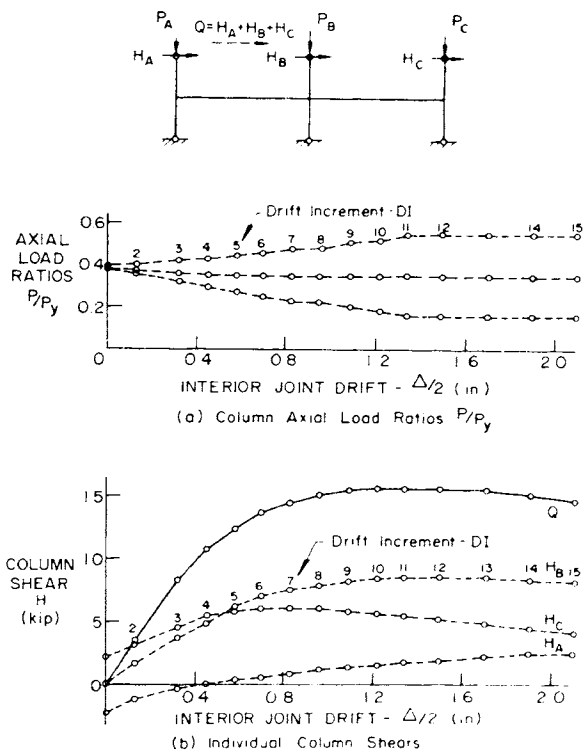

FIGURE 21. SA-2: Experimental column loads and shears

The experimental variations in axial load ratios P/P_y for the three columns of assemblage SA-2 are shown in Figure 21(a). These values were computed using the applied loads P determined from the calibrated tension dynamometers connected to the gravity load simulators and the calculated values of P_y shown in Table II. The applied loads were also checked with the axial loads indicated by the column strain gages.

Figure 21(b) shows the experimental variation in shear at the top of each column of assemblage SA-2. These values were computed using the

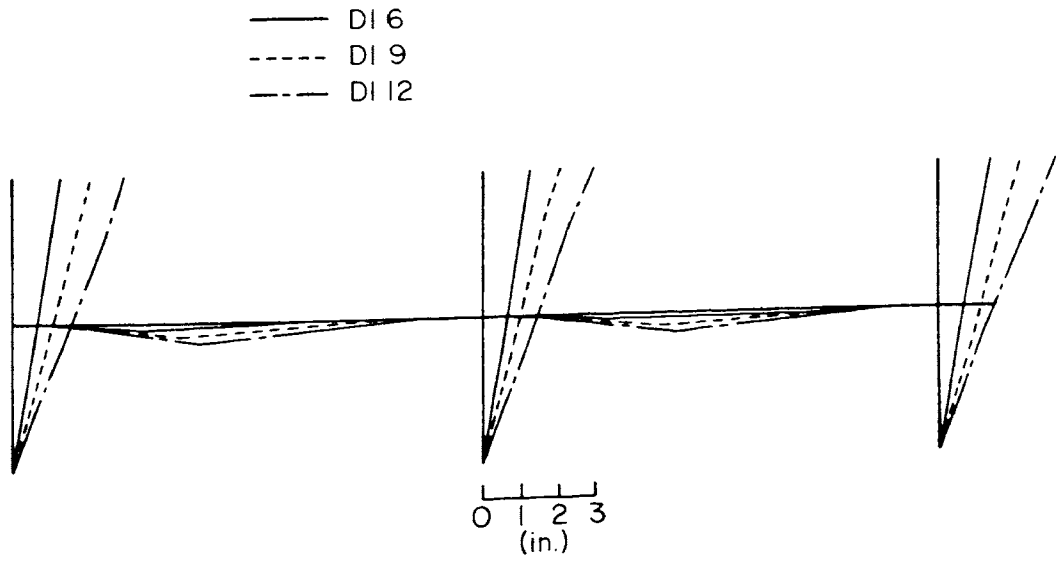

FIGURE 20. SA-2: Experimental drift and beam deflections

calibrated dynamometers in the horizontal struts between the column tops and checked with the shears indicated by the column strain gages. The shear H_A taken by the windward column reversed direction as expected. In addition the shear H_C taken by the leeward column reached a maximum value then began to reduce prior to the drift increment corresponding to the maximum load carrying capacity of the assemblage. The total applied lateral load Q is the sum of the individual column shears, $H_A + H_B + H_C$.

6. Theoretical Analysis and Discussion

6.1 Theoretical Prediction

Several sway subassemblage analyses were performed for each assemblage using the SMOA computer program previously developed at Fritz Engineering Laboratory (14, 15). In the analyses, the lengths of the columns were taken as the total distance between the pinned ends. However, the clear span length (face to face of columns) was assumed for each beam. These assumptions were based on the results of the Phase I studies (8).

Plastic hinges in the test assemblages actually develop over a certain finite length due to the effects of strain hardening, whereas in the analysis the plastic hinges are assumed to occur only at a particular cross-section. To account for this difference three separate analyses were performed for each assemblage. These analyses differed only in the assumed location of a plastic hinge forming in a beam cross-section adjacent to the columns. These cross-sections were assumed as follows:

Analysis 1: The cross-section at the face of a column.

Analysis 2: The cross-section located away from the face of a column a distance equal to the beam depth.

Analysis 3: The cross-section located away from the face of the column a distance equal to one-half the beam depth.

In each analysis plastic hinges in the columns were assumed to form in the cross-section at the center of a joint.

The actual mechanical and cross-section properties of the members, the actual dimensions of the assemblages, as fabricated and erected, and the actual applied beam and column loads were used in the SMOA analyses to determined theoretical load-drift behavior of each test assemblage. Analyses 1 and 2 were performed prior to carrying out the tests. Analysis 3 was performed after testing was completed.

6.2 Analysis of Behavior

6.2.1 Test Assemblage SA-1 The experimental load-drift curve for assemblage SA-1 is shown in Figure 16. Also shown are two theoretical curves plotted from the results of Analyses 1 and 2 of the assemblage. The sequence of formation of the plastic hinges is shown on the theoretical curves and also on the sketch of the assemblage in the figure. Each of the two analyses predicts a slightly different plastic hinge sequence. Analysis 2 requires a larger moment at the interior joint than that required by Analysis 1. As a result in Analysis 2, the first plastic hinge is required to develop in the leeward restrained column. The effect is to substantially increase the stability limit load predicted by Analysis 2.

Figure 16 shows that good correlation between the experimental and Analysis 1 load-drift curves was obtained up to about DI5. Beyond DI5 the assemblage carried substantially higher lateral load than that predicted by Analysis 1. The maximum load (25.75 kips) was only slightly higher than the stability limit load (25.20 kips) predicted by Analysis 2. However, the observed onset of yielding in the assemblage (Article 5.3.1) indicated that the plastic hinge sequence was that predicted by Analysis 1. In addition the lateral

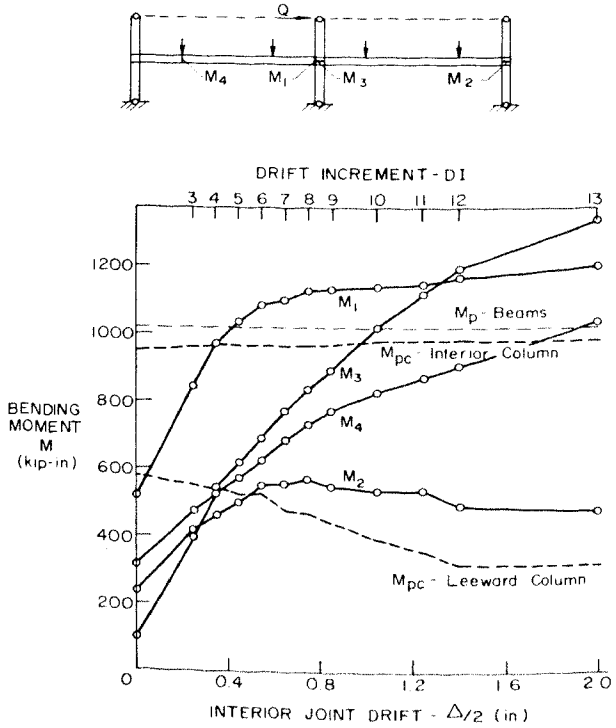

FIGURE 22. SA-1: Experimental moments at predicted plastic hinge locations

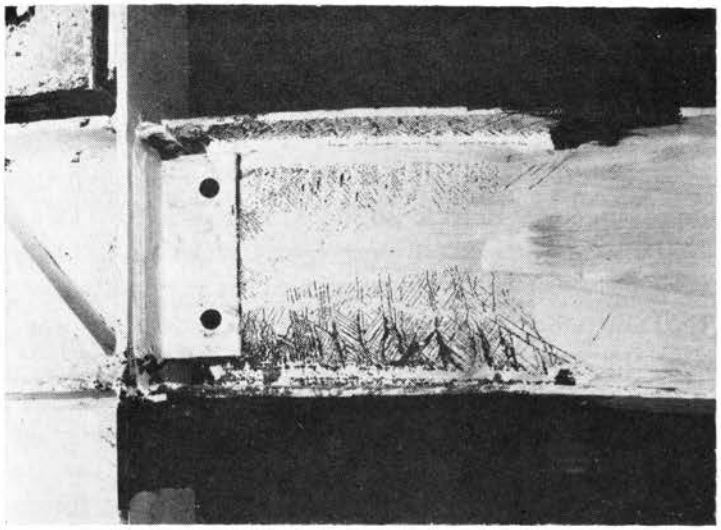

(a) Extent of yielding at plastic hinge location 1

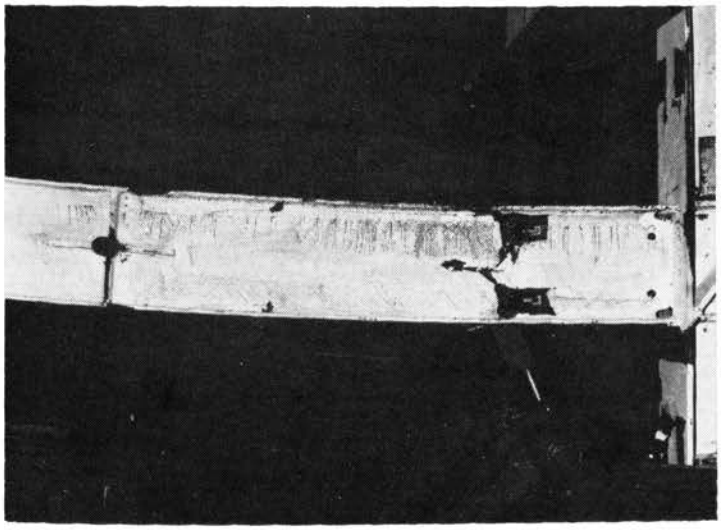

(b) Extent of yielding at plastic hinge location 4

FIGURE 23. Plastic hinges in the windward beam of assemblage SA-1

load did not reduce after a mechanism condition was reached as predicted by either analysis.

The major differences between the observed and the predicted behavior of assemblage SA-1 can be explained by examining Figure 22. This figure shows the experimental bending moment versus drift relationships at each of the plastic hinge locations assumed in Analysis 1. The welding residual moments (Fig. 13) have been included together with the moments resulting from the applied lateral load. It is apparent that by DI5 the plastic moment M_p of the beam was reached and slightly exceeded at hinge location 1. Similarly the M_{pc} of the leeward column had been reached at hinge location 2 by DI7. It is evident therefore that up to about DI5 fairly good correlation between the observed and the predicted behavior from Analysis 1 can be expected. However, between DI5 and DI7 the moments M_1 at hinge location 1 somewhat exceed M_p, thus delaying the formation of the column hinge at location 2. Beyond DI7 the bending moments M_1 and M_2 at both locations exceeded the respective plastic moment capacities of the members. Since these hinge locations are within regions of high moment gradient this increase can be attributed to the effect of strain hardening. This effect was not directly considered in Analysis 1. Thus Analysis 1 predictions can be expected to underestimate the lateral load capacity and overestimate drift for all drifts in excess of DI5.

Analysis 2 considers the effect of strain hardening indirectly in an approximate way by requiring that the M_p at plastic hinge location 1 be reached at a cross-section a beam depth away from the column face. This analysis more closely predicted the maximum load capacity of the assemblage which, of course, is affected by strain hardening.

Observations made during the tests indicated that yielding of the windward beam at hinge location 1 had spread to a distance about equal to the beam depth away from the column face. The extent of yielding at this location is shown in Figure 23. On this basis Analysis 3 was performed, in which the plastic hinge at location 1 was assumed to be more realistically concentrated at a cross-section one-half the beam depth away from the column face. The corresponding bending

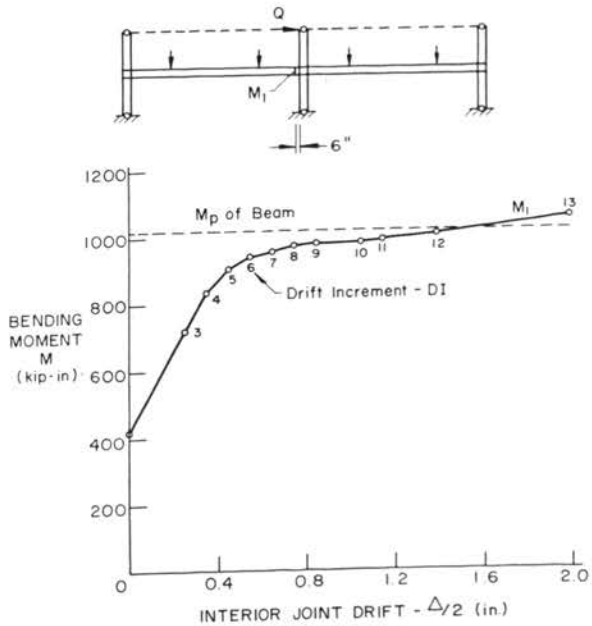

FIGURE 24. SA-1: Experimental moment at predicted plastic hinge location 1

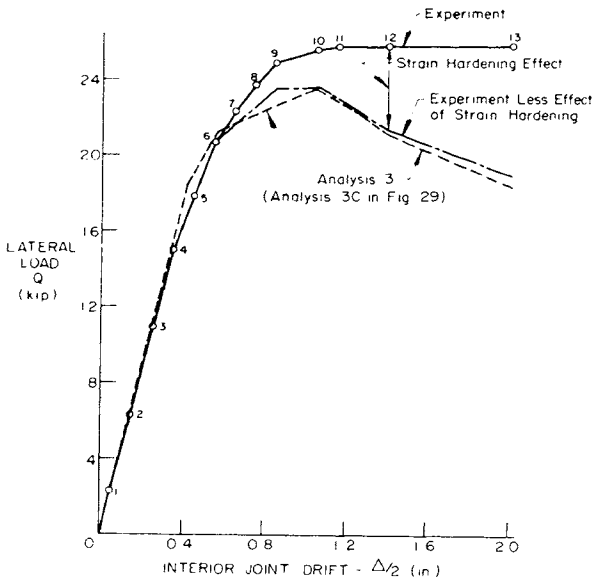

FIGURE 25. SA-1: Comparison of experimental and predicted lateral load vs. drift behavior

moment vs. drift relationship which includes the welding residual moments is shown in Figure 24. Since the moment M_1 at this cross-section more nearly approximates M_p for drifts in excess of DI5, the results of Analysis 3 can be expected to more closely predict the test results if the effect of strain hardening is isolated and eliminated from the test results.

The experimental load-drift curve for assemblage SA-1 is again shown in Figure 25, and compared with the theoretical curve obtained from the results of Analysis 3 for the assemblage considering the actual variation in the column loads (Article 6.3.1). Also shown in the figure is an experimental load-drift curve where the effect of strain hardening has been eliminated. The increments of lateral load attributed to strain hardening were calculated for each drift increment based on the difference between the actual column moments at the centers of the joints and the computed values of M_{pc} based on the actual applied column loads also taking into account the $P\Delta$ effect. It is evident from the figure that the correlation between the results of Analysis 3 and the modified experimental results is quite good.

6.2.2 Test Assemblage SA-2 The experimental load-drift curve for assemblage SA-2 is shown in Figure 19. Also shown are two theoretical curves plotted from the results of Analyses 1 and 2 for the assemblage. The sequence of formation of the plastic hinges is shown on the theoretical curves and also on the sketch of the assemblage shown in the figure. The same plastic hinge sequence is predicted by both analyses.

Figure 19 shows that good correlation between the experimental and Analysis 1 load-drift curves was obtained up to about DI5. Beyond DI5 the assemblage carried a higher lateral load (15.69 kips) than that predicted by Analysis 1 (14.50 kips) but less than that predicted by Analysis 2 (18.05 kips). The lateral load did reduce somewhat after a mechanism condition was reached but not so abruptly as predicted by either analysis.

The major differences between the observed and the predicted behavior of assemblage SA-2 can be explained by examining Figure 26. This figure shows the experimental bending moment vs. drift increment relationships at each of the plastic hinge locations assumed in Analysis 1. Considering the effect of welding residual moments (Article 5.1) it is evident that the M_p of the beam was essentially reached at hinge locations 1 and 2 by DI5. This correlates well with the observed onset of yielding (Article 5.3.2) which occurred simultaneously at both locations at DI3. A plastic hinge condition was not reached at hinge locations 3 and 4 until about DI13 and DI14.

It is evident from Figure 26 that up to DI5 good correlation between observed and predicted behavior can be expected. However, beyond DI5 the bending moments M_1 and M_2 at hinge locations 1 and 2 exceeded the respective plastic moment capacities M_p of the beams. Since both hinge locations are in regions of high moment

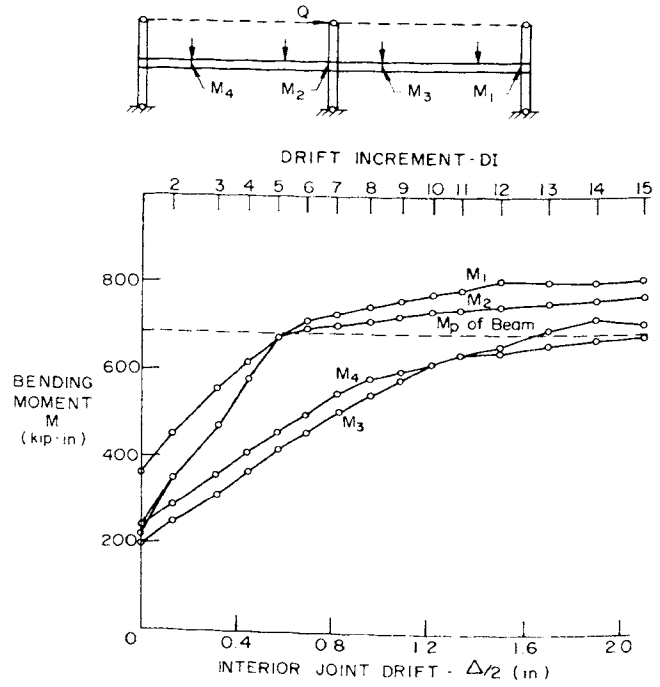

FIGURE 26. SA-2: Experimental moments at predicted plastic hinge locations

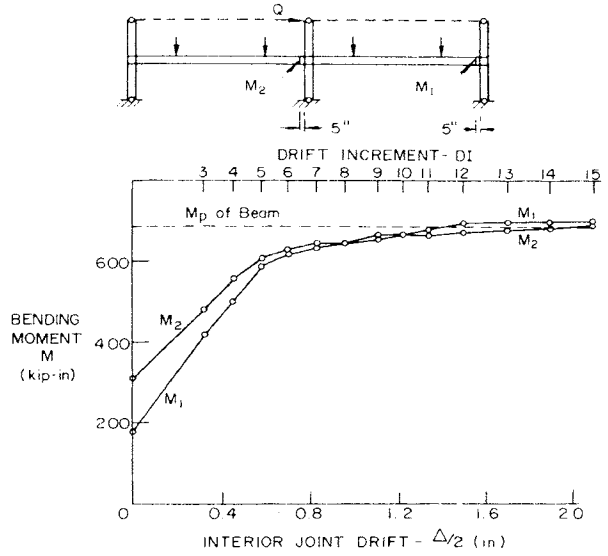

FIGURE 27. SA-2: Experimental moments at predicted plastic hinge locations 1 and 2

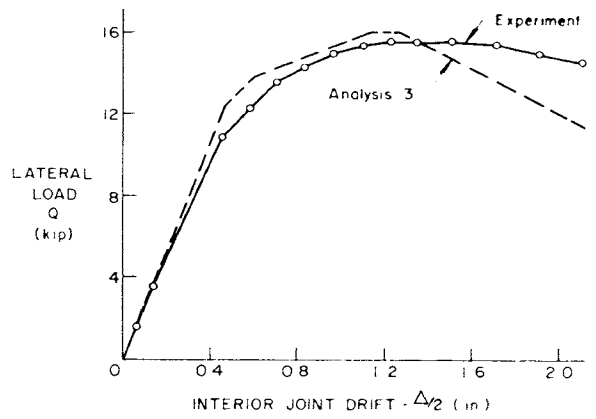

FIGURE 28. SA-2: Comparison of experimental and predicted lateral load vs. drift behavior

gradient this increase can be attributed to the effect of strain hardening. As mentioned in Article 6.2.1, this effect was not considered in Analysis 0. Thus Analysis 1 predictions will underestimate the lateral load capacity and overestimate drift of the assemblage beyond DI5.

Analysis 2 considers the effect of strain hardening indirectly in an approximate way by requiring that the M_p at plastic hinge locations 1 and 2 be reached at a cross-section a beam depth away from the column face. Analysis 2 actually overestimates the lateral load capacity and underestimates drift beyond DI5.

Observations made during the test indicated that as in assemblage SA-1 yielding of the beams at hinge locations 1 and 2 had spread to a distance about equal to the beam depth away from the column face [Fig. 23(a)]. On this basis Analysis 3 was performed, in which the plastic hinges at locations 1 and 2 were assumed to be more realistically concentrated at a cross-section one-half the beam depth away from the column face. The bending moment vs. drift relationships at hinge locations 1 and 2 are shown in Figure 27. The residual welding moments at these locations have been considered. It is evident that the moments at these locations more closely approximates M_p after DI5.

The experimental load-drift curve for assemblage SA-2 is again shown in Figure 28, and compared with the theoretical curve obtained from the results of Analysis 3 of the assemblage. Good correlation between experimental and theoretical results is obtained up to the maximum load level. Beyond that, the excess load capacity may be attributed to the effects of strain hardening in the beams, as was discussed in Article 6.2.1.

6.3 Effect of Variation of Column Loads

Sway subassemblage theory indicates that if the total gravity load carried by the restrained columns in a one-story assemblage is constant there will be no effect on the load-drift behavior of the assemblage due to variations in the distribution of the gravity load to the columns, providing that plastic hinges do not form in the restrained columns (3, 15). Plastic hinges were predicted to form in the interior and leeward restrained columns of assemblage SA-1. Plastic hinges did occur in these columns during the test. An analysis of assemblage SA-1 and a comparison with the experimental results will indicate the significance of variations of the column loads on the load drift behavior of the assemblage.

Figure 29 again shows the experimental load-drift behavior of SA-1 modified to eliminate the effects of strain hardening in the columns (Article 6.2.1 and Fig. 25). The modified experimental results are compared in the figure with three theoretical load-drift curves computed using the Analysis 3 assumptions (Article 6.1). The differences between the three analytical curves are entirely due to variations in the assumed column loads. In the analyses the axial load ratios P/P_y assumed for the windward (column A), interior (column B) and leeward (column C) restrained columns of assemblage SA-1 were as follows (see also Fig. 18)

Analysis 3A: $P_A/P_y = 0.35$; $P_B/P_y = 0.35$; $P_C/P_y = 0.36$.

This corresponds to the assumption of a uniform distribution of total gravity loads. The ratios

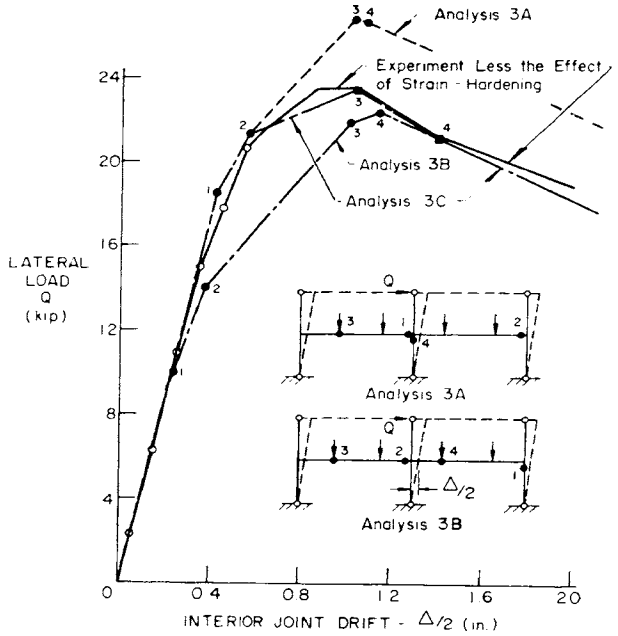

FIGURE 29. SA-1: Effect of variation of column loads on lateral load vs. drift behavior

were computed from the average of the nearly constant total gravity loads in the restrained columns during the test. These ratios were maintained constant in Analysis 3A.

Analysis 3B: $P_A/P_y = 0.11$; $P_B/P_y = 0.33$; $P_C/P_y = 0.65$.

This corresponds to the distribution of the total gravity loads to the columns at the end of the test. These ratios were maintained constant in Analysis 3B.

Analysis 3C:

The load-drift curve in Figure 29 was plotted from the results of 13 separate analyses, one for each drift increment (DI) used in the test. In each analysis the axial load ratio P/P_y selected for each column was held constant. The ratios selected for a particular analysis were those actually applied during the test at a particular drift increment. Thus the load-drift curve in Figure 29 represents the effect of maintaining the total gravity loads constant but varying the distribution to each column as the drift was varied. This closely represents the practical loading case for an unbraced frame.

Also shown in Figure 29 are the locations and sequences of formation of the plastic hinges predicted by each of the three analyses. The behavior predicted by Analysis 3C is identical to that predicted by Analysis 3A up to the second plastic hinge. At this point the moment at the top of the leeward restrained column also reached M_{pc} for that column (M_{pc} is steadily decreasing due to increasing P/P_y in the leeward column). As the lateral load and drift continue to increase the magnitude of M_{pc} at the top of the leeward restrained column continues to decrease (thus causing the moment at the end of the leeward beam to also decrease) and the second plastic hinge shifts from the beam to the top of the restrained column (hinge position 1 in Analysis 3B). With further increases in lateral load and drift the third plastic hinge eventually forms in the windward beam as indicated in the figure. At this stage the maximum lateral load capacity of 23.5 kips is reached. Beyond this point additional drift results in decreasing lateral load. The value of M_{pc} at the top of the leeward restrained column still continues to decrease however because P/P_y in that column is still increasing (Fig. 18), thus maintaining the plastic hinge at that point. Because of the reduction in moment at the leeward end of the leeward beam (joint equilibrium being maintained) the positive moment at the windward loading point of that beam continues to increase even though the bending moment in the beam due to the applied lateral loads is decreasing. Finally, the fourth plastic hinge develops in the leeward beam as predicted by Analysis 3B.

Comparison of the analytical results with the modified experimental load-drift behavior in Figure 29 indicates that excellent correlation was achieved between the two curves. The difference between the observed location and sequence of plastic hinges (Article 5.3.1 and Fig. 16) and that predicted by Analysis 3C above can be readily explained with reference to strain hardening of the interior and leeward restrained columns. In the absence of strain hardening the moments at the interior and leeward joints are somewhat smaller than the moments observed in the test. As a result the third and fourth plastic hinges form as predicted by Analysis 3B. Due to strain hardening, the moment in each restrained column is increased above the theoretical values of M_{pc}. The redistribution of moments in the assemblage is altered so that the third hinge forms in the interior column instead of the windward beam. The fourth hinge finally forms in the windward beam as shown in Figure 23(b).

The theoretical load-drift curve for assemblage SA-2 shown in Figure 28 remains the same regardless of the distribution of gravity loads to the

columns. This is a consequence of the fact that no plastic hinges are predicted to occur in the restrained columns. As shown in the figure, fairly good correlation between the experimental and predicted load-drift behavior of assemblage SA-2 was obtained. The difference that did occur can be attributed partly to the slight strain hardening of the third plastic hinge beyond DI13 (Fig. 26), partly to assumptions used in the analysis which were not exactly attained in the experiment and partly to experimental error. In view of the major effect of the variation of column loads exhibited in assemblage SA-1, it can be concluded that the variation in column loads for assemblage SA-2 had little or no effect on the load-drift behavior of the assemblage.

The implication of the above results on the use of sway subassemblage theory to predict the load-drift behavior of one-story assemblages is as follows:

1. For assemblages in which column plastic hinges are not expected to occur use any reasonable distribution of the total gravity loads to the column when performing the analysis. For instance the distribution obtained under gravity loads alone could be used.

2. For assemblages in which column plastic hinges are expected to occur, or when it is not known if column plastic hinges will occur, consider the probable variation in column loads in the analysis. For the zero drift condition, the distribution of gravity loads to the columns will be for the gravity load alone case as in (1) above. For drifts in the vicinity of the stability limit load or the mechanism load, a reasonable estimate of the column loads can be obtained from a moment balancing solution of the frame or from a prior frame analysis if preliminary designs of the frame are being carried out. For intermediate values of drift the column loads can be obtained from a linear variation of the total changes in the column loads as was performed in this report.

7. Summary and Conclusions

Tests were conducted on two one-story assemblages. One assemblage was designed to simulate the expected behavior of a story close to the top of an unbraced multi-story frame. The other was designed to simulate the expected behavior of a story near the bottom of the frame. Several analyses of the assemblages were carried out by computer using a computer program (SMOA) previously developed from sway subassemblage theory (3, 14, 15). The analyses were used to obtain predicted lateral load versus drift curves for the assemblages. The several predicted load-drift curves differed in the assumed locations of beam plastic hinges adjacent to the columns and in the assumed distribution of the total constant gravity loads to each of the columns. Excellent correlation between experimental and predicted behavior was obtained, especially when the effect of strain hardening, neglected in the analyses, was accounted for in the experimental results.

The major conclusions based on the results of this investigation are as follows:

1. The load-drift behavior of each assemblage was essentially as predicted. The location and sequence of formation of plastic hinges were as predicted.

2. The experimental behavior of both assemblages compared best with predicted behavior when plastic hinges at the leeward ends of the beams were assumed in the analysis to form at a cross-section located one-half the beam depth away from the face of the column.

3. Strain hardening of plastic hinges at the top of restrained columns had a significant effect on the load-drift behavior of an assemblage. Neglecting strain hardening in the analysis had the effect of underestimating the lateral load capacity of the assemblage and overestimating drift.

4. Variation in the distribution of gravity loads to the columns as drift increases has a significant effect on the load-drift behavior of an assemblage only if plastic hinges occur in one or more restrained columns. This conclusion is in accordance with sway subassemblage theory.

References

1. Daniels, J. H., and Lu, L. W., "The Subassemblage Method of Designing Unbraced Multistory Frames," Fritz Engineering Laboratory Report No. 273.37, Lehigh University, Feb. 1966.
2. Daniels, J. H., and Lu, L. W., "Design Charts for the Subassemblage Method of Designing Unbraced Multistory Frames," Fritz Engineering Laboratory Report No. 273.54, Lehigh University, March 1966.
3. Daniels, J. H., "Combined Load Analysis of Unbraced Frames," Ph.D. Dissertation, Fritz Engineering Laboratory Report No. 338.2, Lehigh University, July 1967.
4. Daniels, J. H., and Lu, L. W., "Sway Subassemblage Analysis for Unbraced Frames," Paper presented at the Sept. 30 to Oct. 4, 1968, ASCE Annual Meeting and Structural Engineering Conference held at Pittsburgh, Pa., ASCE Preprint No. 717.
5. Levi, V., Driscoll, G. C., Jr., and Lu, L. W., "Analysis of Restrained Columns Permitted to Sway," *Proc. ASCE*, Vol. 93, No. ST1, Feb. 1967.
6. Kim, S. W., Daniels, J. H., and Lu, L. W., "Technical Proposal No. 1—Restrained Column Tests," Fritz Engineering Laboratory Report No. 346.1, Lehigh University, Sept. 1967.
7. Kim, S. W., Daniels, J. H., and Lu, L. W., "Technical Proposal No. 2—Comparative Behavior of Two One-Story Assemblages," Fritz Engineering Laboratory Report No. 346.2, Lehigh University, June 1969.
8. Kim, S. W., and Daniels, J. H., "Experiments on Restrained Columns Permitted to Sway," Fritz Engineering Laboratory Report No. 346.3, June 1970.
9. Hansell, W. C., "Preliminary Design of Unbraced Multistory Frames," Ph.D. Dissertation, Lehigh University, 1966, University Microfilms, Inc., Ann Arbor, Mich.

10. Yarimci, E., Yura, J. A., and Lu, L. W., "Techniques for Testing Structures Permitted to Sway," Fritz Engineering Laboratory Report No. 273.40, Lehigh University, May 1966.
11. Driscoll, G. C., Jr., et al., "Plastic Design of Multistory Frames —Lecture Notes," Fritz Engineering Laboratory Report No. 273.20, Lehigh University, Sept. 1965.
12. Yarimci, E., "Incremental Inelastic Analysis of Framed Structures and Some Experimental Verifications," Ph.D. Dissertation, Lehigh University, May 1966.
13. Lay, M. G., and Galambos, T. V., "Tests on Beam-and-Column Subassemblages," Fritz Engineering Laboratory Report No. 278.10, Lehigh University, June 1964.
14. Driscoll, G. C., Armacost, J. O., and Hansell, W. C., "Plastic Design of Multistory Frames by Computer," *Journal of the Structural Division, ASCE*, Vol. 96, No. ST1, Jan. 1970.
15. Daniels, J. H., and Lu, L. W., "Subassemblage Analysis for Unbraced Frames," Submitted Sept. 1971 for publication in the *Journal of the Structural Division, ASCE*.

Design Example

The load-deflection behavior of the one-story assemblage at Level 8 of the frame shown in Figure 1 will be determined by the subassemblage method. The uniformly distributed factored gravity loads on the beams (0.321 kips per inch) and the axial loads in the columns are maintained constant. These loads are determined in accordance with the working loads shown in Figure 1, using a load factor of 1.3 and the live load reduction factors suggested by ASA A58.1. The load-drift behavior is determined for the wind from left condition only. Although the analysis is more easily and quickly accomplished by computer, step-by-step manual calculations are presented in Plates I to VI to illustrate the procedure.

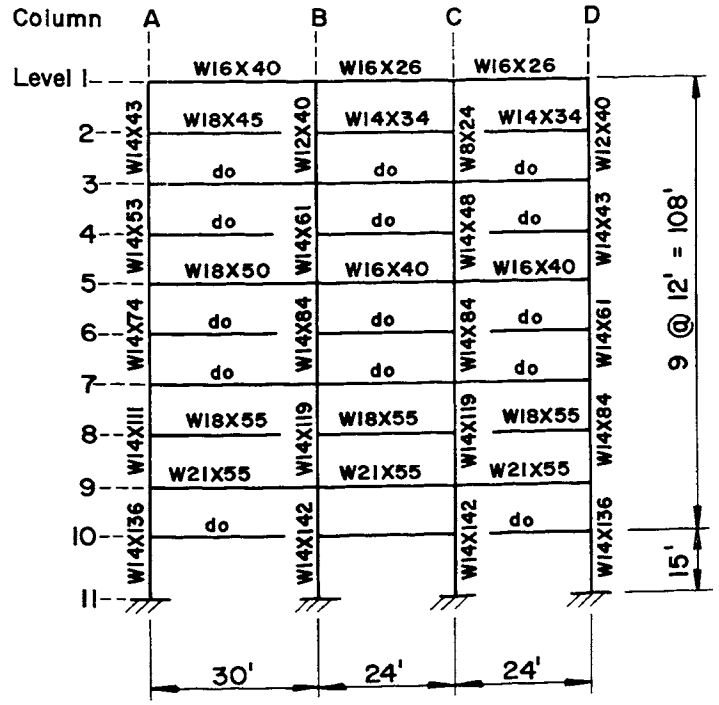

Bent Spacing = 24' ASTM A36 Steel

Working Loads

Level 1	w_D = 60 psf	w_L = 30 psf
Levels 2-10	w_D = 80 psf	w_L = 80 psf
Exterior Wall	w_D = 45 psf	
Wind	w_W = 20 psf	

Percent Live Load Reduction by ASA A58.1

FIGURE 1. Preliminary frame design

The first step is to isolate the one-story assemblage at Level 8 from the frame. The resulting one-story assemblage with known member sizes is shown in Plate I. Also shown are the distribution of bending moments under gravity loads alone ($\Delta/h = 0$), column and beam properties and the initial restraint coefficients.

The analysis of the one-story assemblage initially involves the calculation of the nondimensional rotational restraint stiffnesses M_r at each joint before and after the formation of each plastic hinge. In addition the nondimensional restraining moments M_r at each joint are calculated under the gravity loads alone and under the combined loads at the formation of each plastic hinge.

The comments which follow are intended to clarify the correspondingly lettered items in Plates I and III. Comments concerning calculations in Plate III will also be relevant to corresponding calculations in Plates II and IV.

Plate I

(a) The distribution of bending moments is determined by elastic analysis, assuming each column is laterally restrained at both ends and at mid-height.

(*b*) The column axial forces are computed on the basis of a mechanism condition occurring in each story of the frame under the combined loads, assuming wind from the left.

(c) The reduced plastic moment capacity M_{pc} of each column was computed from Eq. (5) of Part 1 of this Bulletin.

(d) The minimum plastic moment required to resist 1.3 times the working gravity loads is defined as M_{pm}.

$$M_{pm} = \frac{1.3wL^2}{16}$$

where L = beam span center-to-center of adjacent columns and w = uniformly distributed working

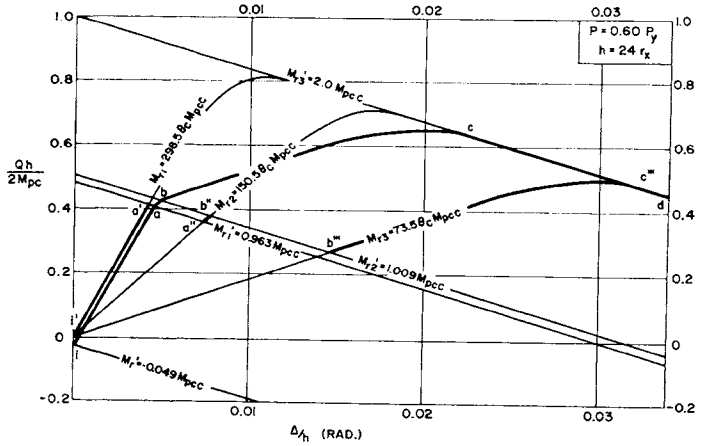

FIGURE 2. Construction of load-drift curve for sway subassemblage B1)

gravity load per unit of span length. It is convenient to use this moment as a nondimensionalizing factor when determining the total sway resistance of a beam.

(e) The initial restraint coefficients are computed from Eq. (15) of Part 1 of this Bulletin.

Plate III

(a) The analysis of interior subassemblage A-C begins by determining the total change in moment in the columns at joint B as sway Δ/h increases from the initial zero drift condition to the occurrence of the first plastic hinge in the subassemblage.

(b) The total change in moment in the columns at joint B is now required as the drift is further increased up to the formation of the second plastic hinge in the subassemblage.

(c) With the first two plastic hinges found to occur at the leeward ends of the two beams, the third or last plastic hinge can only occur somewhere in the windward half span of beam BC or in the columns at joint B.

(d) The initial moment in the columns under the gravity loads alone and zero drift is equal to the net moment from the beams or $M_e = 3514 - 2335 = 1179$ k-in.

(e) The initial value of nondimensional restraining moment M_{r1} is now determined.

(f) The nondimensional restraining moment at joint B when the first plastic hinge occurs is the sum of the initial restraining moment, $0.388M_{pcB}$ and the moment found in (d).

(g) For increased drift beyond the first plastic hinge, beams AB can no longer contribute to the rotational restraint stiffness at joint B. Thus the restraint stiffness in the interval between the first and second plastic hinges decreases to that provided by beam BC alone. The corresponding joint rotation increment $\delta\theta_B$ is 0.00238.

(h) The nondimensional restraining moment at joint B when the second plastic hinge forms is again equal to the sum of the restraining moment at joint B when the first plastic hinge forms, 0.744 M_{pcB} plus the increase in restraining moment up to the second plastic hinge.

(i) Since the second plastic hinge occurred at the leeward end of beams BC, K_{BC} reduces from 5.949 to 3.0 when calculating the restraint stiffness M_{r3} between the second and third plastic hinges.

(j) Since the third and last plastic hinge forms in the columns at joint B the total moment resisted by the two columns M_{r3}' must be equal to twice the reduced plastic moment capacity M_{pcB} of the restrained column.

Load-Drift Behavior of the Four Subassemblages

The construction of the nondimensional load-drift curve for subassemblage B-D, is shown in

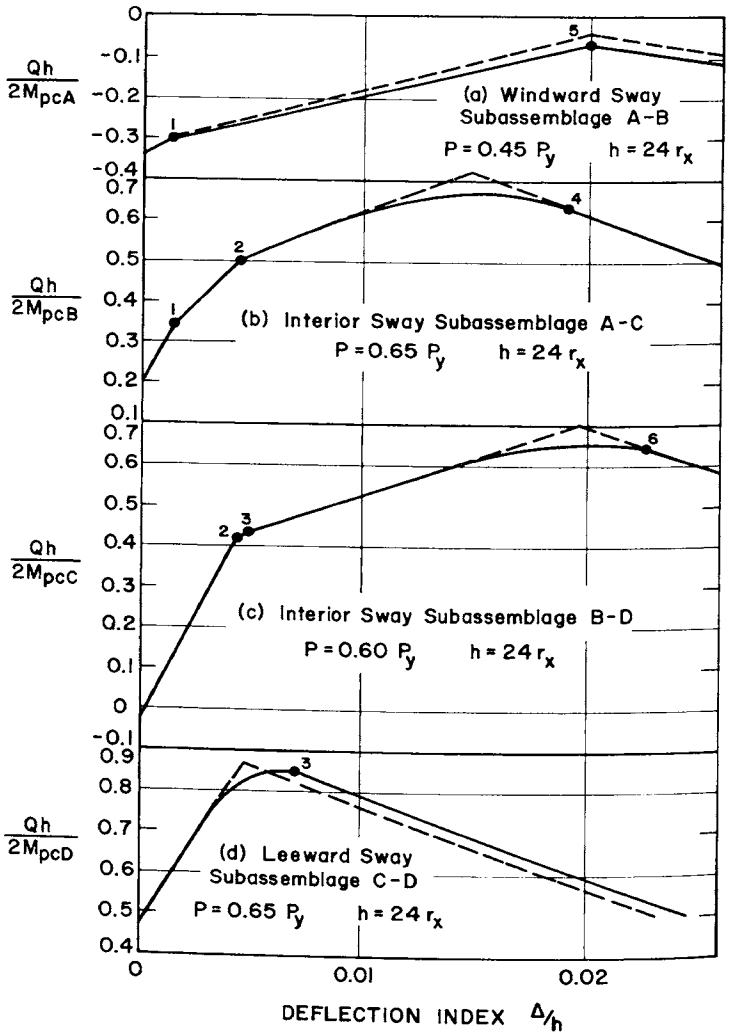

FIGURE 3. Four sway subassemblage curves

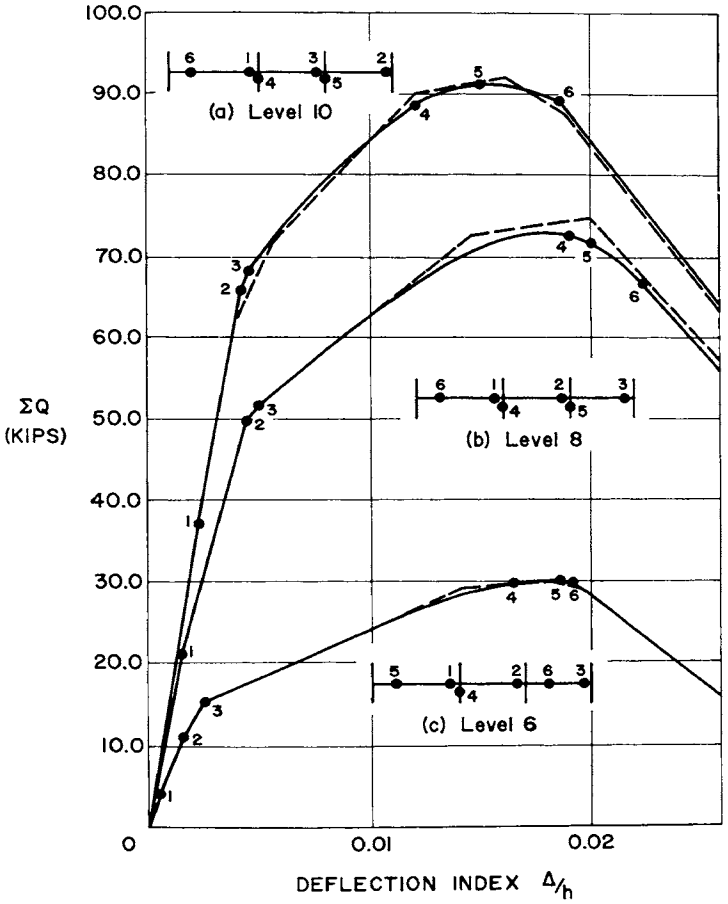

FIGURE 4. One-story assemblage curves for levels 6, 8 and 10

Figure 2. The set of M_r values calculated in Plate IV will determine the three complete restrained column curves o-a′-c, o-a″-c and o-b‴-d shown in the figure. These curves are given by Eq. (8) in Part 1. Similarly the set of M_r' values will define the four sloping straight lines shown in the figure. The initial segment of the load-drift curve is i-a. This segment is parallel to o-a′ of the load-drift curve corresponding to M_{r1}. The first plastic hinge occurs at point a, which lies on the intersection of curve i-a with the straight line corresponding to M_{r1}'. Similarly, the second segment, a-b, is parallel to segment a″-b″, and the third segment, b-c, is parallel to segment b‴-c‴. The last plastic hinge occurs in the columns at point c on the load-deflection curve. The final segment, c-d is the second-order plastic mechanism curve for the subassemblage.

The nondimensional load-drift relationships of the four subassemblages at Level 8 are shown in Figure 3. In each case, the solid curves indicate the behavior determined in this analysis. The dashed curves were obtained using the computer analysis described in Part 1 of this Bulletin.

Load-Drift Behavior of the One-Story Assemblage

Transforming the ordinates to the curves in Figure 3 from $Qh/2M_{pc}$ to Q and summing, results in the load-drift curves for the one-story assemblage at Level 8 as shown in Figure 4. Also shown are the corresponding curves for the one-story assemblages at Levels 6 and 10 as computed manually (solid) and by computer (dashed). The sequence of formation of the plastic hinges in the one-story assemblages are also shown in Figure 4.

ONE-STORY ASSEMBLAGE AT LEVEL 8

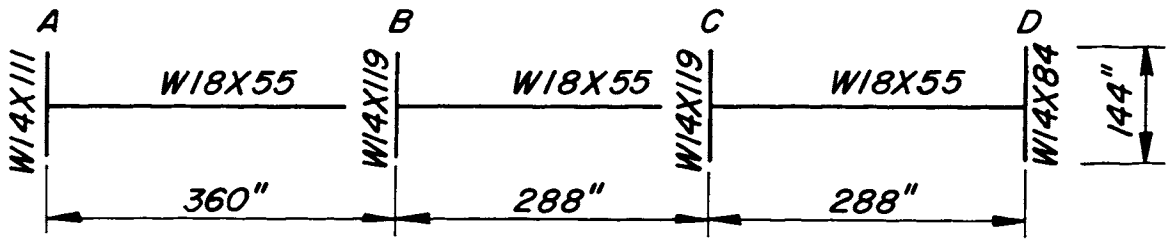

BENDING MOMENTS - Gravity Loads Only and $\Delta/h = 0$ (a)

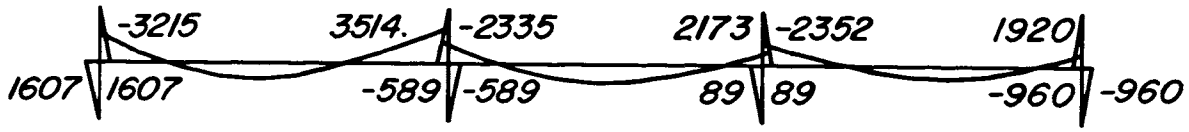

RESTRAINED COLUMN PROPERTIES - Wind From Left Only

Restrained Column	Section	P_y	h/r_x	Wind From Left		
				P (b)	P/P_y	M_{pc} (c)
Units		Kips		Kips		K-in.
A8 - A9	W14X111	1175	23.1	505	0.430	4740
B8 - B9	W14X119	1260	23.0	833	0.661	3040
C8 - C9	W14X119	1260	23.0	745	0.591	3660
D8 - D9	W14X84	889.6	23.5	597	0.671	2040

BEAM PROPERTIES AT LEVEL 8

Girder	Section	M_p	M_{pm} (d)	I	L
Units		K-in.	K-in.	$in.^4$	$in.^4$
A8 - B8	W18X55	4010	2600	889.9	360
B8 - C8	W18X55	4010	1670	889.9	288
C8 - D8	W18X55	4010	1670	889.9	288

INITIAL RESTRAINT COEFFICIENTS (e)

Joint	K_{right}	K_{left}
A8	K_{AB} = 5.750	
B8	K_{BC} 5.949	K_{BA} = 6.286
C8	K_{CD} 6.154	K_{CB} = 6.053
D8		K_{DC} = 5.857

Notes

1. E = 29,000 ksi in the analysis, and
2. Letters in parentheses refer to items which are discussed in the text.

WINDWARD SWAY SUBASSEMBLAGE A-B

First Plastic Hinge:

$$\delta M_{BA} = 496 = 6.286 \times \frac{E \times 889.9}{360} \times \frac{5.750-4}{2}\,\delta\theta_A$$

$$= 13.6\,E\,\delta\theta_A\ ; \qquad \therefore E\,\delta\theta_A = 36.5$$

$$\delta M_{AB} = 5.750 \times \frac{889.9}{360} \times 36.5 = 518\ \text{k-in.}$$

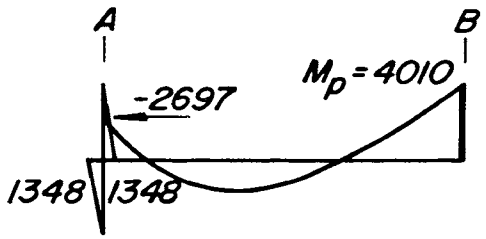

Second Plastic Hinge:

$$\frac{F_1}{F_2} = \frac{16 \times 4010}{0.321 \times 360^2} = 1.54\ ;$$

$$\therefore \frac{M_{min}}{M_{pm}} = 0.38\ ; \quad M_{min} = 0.38 \times 2600 = 987\ \text{k-in.}$$

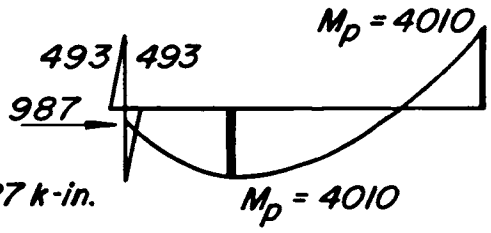

Check: $987 < 2\,M_{pcA}$ (OK) $\quad \delta M_{AB} = 987 - (-2697) = 3684$ k-in.

Determine M_r and M_r' Values:

Initial $(\Delta/h = 0)$: $\quad M_r' = -\frac{3215}{4740}\,M_{pcA} = \underline{-0.678\,M_{pcA}}$

$$M_{r1} = 5.75 \times \frac{29{,}000 \times 889.9}{360 \times 4740}\,\theta_A\,M_{pcA} = \underline{87.0\,\theta_A\,M_{pcA}}$$

$$\delta M_A = 518 = 87.0 \times 4740\,\delta\theta_A \qquad \therefore \delta\theta_A = \frac{518}{412{,}000} = 0.00126\ \text{rad.}$$

$$M_{r1}' = (87 \times 0.00126 - 0.678)\,M_{pcA} = \underline{-0.568\,M_{pcA}}$$

$$M_{r2} = 3.0 \times \frac{29{,}000 \times 889.9}{360 \times 4740}\,\theta_A\,M_{pcA} = \underline{45.4\,\theta_A\,M_{pcA}}$$

$$\delta M_A = 3684 = 45.4 \times 4740\,\delta\theta_A \qquad \therefore \delta\theta_A = \frac{3684}{215{,}500} = 0.0171\ \text{rad.}$$

$$M_{r2}' = (45.4 \times 0.0171 - 0.568)\,M_{pcA} = \underline{0.209\,M_{pcA}}$$

LEEWARD SWAY SUBASSEMBLAGE C-D

First Plastic Hinge: $\delta M_{DC} = 4010 - 1920 = 2090$ k-in.

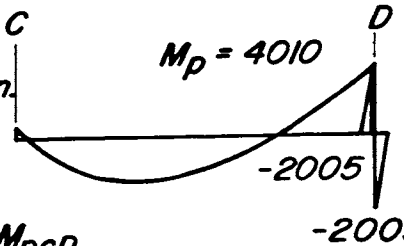

Determine M_r and M_r' Values:

Initial $(\Delta/h = 0)$: $\quad M_r' = \frac{1920}{2040}\,M_{pcD} = \underline{0.941\,M_{pcD}}$

$$M_{r1} = 5.857 \times \frac{29{,}000 \times 889.9}{288 \times 2040}\,\theta_D\,M_{pcD} = 257\,\theta_D\,M_{pcD}$$

$$\delta M_D = 2090 = 257 \times 2040\,\delta\theta_D \qquad \therefore \delta\theta_D = \frac{2090}{525{,}000} = 0.00398\ \text{rad.}$$

$$M_{r1}' = (257 \times 0.00398 + 0.941)\,M_{pcD} = \underline{1.963\,M_{pcD}}$$

INTERIOR SWAY SUBASSEMBLAGE A-C

First Plastic Hinge: (a)

$\delta M_{BA} = 496 = 6.286 \times \frac{E \times 889.9}{360}\ \delta\theta_B = 15.5E\ \delta\theta_B$; $\therefore E\delta\theta_B = 31.9$

$\delta M_{BC} = 5.949 \times \frac{889.9}{360} \times 31.9 = 586$ k-in.; $\delta M_{CB} = 6.053 \times \frac{889.9}{360} \times 31.9 \times \frac{5.949-4}{2} = 581$ k-in.

Second Plastic Hinge: (b)

$\delta M_{CB} = 1256 = 6.053 \times \frac{E \times 889.9}{288} \times \delta\theta_C = 18.7E\ \delta\theta_C$; $\therefore E\delta\theta_C = 67.1$

$\delta M_{BC} = 5.949 \times \frac{889.9}{288} \times 67.1 \times \frac{6.053-4}{2} = 1265$ k-in.

Third Plastic Hinge: (c)

$\frac{F_1}{F_2} = \frac{16 \times 4010}{0.321 \times 288^2} = 2.40$ $\therefore \frac{M_{min}}{M_{pm}} = 2.0$ $M_{min} = 2.0 \times 1670 = 3340$ k-in.

Check: $4010 + 3340 = 7350 > 2M_{pcB}$ (NG) $\therefore M_{min} = 2 \times 3040 - 4010 = 2070$ k-in.

$\delta M_{BC} = 2070 - (-484) = 2554$ k-in.

Calculate M_r and M_r' Values:

Initial $(\Delta/h = 0)$ $M_r' = \frac{1179}{3040} M_{pcB} = \underline{0.388\ M_{pcB}}$ (d)

$M_{r1} = \left(6.286 \times \frac{29{,}000 \times 889.9}{360 \times 3040} + 5.949 \times \frac{29{,}000 \times 889.9}{288 \times 3040}\right) \theta_B M_{pcB}$ (e)

$= (148 + 175)\ \theta_B M_{pcB} = \underline{323\theta_B M_{pcB}}$

$\delta M_B = 1082 = (148 + 175)3040\ \delta\theta_B$; $\therefore \delta\theta_B = \frac{1082}{983{,}000} = 0.00110$ rad.

$M_{r1}' = (323 \times 0.00110 + 0.388)\ M_{pcB} = \underline{0.744\ M_{pcB}}$ (f)

$M_{r2} = \underline{175\ \theta_B M_{pcB}}$ (g)

$\delta M_B = 1265 = 175 \times 3040\ \delta\theta_B$; $\therefore \delta\theta_B = \frac{1265}{533{,}000} = 0.00238$ rad.

$M_{r2}' = (175 \times 0.00238 + 0.744)\ M_{pcB} = \underline{1.161\ M_{pcB}}$ (h)

$M_{r3} = 3.0 \times \frac{29{,}000 \times 889.9}{288 \times 3040}\ \theta_B M_{pcB} = \underline{88.5\ \theta_B M_{pcB}}$ (i)

$\delta M_B = 2554 = 88.5 \times 3040\ \delta\theta_B$; $\therefore \delta\theta_B = \frac{2554}{269{,}000} = 0.0095$ rad.

$M_{r3}' = (88.5 \times 0.0095 + 1.161)\ M_{pcB} = \underline{2.000\ M_{pcB}}$ (Checks) (j)

INTERIOR SWAY SUBASSEMBLAGE B-D

First Plastic Hinge:

$\delta M_{CB} = 1836 = 6.053 \times \frac{E \times 889.9}{288} \delta\theta_C = 18.7 E \delta\theta_C \qquad \therefore E\delta\theta_C = 98.3$

$\delta M_{CD} = 6.154 \times \frac{889.9}{288} \times 98.3 = 1870 \text{ k-in.}; \quad \delta M_{DC} = 5.857 \times \frac{889.9}{288} \times 98.3 \times \frac{6.154-4}{2} = 1918 \text{ k-in.}$

Second Plastic Hinge:

$\delta M_{DC} = 172 = 5.857 \times \frac{E \times 889.9}{288} \delta\theta_D = 18.1 E \delta\theta_D \qquad \therefore E\delta\theta_D = 9.50$

$\delta M_{CD} = 6.154 \times \frac{889.9}{288} \times 9.50 \times \frac{5.857-4}{2} = 168 \text{ k-in.}$

Third Plastic Hinge:

$\frac{F_1}{F_2} = \frac{16 \times 4010}{0.321 \times 288^2} = 2.40 \quad \therefore \frac{M_{min}}{M_{pm}} = 2.0 \quad M_{min} = 2.0 \times 1670 = 3340 \text{ k-in.}$

Check: $4010 + 3340 = 7350 > 2 M_{pcC}$ (NG) $\therefore M_{min} = 2 \times 3660 - 4010 = 3310 \text{ k-in.}$

$\delta M_{CD} = 3310 - (-311) = 3621 \text{ k-in.}$

Calculate M_r and M_r' Values:

Initial $(\Delta/h = 0)$ $M_r' = -\frac{179}{3660} M_{pcC} = -0.049 M_{pcC}$

$M_{r1} = \left(6.053 \times \frac{29{,}000 \times 889.9}{288 \times 3660} + 6.154 \times \frac{29{,}000 \times 889.9}{288 \times 3660}\right) \theta_C M_{pcC}$

$= (148 + 150.5)\theta_C M_{pcC} = \underline{298.5 \theta_C M_{pcC}}$

$\delta M_C = 3707 = (148 + 150.5) 3660 \delta\theta_C \qquad \therefore \delta\theta_C = \frac{3704}{1{,}093{,}000} 0.00339 \text{ rad.}$

$M_{r1}' = (298.5 \times 0.00338 - 0.049) M_{pcC} = \underline{0.963 M_{pcC}}$

$M_{r2} = 150.5 \theta_C M_{pcC}$

$\delta M_C = 168 = 150.5 \times 3660 \delta\theta_C; \qquad \therefore \delta\theta_C = \frac{168}{551{,}000} = 0.000305 \text{ rad.}$

$M_{r2}' = (150.5 \times 0.000305 + 0.963) M_{pcC} = \underline{1.009 M_{pcC}}$

$M_{r3} = 3.0 \times \frac{29{,}000 \times 889.9}{288 \times 3660} \theta_C M_{pcC} = 73.5 \theta_C M_{pcC}$

$\delta M_C = 3621 = 73.5 \times 3660 \delta\theta_C; \qquad \therefore \delta\theta_C = \frac{3621}{269{,}000} = 0.01347 \text{ rad.}$

$M_{r3}' = (73.5 \times 0.01347 + 1.009) M_{pcC} = 2.000 M_{pcC}$ (Checks)

BULLETINS

Steel Research for Construction

No. 1 Current Paving Practices on Orthotropic Bridge Decks—*Battelle Memorial Institute, October, 1965*

No. 2 Strength of Three New Types of Composite Beams—*A. A. Toprac, October, 1965*

No. 3 Research on and Paving Practices for Wearing Surfaces on Orthotropic Steel Bridge Decks, Supplement to Bulletin 1—*Battelle Memorial Institute, August, 1966*

No. 4 Protection of Steel Storage Tanks and Pipe Underground—*Battelle Memorial Institute, May, 1967*

No. 5 Fatigue Strength of Shear Connectors—*R. G. Slutter and J. W. Fisher, October, 1967*

No. 6 Paving Practices for Wearing Surfaces on Orthotropic Steel Bridge Decks, Supplement to Bulletins 1 and 3—*Battelle Memorial Institute, January, 1968*

No. 7 Report on Investigation of Orthotropic Plate Bridges—*D. Allan Firmage, February, 1968*

No. 8 Deformation and Energy Absorption Capacity of Steel Structures in the Inelastic Range—*T. V. Galambos, March, 1968*

No. 9 The Dynamic Behavior of Steel Frame and Truss Buildings—*Dixon Rea, J. G. Bouwkamp and R. W. Clough, April, 1968*

No. 10 Structural Behavior of Small-Scale Steel Models—*Massachusetts Institute of Technology, April, 1968*

No. 11 Response of Steel Frames to Earthquake Forces—Single Degree of Freedom Systems—*M. J. Kaldjian and W. R. S. Fan, November, 1968*

No. 12 Response of Multistory Steel Frames to Earthquake Forces—*Subhash C. Goel, November, 1968*

No. 13 Behavior of Steel Building Connections Subjected to Inelastic Strain Reversals—*E. P. Popov and R. B. Pinkney, November, 1968*

No. 14 Behavior of Steel Building Connections Subjected to Inelastic Strain Reversals—Experimental Data—*E. P. Popov and R. B. Pinkney, November, 1968*

No. 15 Tentative Criteria for Load Factor Design of Steel Highway Bridges—*George S. Vincent, March, 1969*

No. 16 Strength of Plate Girders with Longitudinal Stiffeners—*Lehigh University, April, 1969*

No. 17 Fatigue Strength of Plate Girders—*Lehigh University, April, 1969*

No. 18 Interior Corrosion of Structural Steel Closed Sections—*February, 1970*

No. 19 Criteria for the Deflection of Steel Bridges—*R. N. Wright and W. H. Walker, November, 1971*

No. 20 Addendum Report on Paving Practices for Wearing Surfaces on Orthotropic Steel Bridge Decks—*Battelle Memorial Institute, October, 1971*

No. 21 Cyclic Loading of Full-Size Steel Connections—*E. P. Popov and R. M. Stephen, February, 1972*

No. 22 Seismic Behavior of Multistory Braced Steel Frames—*S. C. Goel and R. D. Hanson, April, 1972*

No. 23 Plastic Subassemblage Analysis and Tests for Rigid High-Rise Steel Frames—*Lehigh University, March, 1973*

Committee of Structural Steel Producers • Committee of Steel Plate Producers

american iron and steel institute

150 East 42nd Street, New York, N.Y. 10017